

DETECTION OF RESERVOIR WATER LEVELS USING LANDSAT REMOTE
SENSING DATA OVER ERMENEK AND ALTINKAYA DAMS

A THESIS SUBMITTED TO
THE GRADUATE SCHOOL OF NATURAL AND APPLIED SCIENCES
OF
MIDDLE EAST TECHNICAL UNIVERSITY

BY

ALİ ULVİ GALİP ŞENOCAK

IN PARTIAL FULFILLMENT OF THE REQUIREMENTS
FOR
THE DEGREE OF MASTER OF SCIENCE
IN
CIVIL ENGINEERING

SEPTEMBER 2019

Approval of the thesis:

**DETECTION OF RESERVOIR WATER LEVELS USING LANDSAT
REMOTE SENSING DATA OVER ERMENEK AND ALTINKAYA DAMS**

submitted by **ALİ ULVİ GALİP ŞENOCAK** in partial fulfillment of the requirements for the degree of **Master of in Civil Engineering** Department, **Middle East Technical University** by,

Prof. Dr. Halil Kalıpçılar
Dean, Graduate School of **Natural and Applied Sciences**

Prof. Dr. Ahmet Türer
Head of Department, **Civil Engineering**

Assoc. Prof. Dr. M. Tuğrul Yılmaz
Supervisor, **Civil Engineering, METU**

Examining Committee Members:

Prof. Dr. İsmail Yücel
Civil Engineering Department, METU

Assoc. Prof. Dr. M. Tuğrul Yılmaz
Civil Engineering, METU

Assoc. Prof. Dr. Uğur Murat Leloğlu
Geodetic and Geographical Information Technologies, METU

Assist. Prof. Dr. Cüneyt Baykal
Civil Engineering Department, METU

Assist. Prof. Dr. Ali Levent Yağcı
Department of Geodetic and Photogrammetric Engineering, GTU

Date: 02.09.2019

I hereby declare that all information in this document has been obtained and presented in accordance with academic rules and ethical conduct. I also declare that, as required by these rules and conduct, I have fully cited and referenced all material and results that are not original to this work.

Name, Surname: Ali Ulvi Galip Őenocak

Signature:

ABSTRACT

DETECTION OF RESERVOIR WATER LEVELS USING LANDSAT REMOTE SENSING DATA OVER ERMENEK AND ALTINKAYA DAMS

Şenocak, Ali Ulvi Galip
Master of Science, Civil Engineering
Supervisor: Assoc. Prof. Dr. M. Tuğrul Yılmaz

September 2019, 129 pages

Detection of water border using remote sensing observations at the visible bands and incorporating them with the digital elevation map is a useful approach for detecting water volume of dams and the water bodies with existing DEM images. In this study, NDWI, NDPI, WI2015 and AWEI indices retrieved using Landsat 8 images and ASTER/SRTM DEM maps are utilized to infer about the water levels of Ermenek and Altinkaya dams' reservoir water levels. To reduce the water level retrieval errors during the cloudy and the snow-covered areas, F-Mask cloud masking algorithm and a TCW-based custom index with optimized parameters have been introduced. Moreover, in order to prevent the affection of pixels that are located far away from the area of interest, a water-area-based shape file and proximity buffer have been introduced. Lastly, after the completion of the analysis, a statistical model has been applied to combine the results with DEM to get the elevation value as a result. Results show RMSE of the water level estimation over Ermenek and Altinkaya are 3.63 m and 3.34 m, respectively for the best index/DEM scenario when the models are trained and calibrated over the same dam. On the other hand, the errors increase to 5.13 m and 5.09 m respectively for Ermenek and Altinkaya dams when the validation and the calibration are done over different dams .

Keywords: Water Elevation, Landsat, Digital Elevation Map, Remote Sensing, Dam Reservoir

ÖZ

ERMENEK VE ALTINKAYA BARAJ REZERVUARLARININ SU YÜKSEKLİKLERİNİN LANDSAT KULLANILARAK UZAKTAN ALGILAMA İLE TESPİT EDİLMESİ

Şenocak, Ali Ulvi Galip
Yüksek Lisans, İnşaat Mühendisliği
Tez Danışmanı: Doç. Dr. M. Tuğrul Yılmaz

Eylül 2019, 129 sayfa

Görülebilir bantları, sayısal yükseklik haritası ile birlikte kullanarak su seviyesini tespit etmek, sayısal yükseklik harita görüntülerine ulaşılabilen barajlar için kullanışlı bir yaklaşımdır. Bu çalışmada, Ermenek ve Altinkaya ve Ermenek barajlarının göllerindeki su seviyelerinin tahmin edilmesi için Landsat 8 görüntüleri kullanılarak hesaplanmış olan AWEI, NDPI, NDWI ve WI2015 indeksleri ve ASTER/SRTM DEM verileri kullanılmıştır. Su seviyesi tahmininde bulut ve kar kaplı alanlar sebebiyle oluşabilecek hataları azaltmak için F-Mask bulut tespit algoritması ile parametreleri optimize edilmiş, TCW bazlı yeni oluşturulmuş bir indeks kullanılmıştır. Ayrıca, coğrafi olarak çalışmanın ilgi alanı ile alakasız olan piksellerin etkilerini ortadan kaldırmak için çalışma alanına dayalı bir sınırlama ve yakınlık bazlı ikinci bir sınırlama kesiti kullanılmıştır. Son olarak, çalışmanın tamamlanmasının ardından, istatistiksel bir model vasıtası ile sonuçların DEM ile kombinasyonu

sonrasında yükseklik deęerinin elde edilmesi gerekleřtirilmiřtir. Sonular gstermektedir ki Ermenek ve Altınkaya baraj gllerinde (en bařarılı model ve DEM kombinasyonunun) kk ortalama kare hatası deęerleri sırası ile 3.63 ve 3.34 metredir. Ancak, doęrulama ve kalibrasyon iřlemleri farklı barajlar ile yapıldığında bu hata deęerlerinin Ermenek ve Altınkaya barajları iin sırası ile 5.13 m ve 5.09 m olduęu gzlemlenmiřtir.

Anahtar Kelimeler: Su Yksekligi, Landsat, Sayısal Ykseklilik Haritası, Uzaktan Algılama, Baraj Rezervuarı

To my beloved family and in the loving memories of my grandmother Fidan Kurt,
my grandfather Ali Faik Şenocak and my uncle Şükrü Özdemir

ACKNOWLEDGEMENTS

First of all, I would like to thank my supervisor Assoc. Prof. Dr. M. Tuğrul Yılmaz, who was also be my advisor during my undergraduate studies. He was there for me even when our meetings about my questions were extended in the evenings and even weekends, and guided my research in a way that I felt both liberty for going after my conceptual ideas about this study without any limitation and safety that I would be guided into the right direction shall my conceptual works fail. I am grateful for his guidance throughout whole process.

During the initial phase of my MSc studies, I had attended courses all of which helped me to gain knowledge on the topics related with this study. However, among these courses, I would like to thank Prof. Dr. İsmail Yücel, Assoc. Prof. Dr. Uğur Murat Leloğlu and Assoc. Prof. Dr. M. Tuğrul Yılmaz specially.

I would like to thank examining committee members for their insightful comments that led to final form of this thesis.

M. Kemal Ardoğa and Hasan Eser, both of whom are PhD candidates in METU and among my best friends, have helped me with their friendship and guidance with their experiences in addition to Kemal's help throughout the final bureaucratic steps. I am grateful for their friendship and contributions.

Writing a thesis sometimes come with struggles like not working codes and having problems that require unique approaches, in addition to diminished social interaction as the defense date gets closer. Through the good and bad days, I always had the support of my friends and complained mostly to them about the struggles whenever I felt like. I would like to thank Bahar N. Can, G. Hazal Ak, Osman Fuat Öztürk, Emirhan Söğütkıran and Dr. Meltem Durğun Küçükdağ for their lifelong friendship and patience.

Throughout my studies, I have felt like a member of a research team and met wonderful friends. I would like to thank İpek Gül Karasu, Dr. Mehdi Hesami Afshar, Eren Düzenli, Burak Bulut, Kaveh Yousefi-Patakchi, Muhammad Amjad, for providing a friendly atmosphere with always existing tea and coffee. I should also thank them for them for using their vacation days in an unplanned way that I could always find a table to study in the room. I would like to underline my gratitude to İpek Gül Karasu for her friendship and help throughout the writing of this thesis.

I would thank Dr. Mehdi Hesami Afshar again for the physical copy of his PhD thesis that I had used as a real-world example for formatting.

In the name of all of their members and their educational tradition that have a huge effect on me, I should thank Middle East Technical University and Beşevler Ankara Atatürk Anatolian Highschool.

I am glad that Doctor Who, Rick and Morty, Futurama and The Big Bang Theory shared half of my computer screen through those times.

I would like to thank USGS, METI, NASA and DSI for providing data that is in this study.

Writing computer code sometimes requires a place that employs wise but not-so-friendly wizards that one may go and ask his questions. I should be thankful for Stackoverflow for being this and Reddit for balancing it. While mentioning about Internet sites, XKCD and PhD Comics should also be mentioned in a way that they make people say that “How do you know about my life and research that well?”.

I would not have chance to pursue the educational path that ended up providing me to have enough discipline and skill-set to fulfill the requirements of carrying out this thesis if my former teacher, Cemile Atasoy would not choose to believe in me, even when her colleagues were thinking otherwise and even I had doubts about myself. I always will fell grateful and indebted to her.

I would like to thank Selçuk Mızrak and Bahadır Gülcüler for being not only two of my best friends but also being like a brother for all these years. I knew that whenever I had a conflict between my research and professional life, I could rely on Selçuk Mızrak to cover me. I wish their newborn daughters Serra Duru Mızrak and Gökçe Gülcüler a long and happy life and thank for keeping their fathers awake while I was staying awake for writing and editing this thesis.

I would like to thank Zeliha-Murat Aküzüm, Yasemin-Sinan Kurt, Serap-Muammer Yılmaz an in the name of my extended family for support, coffee, French fries and joyful conversations I had received and their confidence in me.

Hanife Yılmaz and Serap Yılmaz also have great contributions that affected the person I became. Without their support and efforts, I would be missing a lot.

I will always be thankful to my grandmother Hatice Şenocak and grandfather İdris Kurt for my childhood memories and their wisdom.

I am grateful to my cousins Seval Kamiloğlu, Mustafa Kurt, Safa Kurt, Dr. Necla Gökçe Şenocak, Dr. Elif Göksu Yiğit Tekkanat and Umut Göktuğ Yiğit in the name of all of my cousins for being like a sibling to me through all my life.

My uncle Prof. Dr. Kemal Şenocak and my aunt Prof. Dr. Zarife Şenocak have shown genuine interest in my studies as well as supported my decision of conducting my MSc studies in addition to their helpful guidance and advices. They are and will always be an inspiration for me and my cousins who is pursuing or would like to pursue an academic research.

Last but most, I would like to thank my family, Alptekin Şenocak, Nur Pınar Özdemir, Erdem Şenocak and Zuhale Şenocak. They have always supported me in my decisions, they have guided my way but also provide me to freedom to shape my life for my entire lifetime. Without their constant support and confidence in my decisions, all of these would not be possible. My gratitude towards them are inexpressible by words.

TABLE OF CONTENTS

ABSTRACT	v
ÖZ	vii
ACKNOWLEDGEMENTS	x
TABLE OF CONTENTS	xiii
LIST OF TABLES	xvi
LIST OF FIGURES	xviii
LIST OF ABBREVIATIONS	xxi
LIST OF SYMBOLS	xxiv
1. INTRODUCTION	1
1.1. Goal of This Study	1
1.2. Studies Focusing on Water Level Detection using VIS/NIR/SWIR Images and DEMs.....	3
1.3. Relevant Studies over Turkey	5
1.4. Added Utility of This Study	7
2. METHODOLOGY	9
2.1. Definitions	9
2.2. Overview of the Study	11
2.3. Flow of The Model.....	13
2.4. Study Area	20
2.4.1. Ermenek Dam.....	20
2.4.2. Altinkaya Dam	23
2.5. Utilized Input Data	26

2.5.1. Ground Data.....	26
2.5.2. Digital Elevation Data.....	27
2.5.2.1. ASTER GDEM.....	27
2.5.2.2. SRTM GDEM.....	29
2.5.3. Landsat Images	30
2.5.3.1. Selection of Landsat-8 Images.....	30
2.5.3.2. Selection of Digital Numbers Instead of Surface Reflectance	31
2.5.3.3. TOA Reflectance, Radiance and Brightness Temperature Calculations	33
2.6. Post-Processed Data.....	34
2.6.1. Selected Water Area Detection Indices	34
2.6.1.1. AWEI.....	35
2.6.1.2. 8 NDPI.....	35
2.6.1.3. NDWI	35
2.6.1.4. WI2015	36
2.6.2. Applied Buffers and Masks.....	36
2.6.2.1. Region of Interest Subset.....	36
2.6.2.2. Proximity Mask	38
2.6.2.3. Cloud Mask.....	40
2.6.2.4. Snow and Shadow Mask.....	49
2.7. Optimization of Water Level Detection Estimations	53
2.7.1. Optimization Method and Design Decisions	53
2.7.2. Initial Threshold Selection for Water Detection Indices	55
2.7.3. Objective Function.....	58

2.7.4. Training and Test Data	59
2.8. Alternative Statistical Methods to Retrieve Water Level Estimation	59
2.9. Used Software and Web Apps.....	60
3. RESULTS AND DISCUSSION.....	61
3.1. Optimized Parameters	61
3.2. Water-Land Border Detection	63
3.3. Ermenek Dam Estimations	64
3.4. Altinkaya Dam Estimations.....	80
4. SUMMARY AND CONCLUSION	93
REFERENCES.....	97
A. Results Other Statistical Models	105

|

LIST OF TABLES

TABLES

Table 2:1 Band Coefficients of TCW-Crist and mTCW	50
Table 2:2 Predetermined Step Sizes of Applied Water Indices.....	55
Table 3:1 <i>Optimized parameters for training data based on Ermenek Dam and Altinkaya Dam</i>	62
Table 3:2 Average Error Values of Both Local and Remote Trained Models over Ermenek Dam (ErmT means Ermenek Trained and AltT means Altinkaya Trained; AWEI_S, NDPI, NDWI_MCF and WI2015 are Water Detection Indices, ASTER and SRTM are DEMs, E means that model is estimating Ermenek Dam's water level and A means model is estimating Altinkaya Dam's water level)	71
Table 3:3 Average Error Standard Deviation Values of Both Local and Remote Trained Models over Ermenek Dam (ErmT means Ermenek Trained and AltT means Altinkaya Trained; AWEI_S, NDPI, NDWI_MCF and WI2015 are Water Detection Indices, ASTER and SRTM are DEMs, E means that model is estimating Ermenek Dam's water level and A means model is estimating Altinkaya Dam's water level).....	72
Table 3:4 Average RMSE Values of Both Local and Remote Trained Models over Ermenek Dam (ErmT means Ermenek Trained and AltT means Altinkaya Trained; AWEI_S, NDPI, NDWI_MCF and WI2015 are Water Detection Indices, ASTER and SRTM are DEMs, E means that model is estimating Ermenek Dam's water level and A means model is estimating Altinkaya Dam's water level)	73
Table 3:5 Correlation Coefficient of Ermenek Dam Models	76
Table 3:6 RMSE Results of Best Models based on Different Statistical Models for Estimation of Water Level of Ermenek Dam.	77
Table 3:7 Average Error Values of Both Local and Remote Trained Models over Altinkaya Dam (ErmT means Ermenek Trained and AltT means Altinkaya Trained; AWEI_S, NDPI, NDWI_MCF and WI2015 are Water Detection Indices, ASTER and	

SRTM are DEMs, E means that model is estimating Ermenek Dam’s water level and A means model is estimating Altinkaya Dam’s water level).....	85
Table 3:8 Average Error Standard Deviation Values of Both Local and Remote Trained Models over Altinkaya Dam (ErmT means Ermenek Trained and AltT means Altinkaya Trained; AWEI_S, NDPI, NDWI_MCF and WI2015 are Water Detection Indices, ASTER and SRTM are DEMs, E means that model is estimating Ermenek Dam’s water level and A means model is estimating Altinkaya Dam’s water level)	86
Table 3:9 Average RMSE Values of Both Local and Remote Trained Models over Altinkaya Dam (ErmT means Ermenek Trained and AltT means Altinkaya Trained; AWEI_S, NDPI, NDWI_MCF and WI2015 are Water Detection Indices, ASTER and SRTM are DEMs, E means that model is estimating Ermenek Dam’s water level and A means model is estimating Altinkaya Dam’s water level).....	87
Table 3:10 Correlation Coefficient of Altinkaya Dam Models	90
Table 3:11 RMSE Results of Best Models based on Different Statistical Models for Estimation of Water Level of Altinkaya Dam.	92

LIST OF FIGURES

FIGURES

Figure 2.1 Demonstration of Elevation Change Within a Pixel and Half Pixel with respect to Slope.....	11
Figure 2.2 Flow Chart of the Model up to the Calculation of Cropped DEM.....	14
Figure 2.3 Flow Chart of the Model up to the Calculation of Final Water Area Mask	14
Figure 2.4 Flow Chart of the Model about Water Elevation Detection.....	15
Figure 2.5 Satellite View of the Ermenek Dam and its Reservoir (Google, n.d.-b)..	22
Figure 2.6 Slope Map (in Degrees) of Ermenek Dam Buffer Area Based on SRTM DEM	22
Figure 2.7 Slope Map (in Degrees) of Ermenek Dam Buffer Area Based on ASTER DEM	23
Figure 2.8 Satellite View of the Altinkaya Dam and its Reservoir (Google, n.d.-a).	25
Figure 2.9 Slope Map (in Degrees) of Altinkaya Dam Buffer Area Based on SRTM DEM	25
Figure 2.10 Slope Map (in Degrees) of Altinkaya Dam Buffer Area Based on ASTER DEM	26
Figure 2.11 ASTER DEM over Ermenek Dam	28
Figure 2.12 ASTER DEM over Altinkaya Dam.....	28
Figure 2.13 SRTM DEM over Ermenek Dam.....	29
Figure 2.14 SRTM DEM over Altinkaya Dam	30
Figure 2.15 NDWI-XU Result (SWIR = B6) based on DN of Landsat 8 (LS8) Image LC08_L1TP_177035_20180418_20180501_01_T1.....	32
Figure 2.16 NDWI-XU Result (SWIR = B6) based on SR of LS8 Image LC08_L1TP_177035_20180418_20180501_01_T1.....	32
Figure 2.17 Initial Subset Marked (with Red) over the Altinkaya RGB Image	37

Figure 2.18 Initial Subset Marked (with Red) over the Ermenek RGB Image.....	37
Figure 2.19 Proximity Buffer Area for Ermenek Dam	39
Figure 2.20 Proximity Buffer Area for Altınkaya Dam.....	39
Figure 2.21 RGB Image (Left) and Related Cloud Mask Result (Right) of the LS8 Image LC08_L1TP_177035_20160802_20170322_01_T1	41
Figure 2.22 PCP (Left) and Water Mask (Right) results of LS8 Image LC08_L1TP_177035_20180402_20180416_01_T1	43
Figure 2.23 Clear Sky Water Mask results of LS8 Image LC08_L1TP_177035_20180402_20180416_01_T1	43
Figure 2.24 Brightness Temperature (Kelvin) Result of LS8 Image LC08_L1TP_177035_20180402_20180416_01_T1 (Axes Represent UTM Coordinates).....	44
Figure 2.25 Temperature Based Water Probability Mask (Left) and Brightness based Probability Mask (Right) of LS8 Image LC08_L1TP_177035_20180402_20180416_01_T1	45
Figure 2.26 Clear Sky Land Mask (Left) and Temperature Based Cloud Probability Mask (Right) of LS8 Image LC08_L1TP_177035_20180402_20180416_01_T1....	46
Figure 2.27 Whiteness Mask (Left) and Land Variance Mask (Right) calculations of the Cloud Mask of LS8 Image LC08_L1TP_177035_20180402_20180416_01_T1	47
Figure 2.28 RGB image of LS8 Image LC08_L1TP_177035_20180402_20180416_01_T1	48
Figure 2.29 Final Cloud Mask of LS8 Image LC08_L1TP_177035_20180402_20180416_01_T1	49
Figure 2.30 Results of AWEI-S (Left) and mTCW (Right) Calculations of Landsat-8 Image LC08_L1TP_173033_20180201_20180220_01_T1	51
Figure 2.31 RGB Image of Landsat-8 Image LC08_L1TP_176031_20170219_20170301_01_T1 (Image obtained from USGS).	52
Figure 2.32 Resultant Image (Introduction of mTCW to Water Detection Index) of Landsat-8 Image LC08_L1TP_176031_20170219_20170301_01_T1	53

Figure 2.33 Histogram of NDWI.MCF Result of Ermenek Dam for Date 09.07.2013	56
Figure 2.34 Plot of NDWI.MCF Result of Ermenek Dam for Date 09.07.2013.....	57
Figure 2.35 Result Plots of Ermenek Dam Area based on Different NDWI.MCF Thresholds.....	57
Figure 2.36 Result Plots of Ermenek Dam Area based on Different NDWI.MCF Thresholds.....	57
Figure 3.1 Detected Water Area of Ermenek Dam for 18/08/2016 (Green areas are land pixels).....	63
Figure 3.2 Detected Water Border of Ermenek Dam for 18/08/2016	64
Figure 3.3 Time Series of Best (NDPI + SRTM) Model for Estimating Ermenek Dam's Water Level.....	69
Figure 3.4 Ground Elevation vs Estimated Elevation Data Scatter Plot of Best Model for Ermenek Dam	70
Figure 3.5 Average Statistics of Local Models 'Results over Ermenek Dam	74
Figure 3.6 Average Statistics of Remote Models 'Results over Ermenek Dam.....	75
Figure 3.7 Water Area Detection based on NDPI Index over Ermenek Dam, Before Masking (24.10.2017).....	78
Figure 3.8 Water Area Detection based on NDPI Index over Ermenek Dam, Before Masking (15.07.2017).....	78
Figure 3.9 Elevation Histogram of Ermenek Dam showing Ground Data and Estimations of Different Statistical Approaches (01.03.2017).....	79
Figure 3.10 Time Series of Best (AWEI-S + ASTER) Model for Estimating Altinkaya Dam's Water Level.....	83
Figure 3.11 Ground Elevation vs Estimated Elevation Data Scatter Plot of Best Model for Altinkaya Dam	84
Figure 3.12 Average Statistics of Local Models 'Results over Altinkaya Dam.....	88
Figure 3.13 Average Statistics of Remote Models 'Results over Altinkaya Dam	89
Figure 3.14 Elevation Histogram of Altinkaya Dam showing Ground Data and Estimations of Different Statistical Approaches (01.11.2017).....	91

LIST OF ABBREVIATIONS

ABBREVIATIONS

ANG	Angle Coefficient File The Advanced Spaceborne Thermal Emission and Reflection
ASTER	Radiometer
AWEI	Automated Water Extraction Index
AWEI-NS	Automated Water Extraction Index (No Consideration of Shadows)
AWEI-S	Automated Water Extraction Index (Considering Shadows)
BDA	Bulk Download Assistant
BT	Brightness Temperature
CRS	Coordinate Reference System
DEM	Digital Elevation Map
DN	Digital Number
DSI	The General Directorate of State Hydraulic Works of Turkey
ECDF	Empirical Cumulative Distribution Function
EROS	Earth Resources Observation Satellite
ESA	European Space Agency
ETM	The Enhanced Thematic Mapper
ETM+	The Enhanced Thematic Mapper Plus
GB	Gigabyte
GDEM	Global Digital Elevation Map
GEV	Generalized Extreme Value
GIS	Geographic Information System
km	kilometer
LS8	Landsat 8
m	meter

METI	Ministry of Economy, Trade, and Industry of Japan
mm	millimeter
MGM	Turkish State Meteorological Service
MODIS	The Moderate Resolution Imaging Spectroradiometer
mTCW	Modified Tasseled Cap Wetness
MTL	Landsat Metadata File
MW	Megawatts
m/s	meters per second
NA	Not Available
NaN	Not a Number
NASA	The National Aeronautics and Space Administration
NDPI	Normalized Difference Pond Index
NDVI	Normalized Difference Vegetation Index
NDWI	Normalized Difference Water Index
NDWI.MCF	Normalized Difference Water Index – Mcfeeter’s Variation
NIR	Near Infrared
NMS	Nelder-Mead Simplex
OS	Operating System
PCP	Potential Cloud Pixel
R	R-Programming Language
RAM	Random Access Memory
RGB	Red Green Blue
RMSE	Root Mean Square Error
SAR	Synthetic Aperture Radar
SE	South East
SLC	Scan Line Corrector
SR	Surface Reflectance
SRTM	Shuttle Radar Topography Mission
SW	South West

SWIR	Short Wave Infrared
TCW	Tasseled Cap Wetness
TIR	Thermal Infrared
TOA	Top of Atmosphere
U.S.	United States
U.S.A.	United States of America
USGS	United States Geological Survey
UTM	Universal Transverse Mercator
UV	Ultraviolet
VIS	Visible Range
WI2015	Water Index 2015

LIST OF SYMBOLS

SYMBOLS

μ	Mean
σ	Standard Deviation
$^{\circ}$	Degree
\leq	Smaller Than or Equal to
\geq	Greater Than or Equal to
$<$	Smaller Than
$>$	Greater Than
\pm	Plus, or Minus
Σ	Sum Operator
Δ	Delta
\Rightarrow	Then
\equiv	Is Equal to?
$=$	Equal to
$^{\circ}\text{C}$	Degree Celsius
$\sin()$	Sinus
$\sqrt{\quad}$	Square Root Operator
,	Thousand Separator (When Used in Combination with Numeric)
.	Decimal Separator (When Used in Combination with Numeric)

CHAPTER 1

INTRODUCTION

1.1. Goal of This Study

Water is an important commodity for maintaining the existence of human life and its accumulated civilization. In the modern world water is used for irrigation, hydropower generation, sanitation and sustaining human life among others. However, as the cities grow, natural water budget can be expected to be stretched to the point that it cannot be considered as sufficient and water transportation may be needed. This transportation requires delicate assessment of water budgets of both providing and receiving areas. Moreover, in addition to irrigation and sustaining human life, hydropower is an important energy source for countries including Turkey that has 27,912 Megawatts (MW) of installed capacity shared among 636 facilities that covers 32% of country's total installed capacity as of June, 2018 (T.R. Ministry of Energy and Natural Resources, 2018). In order to maximize its usage and prevent scarcities, detecting water storage is an important aspect of water body management.

Water storage detection has been performed by using various methods, such as use of ground observations and remote sensing methods. Among these models, manual inspection of remote reservoirs (e.g., lakes) may not be technically easy (i.e., particularly under harsh winter or storm conditions) and cost effective. Besides, there could be some limitations about the water level observations in case the water body of interest lays in another country than the user lives. On the other hand, remote sensing-based observations have the ability to infer about the ground conditions with more conveniently than ground observations. Such remote sensing-based methodologies rely on various methods involving Synthetic-Aperture Radar (SAR) or Interferometric SAR (InSAR) images (Du et al., 2016; Huang, Nguyen, Zhang, Cao,

& Wagner, 2017; Karaman, Özelkan, & Taşdelen, 2018; Okeowo, Lee, Hossain, & Getirana, 2017; Wdowinski et al., 2008) or combination of Digital Elevation Model (DEM) raster images with remote sensing observations at the visible (VIS) and short wave infrared (SWIR) bands of the spectrum (Avisse, Tilmant, François Müller, & Zhang, 2017; Tseng et al., 2016). SAR and InSAR models can penetrate through the atmospheric clouds but are either depend on platforms like JASON (which was designed to operate over the oceans without ice cover (ESA, n.d.-a)) or JERS-1 (now dysfunctional) that have a lower temporal resolution of 44 days (Kramer, 2002) than Landsat's temporal resolution of 16 days (Department of the Interior U.S. Geological Survey, 2019). Moreover, SAR based models' data acquisition process includes side-looking geometry and topographical obstacles such as mountains and dense forests may interfere with the microwave pulses with a consequence of introducing blind areas on the resultant images (Huang et al., 2017). Accordingly, VIS&SWIR bands combination incorporated with DEM have high potential to estimate the water levels over remote locations.

Water detection methods based on Landsat images are widely used to infer about the extent of water bodies utilizing Landsat's VIS, near infrared (NIR), SWIR and thermal infrared (TIR) bands. Using these bands, various indices have been developed to detect water extent (e.g., Automated Water Extraction Index, AWEL; Normalized Difference Water Index, NDWI; Water Index 2015, WI2015; and Normalized Difference Pond Index, NDPI). Since water extent datasets alone do not have sufficient information to infer about the water level estimations, and studies generally utilize also DEM datasets to get water level estimates (Avisse et al., 2017; Tseng et al., 2016).

Among satellite-based images at the visible portion of the spectrum Sentinel based models have the advantage of being higher resolution (10 m) and may utilize the C-SAR band of Sentinel-1 (ESA, n.d.-b). Sentinel's resolution is better than the 500 m resolution of The Moderate Resolution Imaging Spectroradiometer (MODIS) and 30 m resolution of Landsat but Sentinel also have disadvantage of having a smaller

(5 years) historical archive (ESA, n.d.-c) compared to ~47 years of Landsat archive (Earth Resources Technology Satellite, EROS, renamed to Landsat later, was launched in 1972, while the most recent Landsat mission continues to retrieve observations in 2019) (USGS, 2008). Landsat platform with such a long historical archive with high spatial resolution, offers a very unique and valuable opportunity to study historical conditions. Accordingly, studies utilize Landsat datasets to obtain water level estimates are needed to understand the utility of acquired historical water level estimates.

There are various variables impacting the accuracy of the final water level estimates using Landsat & DEM image combination, such as remote sensing image-based indices, DEM dataset selection, and the training dataset. More specifically, there are different water detection indices that are used in the literature (e.g., AWEL, NDWI, WI2015, and NDPI). Similarly, there are different DEM images available that the literature utilizes to obtain water level estimation (e.g., The Advanced Spaceborne Thermal Emission and Reflection Radiometer, ASTER and Shuttle Radar Topography Mission, SRTM). Training data to improve the accuracy of the water level estimates may not be always available at the region of interest; instead for such cases remote datasets (i.e., obtained from different regions) are used to obtain water level estimates. Such factors may significantly impact the accuracy of the water level estimates. Accordingly, relative added benefits of different indices, DEM datasets, and local/remote validation datasets in the framework of water level estimation need to be explicitly investigated in dedicated studies.

1.2. Studies Focusing on Water Level Detection using VIS/NIR/SWIR Images and DEMs

Water level detection by utilizing remote sensing, especially with Landsat and Sentinel images have been researched globally. One notable study is the one performed over Hoover Dam of the United States of America (U.S.A.) by using a statistical model that utilizes Generalized Extreme Value (GEV) distribution in

combination of recreating reservoir bathymetry by using average slopes and triangular topography assumption (Tseng et al., 2016). Landsat imagery, in addition to ASTER and SRTM DEMs were utilized in this study. They found 1.90 ± 0.45 m of root mean square error (RMSE) in estimation of the water level of the dam. The region that this study had focused on has warm climate and have hardly any snow cover (i.e., close to Nevada Desert). Accordingly, this study had not implemented any snow mask. On the other hand, water levels of dams that are fed by snow-melt could be severely impacted from the snow cover around the dam area. Hence, an explicit snow cover mask should be implemented in addition to such water level estimation methodologies. Additionally, this study only investigates the Hoover Dam, where their water level estimation methodology is calibrated and validated over the same area. Given that, it is viable that independent validation over different regions may yield higher errors, such methodologies should be implemented with selection of different calibration and validation regions.

Another notable study has been performed over the water bodies of Jordan by combining Landsat imagery with DEMs and using frequency based statistical model to obtain the water elevation of the water bodies (Avisse et al., 2017). This study had separated the calibration and the validation implementation of their water level estimation methodology. As a result, they have found correlations with the ground observations between 0.31 and 0.98, depending on the water body. On the other hand, similar to Hoover Dam case this study did not implement any snow cover mask in their methodologies too.

Here above only two studies are given as an example for the combination of Landsat & DEM images to retrieve dam water levels. On the other hand, there are not many other studies investigated this potential of Landsat & DEM images particularly over regions with seasonal snow cover (similar to Turkey). Hence, more dedicated studies are necessary in this topic.

Even though indices like AWEI, NDWI, WI2015, and NDPI are particularly used for water area extent estimation (Feyisa, Meilby, Fensholt, & Proud, 2014; Fisher, Flood, & Danaher, 2016; Lacaux, Tourre, Vignolles, Ndione, & Lafaye, 2007; Xu, 2006), their potential in water level estimation has not been investigated in detail with a study that compares their relative utility. Accordingly, more studies over different locations are necessary to clearly highlight the added utility of these indices in water level estimation.

1.3. Relevant Studies over Turkey

Because this study has been carried out using datasets obtained over Turkey, it is relevant to revise the literature about the studies focusing over regions of interests laying over Turkey. Here, under this sub-section brief information about the studies using remote sensing-based images to infer about the water area extent in addition to water level estimates is given, as the number of studies focused on water level estimation is very limited.

There are some studies focused on water extent estimation over various regions in Turkey (Bahadır, 2013; Geymen, 2017; Karabulut, 2015; Peker, 2019). However, there are only a few studies so far focused on the estimation of water level using remote sensing data (Ataol, 2010; Ozdemir & Leloglu, 2014), while combination of Landsat datasets with DEM images to get water level estimation has not been investigated so far. Overall, the studies implemented so far with a study area over Turkey focus more on water area extent estimation rather than water level estimation. Accordingly, there is still a need for more studies investigating estimation of water levels using remote sensing datasets over Turkey.

Lake Burdur is one of the regions with a lake area extent that is very sensitive to seasonal and inter-annual climate variability. There are various studies over the lake area estimation using different methodologies. Among them, the study by Ataol (2010) used two Landsat images (obtained in 1987 and 2000), one SPOT image (obtained in 2008), ground observations acquired from The General Directorate

of State Hydraulic Works of Turkey (DSI), DEM images with spatial resolution of 90 m., and 1:100.000 topography map to get the lake water area extent. They concluded that the lake water extent has dropped 9.50 m. from year 1987 to 2000.

In another study used 5 Landsat TM images (1975, 1987, 1990, 2000 and 2002) and 1 SPOT XS (1996) images and the bathymetry map to determine the lake area extent of Burdur Lake and later validated them using ground observations of water area extent (Şener, Davraz, & İsmailov, 2005). This study concluded that the area of the lake has dropped from 210 km² to 153 km² and the lake water level has dropped 10 m from year 1975 to 2002.

Elmalı Basin, one of the drinking water sources of İstanbul, was studied in terms of land usage by utilizing 3 Landsat Enhanced Thematic Mapper (ETM) images for the dates of 1995, 2005 and 2013, in combination with Geographic Information Systems (Geymen, 2017). They found the basin has increasing water risk in years.

If scope of inspecting local studies is expended in a way that it covers bathymetry mapping of shallow waters by utilizing remote sensing, a research about bathymetry mapping of Serçin Lake by utilizing Hyperion images in combination with statistical error correction and optimization algorithms (Ozdemir & Leloglu, 2014) can be included. This study not only maps the bathymetry but finds chlorophyll content of the water and concluded that the depth estimates are consistent with visual information.

Among aforementioned local studies, even the ones implementing areal measurements do not utilize any statistical models, they have the limitations of area detection algorithms such as blocked areas by clouds and they, except Peker (2019), utilize only a handful of Landsat images since their time series is based on change of water content in terms of years and even half a decade. The water area extent change is investigated over 16 lakes using Landsat and Sentinel images and found major lakes' (Burdur and Akşehir) water area extent shrunk (i.e., water levels dropped) between 1987 and 2017 (Peker, 2019).

There are other studies as well investigated the water area extent using remote sensing based datasets (Bahadır, 2013; Demirkesen, 2003; Karabulut, 2015; Özdemir, 2008) and found satisfactory results. However direct water level estimation related studies over Turkey have not been investigated in detail so far; hence there is still a need for such studies.

1.4. Added Utility of This Study

This study focuses on monthly water level measurements over Ermenek and Altinkaya dams using Landsat 8 images between May 2013 and May 2019, while these estimates were validated using ground measurements (provided by DSI) as the truth. Here, the added utility of four different indices (AWEI, NDWI, WI2015, and NDPI), two different DEM datasets (ASTER and SRTM), two training datasets (i.e., local and remote) and five different statistical model (Empirical Cumulative Distribution Function, ECDF; GEV, mean, mode and median based models) are investigated. F-Mask cloud detection algorithm is utilized and a Modified Tasseled Cap Wetness (mTCW) algorithm is developed for snow and shadow detection.

One of the premises of the remote sensing-based methodologies is the ability to infer over regions that ground observations are not available. Accordingly, error estimates of the remote sensing-based methodologies that do not rely on observations obtained directly over the region-of-interest is needed. On the other hand, earlier studies in the literature estimated water level change via VIS/SWIR observations and DEM images mostly use the same site to train their algorithms and validate their results (i.e., error statistics might suffer from overfitting; Tseng et al., 2016), while only a few studies (Avisse et al., 2017) investigate the impact of training models on different sites. By explicitly investigating the performance of the estimation methodologies over independent regions (i.e., independent validation), this study contributes significantly to the existing literature.

Existing snow/cloud/shadow filters used in the studies in the literature may not necessarily perform well in discriminating snow and shadow covered areas from other

regions. Tasseled Cap Wetness (TCW) index classifies the soils based on their wetness using 6 different (Red Green Blue, RGB; 1 NIR; and 2 SWIR) bands of Landsat images. In this study, a modified version of Tasseled Cap Wetness (mTCW) index that uses 6 different (RGB, 1 NIR, 1 SWIR and 1 TIR) bands of Landsat 8 images is developed to detect snow and shadow covered areas. With this aspect, this study contributes to the existing literature by introducing a new snow and shadow filter.

Below Chapter 2 gives the details about the methodology and the datasets used in this study, Chapter 3 presents the results, and Chapter 4 gives the discussion and the conclusion of these results.

|

CHAPTER 2

METHODOLOGY

2.1. Definitions

Used terminology among this study should be explained before going into the details of the study.

Raster: Rectangular (satellite for this study) image that has been computerized and consisting of pixels (Cambridge University Press, 2013).

Spatial Resolution: A numerical value that is defined for a standard unit (meters in this study) and defines the ground area that each pixel in the raster covers. For example, a raster image with a spatial resolution of 30 m covers an area of 900 square kilometers for each pixel.

Temporal Resolution: A numerical value that is defined for a standard unit (days in this study) and defines the revisit time of the satellite platform. For example, a temporal resolution of 16 days means that a new raster is generated every 16 days.

Aerosol – Ultraviolet Band: Band-1 of Landsat-8 platform that covers the 0.433–0.453 μm interval of the electromagnetic spectrum (Department of the Interior U.S. Geological Survey, 2019).

Blue Band: Band-2 of Landsat-8 platform that covers the 0.450–0.515 μm interval of the electromagnetic spectrum (Department of the Interior U.S. Geological Survey, 2019).

Green Band: Band-3 of Landsat-8 platform that covers the 0.525–0.600 μm interval of the electromagnetic spectrum (Department of the Interior U.S. Geological Survey, 2019).

Red Band: Band-4 of Landsat-8 platform that covers the 0.630–0.680 μm interval of the electromagnetic spectrum (Department of the Interior U.S. Geological Survey, 2019).

Near Infrared (NIR): Band-5 of Landsat-8 platform that covers the 0.845–0.885 μm interval of the electromagnetic spectrum (Department of the Interior U.S. Geological Survey, 2019).

Short Wave Infrared (SWIR): Band-6 (SWIR-1) and Band-7 (SWIR-2) of Landsat-8 platform that covers the 1.560–1.660 μm (Band-6) and 2.100–2.300 μm (Band-7) intervals of the electromagnetic spectrum (Department of the Interior U.S. Geological Survey, 2019).

Cirrus Band: Band-9 of Landsat-8 platform that covers the 1.360–1.390 μm interval of the electromagnetic spectrum (Department of the Interior U.S. Geological Survey, 2019).

Thermal Infrared (TIR): Band-10 (TIR-1) and Band-11 (TIR-2) of Landsat-8 platform that covers the 10.6–11.2 μm (Band-10) and 11.5–12.5 μm (Band-11) intervals of the electromagnetic spectrum (Department of the Interior U.S. Geological Survey, 2019).

RGB: An image that combines blue, green and red bands in a single image.

VIS: An image or matrix that includes the bands that operate within the visible parts of the electromagnetic spectrum. VIS, covers blue, green and red bands.

Sub-Pixel: Spatial area that is smaller than the spatial resolution of raster and hence cannot be represented in the image although it exists and affects the digital number (DN) value. For example, for a platform with 30 m of spatial resolution, sub-pixel means an object that is smaller than 30 m.

Half Pixel: Sub pixel, that covers an area equal to half of the spatial resolution of the raster image. For example, for a platform with 30 m of spatial resolution, half a

pixel means an object that is 15 m long. See Figure 2.1 for elevation change demonstration and relation between whole pixel and half pixel.

Binary Mask, Binary Image: An image or mask that includes only zero or one valued pixels.

Local Dataset/Model: Case, where the ground data used for model training is the same with the dam that the model is used to estimate its water level (ex. Using models trained with Ermenek Dam’s ground measurements to estimate the Ermenek Dam’s water level)

Remote Dataset/Model: Case, where the ground data used for model training is not the same with the dam that the model is used to estimate its water level (ex. Using models trained with Altinkaya Dam’s ground measurements to estimate the Ermenek Dam’s water level)

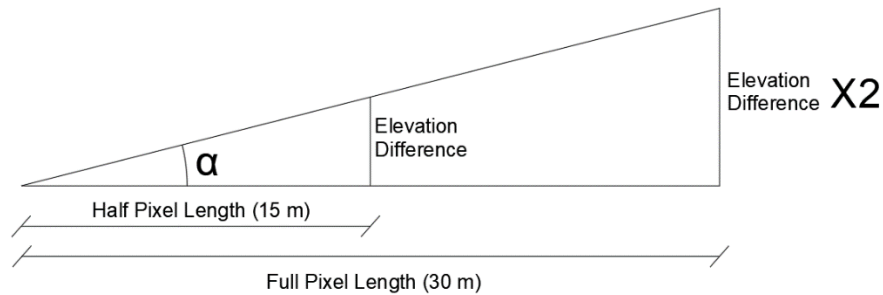


Figure 2.1 Demonstration of Elevation Change Within a Pixel and Half Pixel with respect to Slope

2.2. Overview of the Study

This study focuses on estimation of water levels over Ermenek and Altinkaya dams using Landsat 8 images between May 2013 and May 2019. In order to estimate the water level of these dams for each Landsat 8 image date, first the Landsat image and the DEM maps are post-processed (Section 2.6) so that they could all be input to the Nelder-Mead Simplex (NMS) optimization methodology (Section 2.7). Initially,

the Landsat and the DEM datasets are cropped to a region (Section 2.6.2.1) that contains the dams to reduce the computational time and to improve the accuracy of the cloud filter applied later. Then proximity mask is calculated to prevent water bodies that are around the dam but not part of the dam reservoir to impact the results (Section 2.6.2.2). Similarly, cloud mask (Section 2.6.2.3), snow and shadow mask (Section 2.6.2.4), and water detection indices (Section 2.6.1) are calculated.

All of these masks and indices (before threshold application) are static and are not impacted from the implemented NMS methodology that uses these masks and indices as input. Here, this optimization uses several different thresholds (water area extent detection threshold, water level detection threshold, and statistical outlier detection threshold) as parameters to minimize the errors of the water elevation. NMS at the same time also estimates the water area extent as an intermediate product, which is used as input to water-land border detection within the NMS methodology.

The water level detection methodology introduced in this study relies on estimation of water-land border first using NMS methodology, then retrieval of DEM values at the water-land border pixels again using NMS methodology, and then utilizing several different methods (ECDF, GEV, mean, median, and mode) to obtain the water level estimate. Here, the method ECDF also relies on NMS for the estimation of water level elevation detection threshold. In other words, other four statistical methods (GEV, mean, median, and mode; explained in Section 2.8) obtain the water level estimates using the histograms of the DEM values of the pixels at the water-land border estimated via NMS methodology. Here GEV, mean, median and mode statistics-based methodologies require water-land discrimination before they can be implemented to obtain water level estimates. There could be other methods independent from NMS to obtain water-land border (e.g., directly using the Landsat-based index results to acquire water-land delineation); however such methodologies might introduce high errors as the index values over different dates might have very different values. Accordingly, in this study NMS methodology based water-land

discrimination results are used in GEV, mean, median, and mode statistics-based water level estimations.

Sensitivity of the water level results to the utilized indices, DEM images, and the selection of training dataset is investigated. Above methodologies are repeated for different scenarios using four indices (AWEI, NDWI, WI2015, and NDPI), two DEM images (ASTER and SRTM), two training datasets (i.e., local and remote), and five statistical approaches to retrieve water level from water extent (i.e., ECDF, GEV, mean, median, mode), and two dams. Accordingly, in this study $4*2*2*5*2=160$ scenarios are investigated.

2.3. Flow of The Model

Main flow of the model is explained with 3 flow charts (Figure 2.2, Figure 2.3 and Figure 2.4). The predictive model in this research includes Landsat and DEM (from ASTER and SRTM) raster images as input. Both Landsat and DEM images have been obtained by Earth Explorer web portal of USGS. Downloading of the DEM images was performed manually but the Landsat images were downloaded via Bulk Download Application (BDA) software of the United States Geological Survey (USGS).

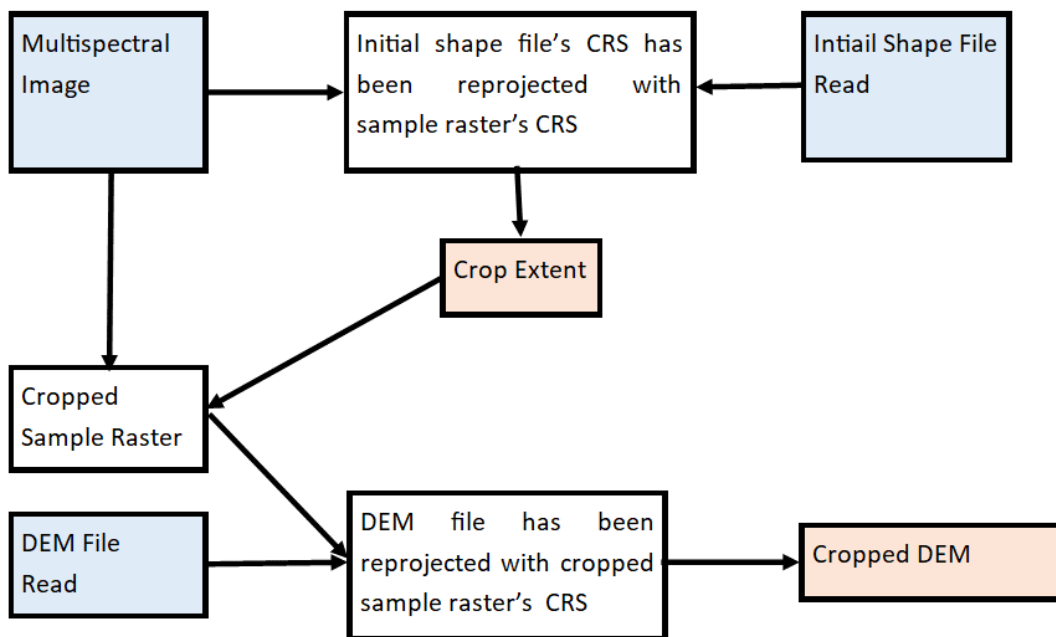


Figure 2.2 Flow Chart of the Model up to the Calculation of Cropped DEM

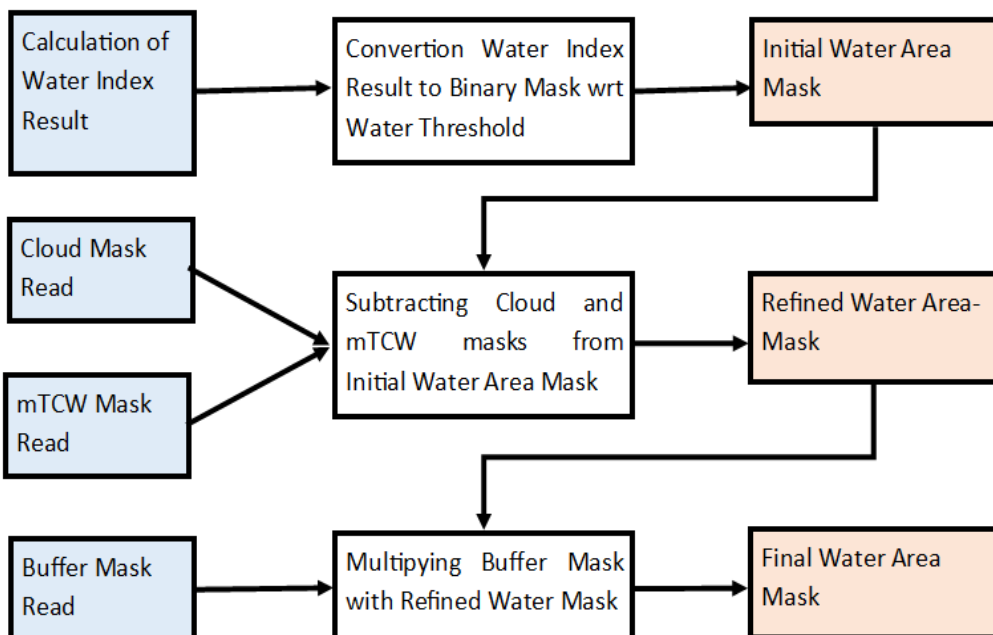


Figure 2.3 Flow Chart of the Model up to the Calculation of Final Water Area Mask

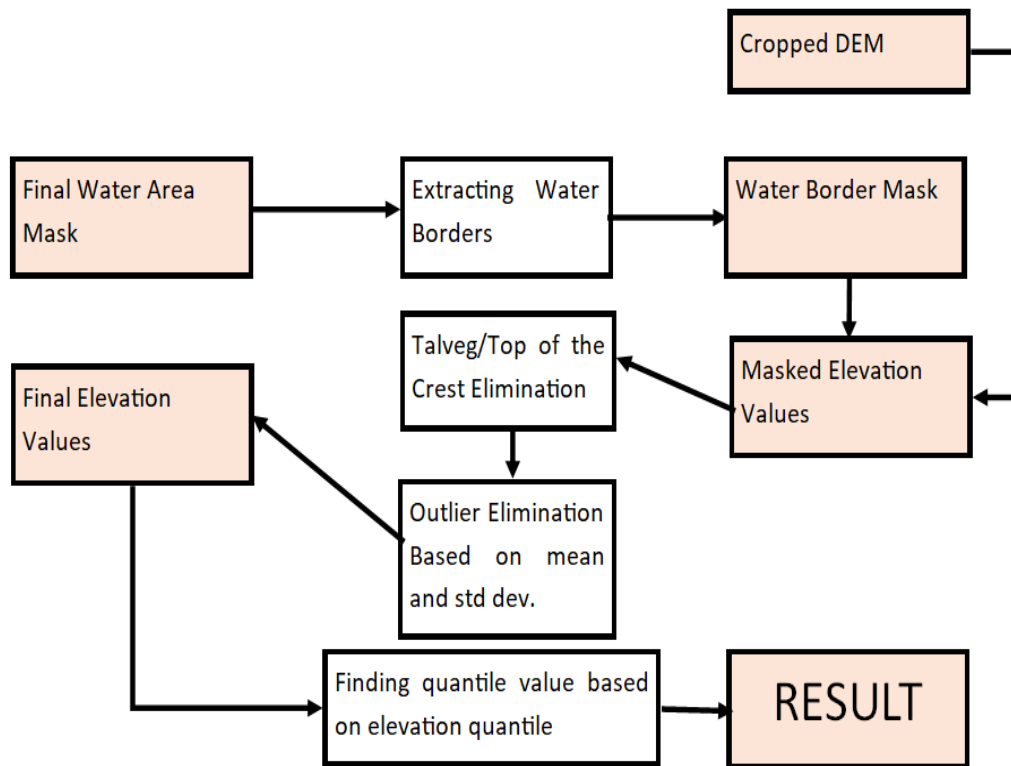


Figure 2.4 Flow Chart of the Model about Water Elevation Detection

Each Landsat-8 image contains approximately 1.70 Gigabytes (GB) of unzipped data including 11 band (1 of them is panchromatic), 1 quality assessment raster, 1 angle coefficient file (ANG) and 1 Landsat Metadata File (MTL) file containing the Sun Elevation Angle, Top Of Atmosphere (TOA) reflectance and radiance coefficients, K1 and K2 values that are used throughout the calculations.

DEM raster images contain 30-40 Mb of data and ASTER Global Digital Elevation Map (GDEM) contains a quality assessment raster in addition to the elevation raster. Downloaded DEM file projections are based on Geographic Coordinate Reference System (CRS) and in order to be able to incorporate them with Landsat images, they have been reprojected on Universal Transverse Mercator (UTM) based CRS. This reprojection was performed with QGIS.

Landsat images contain more than 60 million pixels over an area larger than 34.000 km^2 . To reduce the computational time, Landsat images are first cropped to

smaller subsets containing the dam that is being investigated. Borders of this subset area was defined visually using Google Earth Pro by ensuring no other major water body will lay within this subset area.

In addition to the subset images, buffer masks are further used to further reduce the errors by eliminating the possibility of misclassification of remote locations as water. Here buffer masks are created using DEM images that pixels having higher elevation than the dam's highest elevation (i.e., theoretical maximum lake area extent) are labeled as 0 while pixels having elevation lower than the dam's highest elevation are labeled as 1. Later such buffer masks are multiplied by the water area extent estimations so that water area extent is limited with the theoretical maximum lake area.

Cloud and mTCW masks have been generated for each date of the Landsat images and stored in the computer in raster form. Initial shape file was read and band raster images were cropped with respect to the initial shape file before calculation of these masks. These masks are independent from the parameter optimization steps and hence calculating them before running the main function shortens computational time. Cloud and mTCW mask values are stored as raster images containing values either 1 or 0.

Results of water detection indices (NDWI, NDPI, AWEI and WI2015) were calculated and stored in the computer. Initial shape file was read and band rasters were cropped with respect to the initial shape file before calculation of these results. Results of the indices were not converted into a binary mask at this step since that conversion requires a threshold value that defines what is water and what is not, and that threshold is one of the parameters that have been optimized. Hence, the stored images of this step include complete range of results in terms of pixel values.

Assigning binary values to the pixels based on a threshold takes shorter time than recalculating the index results and applying the threshold. That is the reason of

this calculation and saving in the computer. After completing these steps, the main function is run in order to calculate the results.

Main function takes path of water index, DEM file, initial shape file, cloud masks, mTCW results, proximity buffer mask raster in addition to the values of water detection threshold, which (smaller or bigger) part of the histogram to label as water with respect to threshold, elevation detection threshold, outlier elimination threshold, talveg elevation and top of the crest elevation as parameters.

Water detection threshold value is an either integer or decimal value, depending on the water area detection index. Initial assessment of this threshold is defined by inspecting the histogram of the water index result raster. After the initial assessment, the value is optimized in order to minimize the RMSE value.

Decision of labeling which part of the image as water has been made based on a threshold (whose initial value was provided by inspection of histogram and then final value is obtained by optimization) parameter, where 1 means that any value smaller than or equal to the water detection threshold is water and 0 means that any value greater than or equal to the water detection threshold is water.

Elevation detection threshold is a floating-point numeric value that is between 0.0 and 1.0. This value defines the quantile percent that is returned as the final water elevation.

Outlier elimination threshold is used to eliminate the extreme values that may be caused by either the error related to the DEM or complications due to Landsat's spatial resolution. Values to be eliminated are selected with Eqn-(1, where μ is the mean and σ is the standard deviation of the values.

$$\varepsilon = \mu \pm \beta * \sigma \quad (1)$$

where ε is the limit for values to eliminate, β is the outlier elimination threshold. Here values $\beta * \sigma$ away from the mean are considered as outliers, where β is selected as 1.75 in this study.

Talveg (of the downstream) and top of the crest elevations are used as the physical limits of the water level elevations and as thresholds to filter unrealistically low or high elevations.

Main function initially reads sample raster and initial shape file. These datasets are later utilized to transform shape file's CRS into UTM. Then, DEM file is read, and this file's CRS has also been converted into UTM. Afterwards, DEM file and the crop extent (CRS-corrected-shapefile) have been incorporated to have a raster named "Cropped DEM".

After producing the cropped DEM raster, the algorithm proceeds to read water area detection index results. Type of the water area detection method was provided by the user before the run of the main function by providing the related folder. After the reading process, algorithm proceeds to transform the results into a binary mask with respect to the provided water threshold and the value of the parameter that defines the relation of water labeling and threshold in terms of being smaller or greater than the threshold. The result of this step is named as initial water mask.

After generating the initial water mask, algorithm proceeds and reads the related cloud and mTCW masks. Both cloud and mTCW masks had been saved as a binary mask and hence this step deducts these masks from the initial water mask. The negative valued pixels are the ones that do not have right to be classified as water and their values are set to 0 in order not to have underestimation problems in the upcoming steps due to their negativity. The result of this step is named as refined water area mask.

Proximity buffer mask of binary values are read after the generation of the refined water area mask. Buffer mask defines the area of interest in a narrower manner than the initial shape file. Pixels in the buffer zone have their values assigned as 1 and the others have their values assigned as 0. After reading the mask file, buffer mask is multiplied with refined water area mask. This multiplication eliminates the false positive values in addition to the statistical interference of other genuine water areas that are located further than the buffer distance. Result of this step is named as final water area mask.

Water area mask is a binary mask which have all of the pixels located in the water body valued as 1 and the others valued as 0. Dams and other artificial water bodies that start their water retention after the construction date of the DEMs may be analyzed after this mask by multiplying this mask with cropped DEM but this solution cannot be applied for natural or artificial water bodies that have water before the construction date of the DEM. Hence, extracting the border line between the land and water pixels is a more general approach. This border extraction is done by using R-Programming Language. After the border extraction, only the border pixels have their values assigned as 1 and the others' values are assigned as 0. Result of this step is named as water border mask.

After water border mask generation, this mask is multiplied with cropped DEM values in order to have masked elevation values. Since water border mask is a binary mask and the cropped DEM contains the elevation values, multiplication of these two provides a result that have elevation values for the water borders and zeros for everywhere else.

It is not physically possible to have water elevation below the talveg elevation or above the top of the crest elevation. Hence, values that is out of these boundaries are eliminated.

Even after the elimination of extreme values, the masked elevation values have outlier values due to either Landsat's spatial resolution, standard errors of DEM

products, or thin clouds that are not eliminated in the Landsat image. Hence a second filter is applied based on statistical analysis of the resultant histogram and based on the provided outlier elimination threshold. Result of this process is called as final elevation values. Finally, the value belongs to the provided quantile value is returned among the final elevation values by the algorithm as the final result.

2.4. Study Area

Even though above given methodology can be implemented over any location, in this study it is implemented over Ermenek and Altinkaya dams as proof of concept.

2.4.1. Ermenek Dam

Ermenek Dam (Figure 2.5) has 58.74 km^2 of reservoir area and is located in a basin with an area of 2304 km^2 . The maximum depth of dam reservoir is 204.0 m and the mean depth of the reservoir is 78.0 m . Total reservoir capacity is $4,582 \text{ hm}^3$. Crest height of dam is 210 m from the talveg level and 218 m from the foundation level. Top of the crest elevation of the dam is 700.0 m (Çevlik, 2013).

Climate of the area changes from Mediterranean to continental as elevation increases. Dominant wind direction is South East (SE) and maximum wind speed has been measured as 18.9 m/s as of 2013. The coldest month is January with average temperature of 3.3°C and the hottest month is July with average temperature of 22.7°C . Mean temperature is 8.1°C for winter and 17.2°C for summer. Mean rainfall is $600 \text{ millimeters (mm)}$ per year where the December – February period's rainfall amount is twice of the other months (Çevlik, 2013).

Main water resource for dam is the Ermenek River, whose most recent mean flow amount has been calculated as $1,289.6 \text{ hm}^3 / \text{year}$. In addition to the Ermenek River, other rivers also carry considerable amount of water to the reservoir: Gevne River, Göktepe River, Nadire Spring, Küçüksu River, Zeyve Spring and Zeyve River. Among those sources, Nadire Spring have been covered completely by the dam reservoir (Çevlik, 2013).

Water replenishment time, average amount of time that requires an incoming water stream to leave the reservoir lake, was calculated as 3.55 years and this value is higher when compared to Hirfanli Dam's 2.60 years and Kesikköprü Dam's 0.05 years. Increased water replenishment time results in increased algae levels and hence eutrophication that causes inaccuracies among the results of water detection indices that takes green band into account (Çevlik, 2013).

Dam lake is located in the mild temperate climate zone; hence, water turbidity is increased due to melting of ice that was covering the lake area or circulation due to temperature differences. This turbidity may affect temperature-based calculations in a negative way.

DEM images are cropped to an initial area of interest (section 2.6.2.1). Average slope near the Ermenek Dam is calculated as 14.99 degrees using the ASTER DEM and 14.54 degrees using the SRTM DEM. Following Eqn-2, a Landsat pixel with 30 m of spatial resolution may contain an elevation difference of ~7.8 m within the respect. These values also mean that even half pixel may contain ~3.90 m of elevation difference (Figure 2.1). This elevation difference implies on average 1.95m error may just stem from the coarse spatial resolution of Landsat image for mixed pixels that contain both water and land areas. Moreover, it can be observed that the slope value increases especially through the South Western (SW) part, where the dam is located (Figure 2.6 and Figure 2.7).

$$MeanED = SpaRes * \sin (meanSlope) \quad (2)$$

where MeanED denotes average elevation difference per pixel, SpaRes resembles the spatial resolution of the platform and meanSlope resembles the average slope calculated by using the DEM raster.

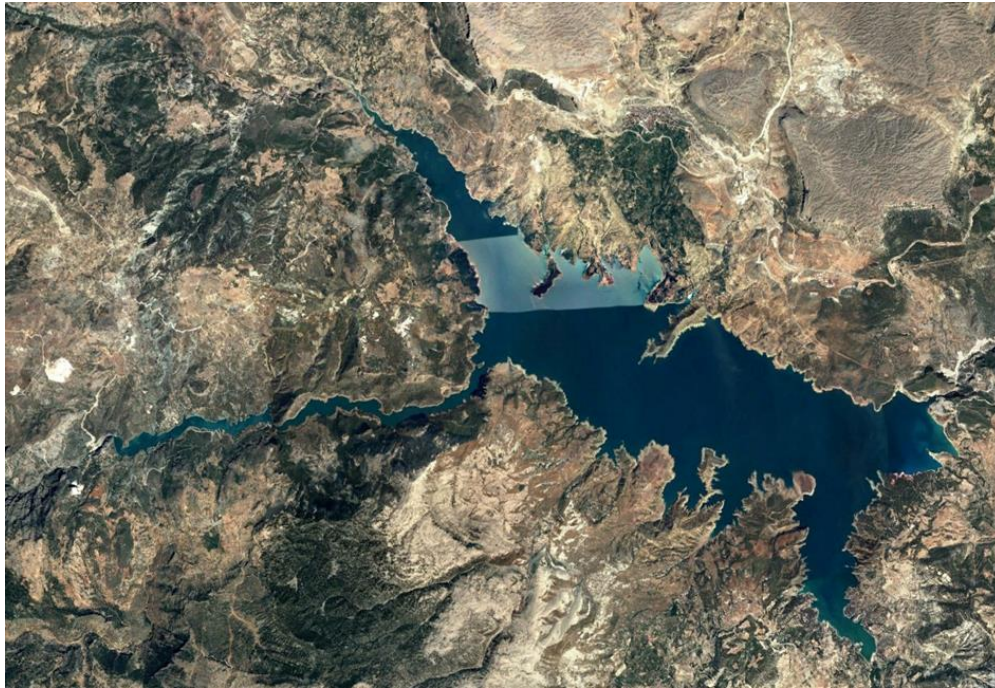


Figure 2.5 Satellite View of the Ermenek Dam and its Reservoir (Google, n.d.-b)

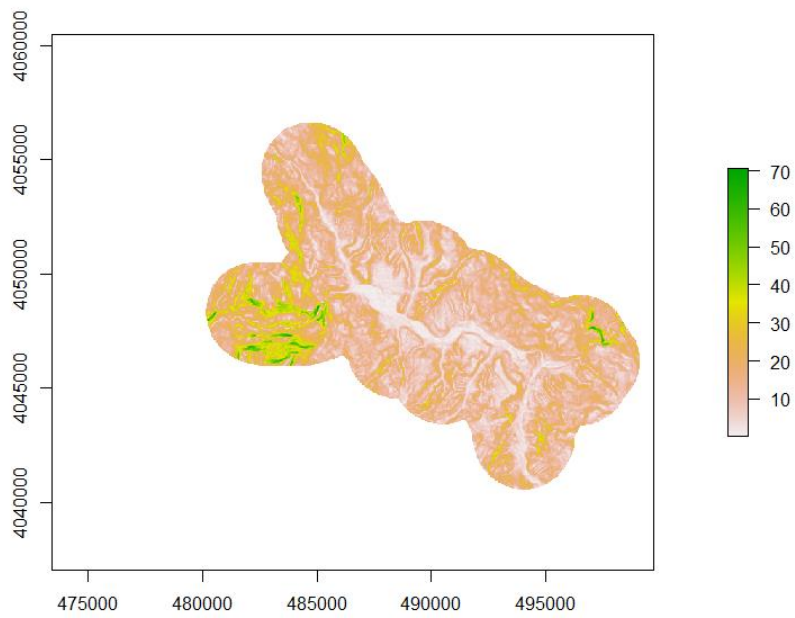


Figure 2.6 Slope Map (in Degrees) of Ermenek Dam Buffer Area Based on SRTM DEM
(Axes represent UTM coordinates)

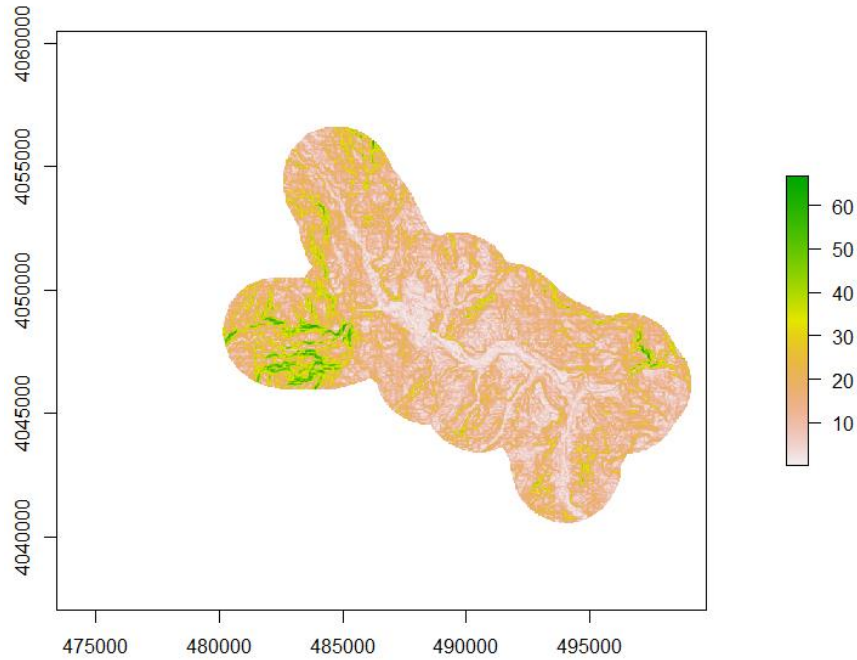


Figure 2.7 Slope Map (in Degrees) of Ermenek Dam Buffer Area Based on ASTER DEM

(Axes represent UTM coordinates)

2.4.2. Altinkaya Dam

Altinkaya Dam (Figure 2.8) is located 35 km SW of the Bafra province of Samsun. The dam is constructed in 1988 on Kızılırmak River, which is the longest river in Turkey and has annual flow values as high as $6.0 \text{ km}^3/\text{year}$. Drainage area of the dam, the basin, is $74,515 \text{ km}^2$ and mean yearly flow value is $5.8 \text{ km}^3/\text{year}$ as of 2011. Reservoir capacity of dam is 5.8 km^3 , whereas the active volume is half of that value. Lake area for the highest water level that the dam has been designed for is 118.0 km^2 . Crest height of the dam is 140.0 m from talveg elevation where talveg elevation is 55.0 m. Altinkaya Dam is the 4th biggest dam of Turkey (Öztan, 2011).

According to the Turkish State Meteorological Service (MGM) statistics, average temperature of the Samsun province is 14.5°C and the coldest month is February with a mean temperature of 3.9°C while the hottest month is August with a

mean temperature of 19.6 °C. Mean rainfall is 717.1 mm/month and 165.5 mm of that rainfall has being observed in months November and December (MGM, 2010).

Average slope determination and slope mapping processes were carried out for Altinkaya Dam by using the same methodology explained in Ermenek Dam (Section 2.4.1). According to those calculations, average slope near of the Altinkaya Dam is 14.44 degrees for ASTER DEM and 14.38 degrees for SRTM DEM. Considering the Eqn-2 these values means that a Landsat pixel with 30 m of spatial resolution (Department of the Interior U.S. Geological Survey, 2019) may contain an elevation difference ~7.5m. This value implies an error of ~1.9 m might be added just because of the local slope and the spatial resolution Landsat images for the water-land mixed pixels (See Figure 2.1). The slopes particularly increases along the sides of the water body area (Figure 2.9 and Figure 2.10), where the added errors independent from the methodology but due to input dataset and the study region might be even higher than average 1.9 m.

Also note that the slope maps of Altinkaya Dam Buffer have zero valued pixels over the dam reservoir area because of the water existence preceding the construction of DEM images. In order to cope with this problem, an older topographic elevation map have been incorporated with DEM raster images so that inner regions of the dam reservoir have available DEM values. This new modified DEM image still has missing values, however, the dam reservoir water level never drops to the levels that DEM data will be missing.



Figure 2.8 Satellite View of the Altinkaya Dam and its Reservoir (Google, n.d.-a)

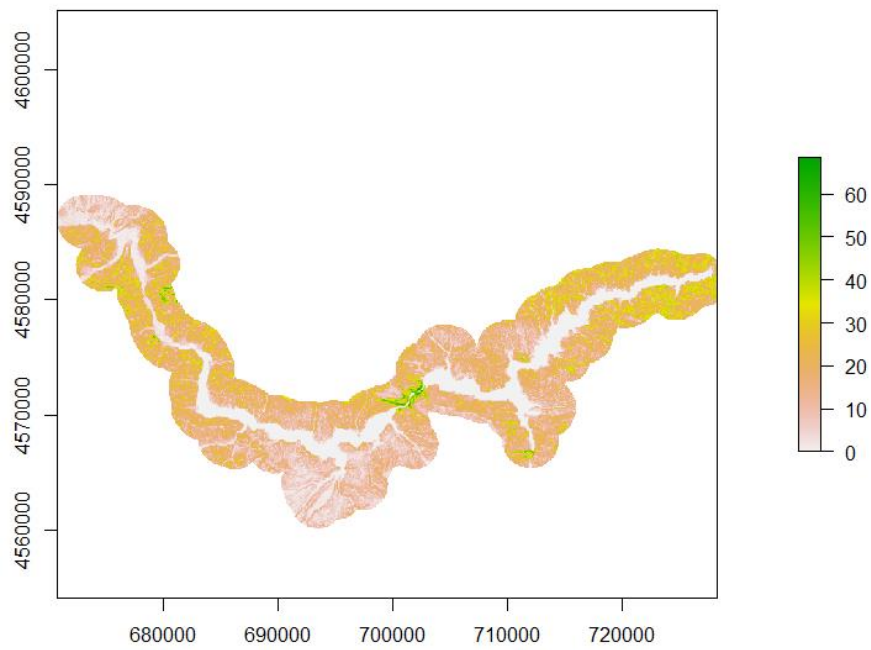


Figure 2.9 Slope Map (in Degrees) of Altinkaya Dam Buffer Area Based on SRTM DEM
(Axes represent UTM coordinates)

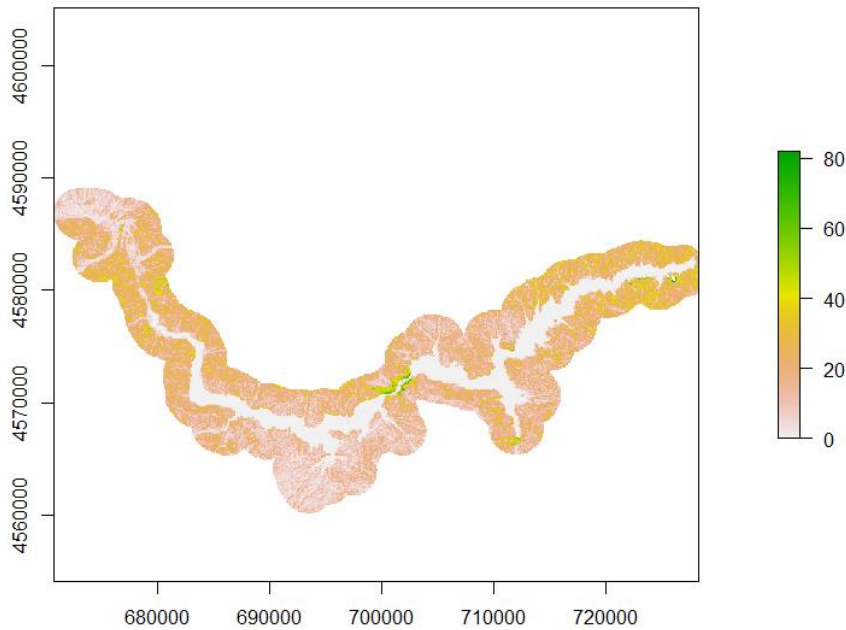


Figure 2.10 Slope Map (in Degrees) of Altinkaya Dam Buffer Area Based on ASTER DEM
(Axes represent UTM coordinates)

2.5. Utilized Input Data

2.5.1. Ground Data

Ground data availability plays an important role during the determination of study area because of the need of independent data for both training and testing phases of the models in this study.

Monthly reservoir water level data continuously measured by DSI over the two dams have been obtained for validation purposes. Data obtained from DSI reflects the water levels at the beginning of each month between May 2013 and May 2019. Data unit is meters. Accordingly, these datasets are interpolated to retrieve the water levels for the same days that 16-daily Landsat datasets are available.

2.5.2. Digital Elevation Data

DEMs are topographic models that provides the elevation value of an area in numerical form. DEMs can be produced via stereo or SAR imaging. In this study, the required DEM data obtained from ASTER and SRTM platforms were used. Here the CRS of these two DEM images is consistent with the CRS of Landsat images, hence one to one comparison, or direct calculations, are possible.

2.5.2.1. ASTER GDEM

ASTER GDEM (Figure 2.11 and Figure 2.12) is based on stereo images taken by satellite platform that had been developed and are being operated by The National Aeronautics and Space Administration (NASA) and The Ministry of Economy, Trade and Industry of Japan, METI (METI, NASA, & ERSDAC, 2011). Its second version (GDEM2) was used in this study. GDEM2 was released in October 2011. It was an improved version of the GDEM1, first iteration, that had been released in June 2009 (METI et al., 2011). Dataset has a spatial resolution of 30 m and each raster file published by the operating bodies cover and area of one degree by one degree in terms of spatial coverage (METI et al., 2011).

RMSE value for ASTER raster images can go as high as 15.1 m for mountainous areas (Tachikawa, Kaku, & Iwasaki, 2011) and this errors have a potential to affect the estimations in a way that they cause higher water level estimation error. Hence the effect of these errors should be decreased by utilizing higher resolution and/or lower error DEM datasets.

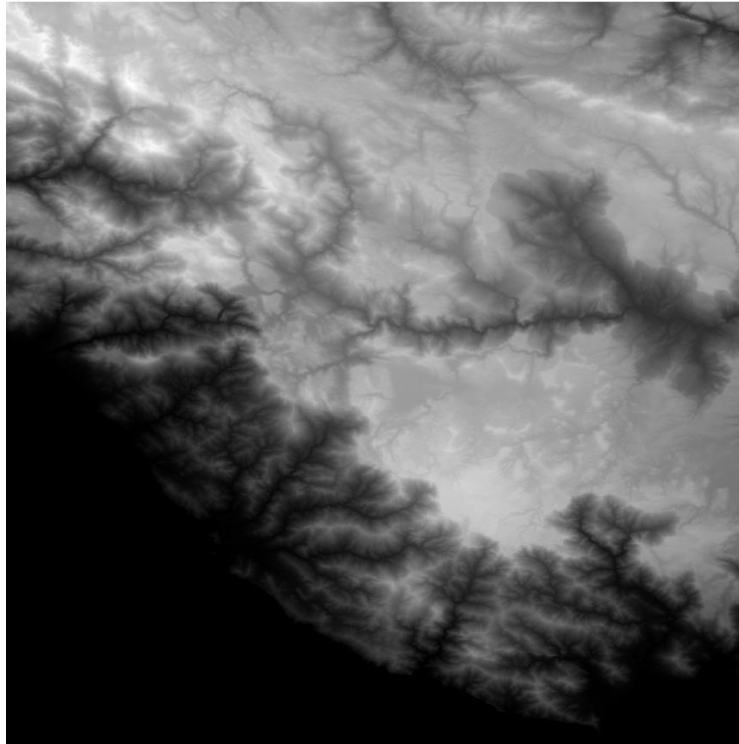


Figure 2.11 ASTER DEM over Ermenek Dam

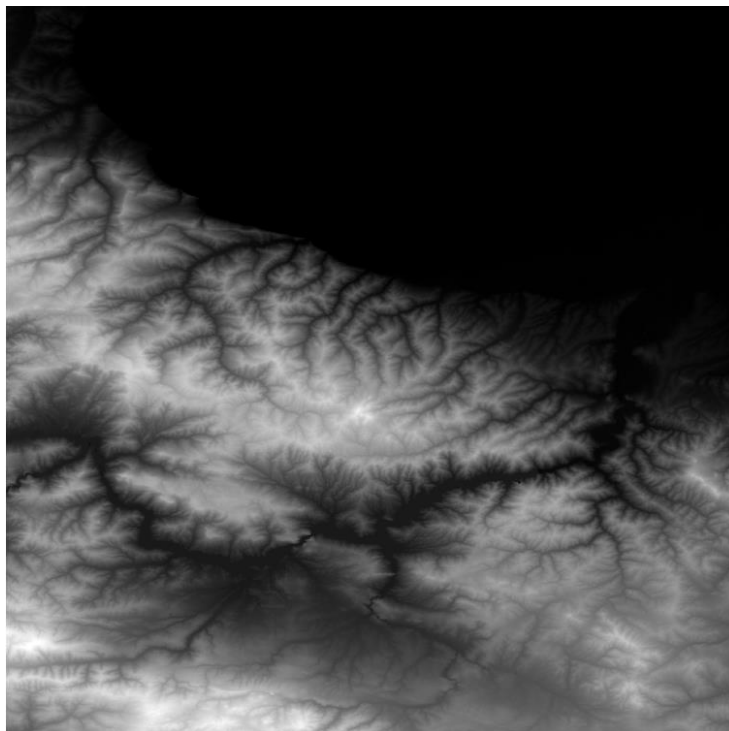


Figure 2.12 ASTER DEM over Altinkaya Dam

2.5.2.2. SRTM GDEM

SRTM GDEM (Figure 2.13 and Figure 2.14) is a DEM that has been constructed based on the images taken by the Shuttle Radar Topography Mission in 2000 (Jain, Thaker, Chaurasia, Patel, & Singh, 2018). Its DEM with highest resolution, 30 m spatial resolution, was released in 2003 (Elkhrachy, 2018).

Dataset has a spatial resolution of 30 m and each raster file published by the operating bodies cover an area of one degree by one degree in terms of spatial coverage (NASA, n.d.). However, SRTM is known to include void pixels over mountainous areas with steep slopes (Berthier, Arnaud, Vincent, & Rémy, 2006; Kolecka & Kozak, 2014).

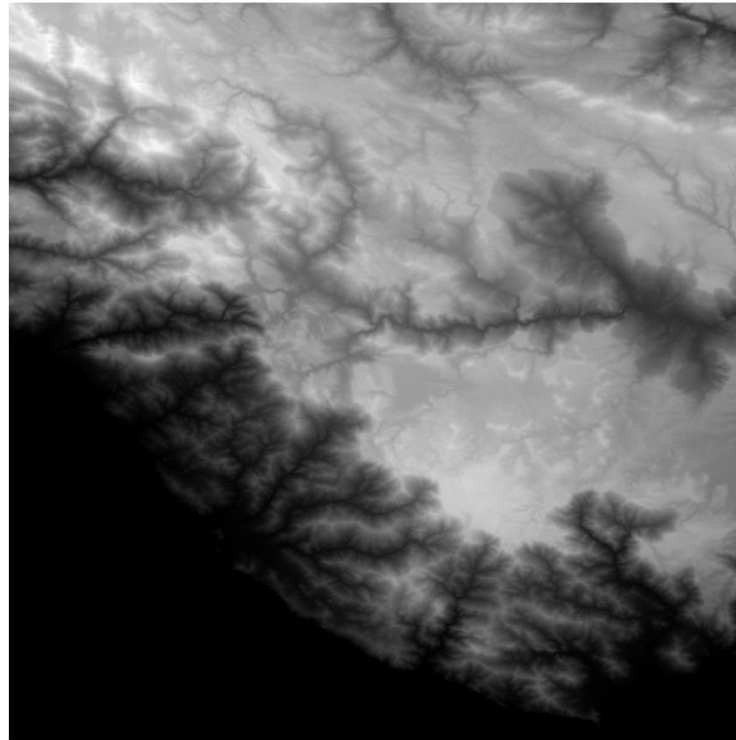


Figure 2.13 SRTM DEM over Ermenek Dam

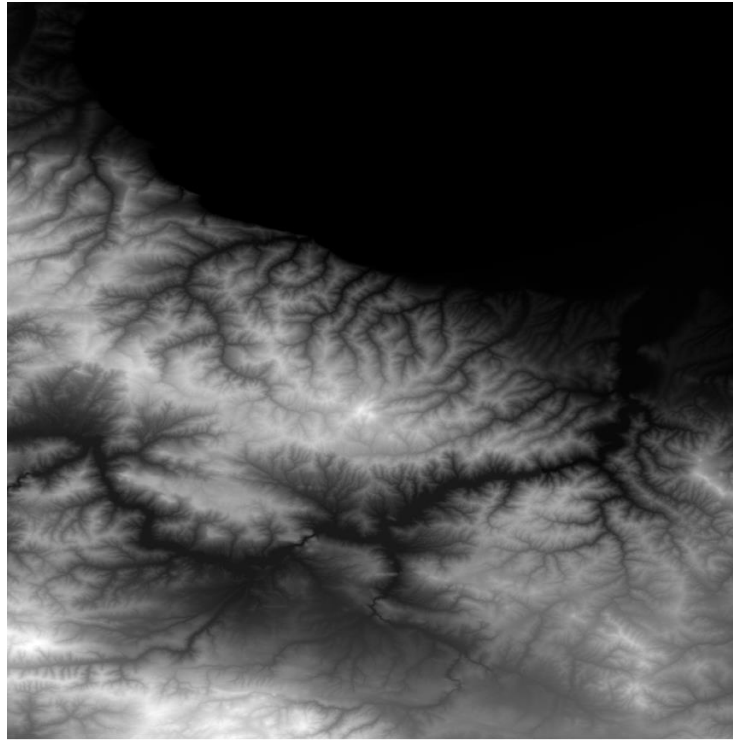


Figure 2.14 SRTM DEM over Altunkaya Dam

2.5.3. Landsat Images

2.5.3.1. Selection of Landsat-8 Images

In order to detect the clouds, improved F-Mask algorithm (Frantz, Haß, Uhl, & Hill, 2018) was utilized in this study. This algorithm utilizes the Band-9 (Cirrus Band) of Landsat-8 that covers the spectral interval of 1.36 - 1.38 μm (Department of the Interior, U.S. Geological Survey, 2019). This band has not been included in previous Landsat satellites (NASA, 2011) and only available in the Landsat-8 images that are used for this research. Having 6 years of data since its launch, the length of available Landsat-8 data limits the duration of this study as Scan Line Corrector (SLC) malfunction problem of Landsat-7 (USGS, 2003) limits its use in this study. While Landsat-6 failed to reach its desired orbit (Viets, 1995), Landsat-5 provides a long archive (its datasets are available between 1984 and 2013; Usgs.gov, 2013); yet, in this study Landsat 5 datasets are not used along with Landsat 8 images as some bands used in this study are only available in Landsat 8 but not in Landsat 5. New Landsat

mission, Landsat-9, is planned to be launched in December 2020 and to include exactly the same bands and spectral intervals as Landsat-8 (U.S. Geological Survey, 2019). Availability of Landsat 8 and 9 images simultaneously would reduce the revisit time of Landsat over any part of the globe.

In this study Landsat 8 Level-1 data is utilized instead of higher level datasets. Level-1 images have been corrected both geometrically and radiometrically in order to get rid of distortions of Level-0 images caused due to sensors, deviations in attitude, shape of Earth (Department of the Interior U.S. Geological Survey, 2019).

2.5.3.2. Selection of Digital Numbers Instead of Surface Reflectance

The decision based on using DN directly versus utilizing surface reflectance (SR) first were made on the fact that although the analyses based on SR calculations seem to yield a more informative initial results, the proposed methods for Brightness Temperature (BT), TOA radiance and reflectance calculation formulas provided in data manual of Landsat-8 utilizes DNs (Department of the Interior U.S. Geological Survey, 2019). In addition to the SR calculation's addition of another artificial layer, utilization of DN instead of calculating SR is commonly applied in literature (Danaher & Collett, 2006).

To see the difference between SR- and DN-based indices, NDWI water index is calculated using both level datasets for Landsat-8 image LC08_L1TP_177035_20180418_20180501_01_T1 (below Figure 2.11 and Figure 2.12). SR-based NDWI images have some artificial strips while DN-based image does not. Accordingly, DN-based level 1 datasets are used in this study rather than SR-based higher level datasets.

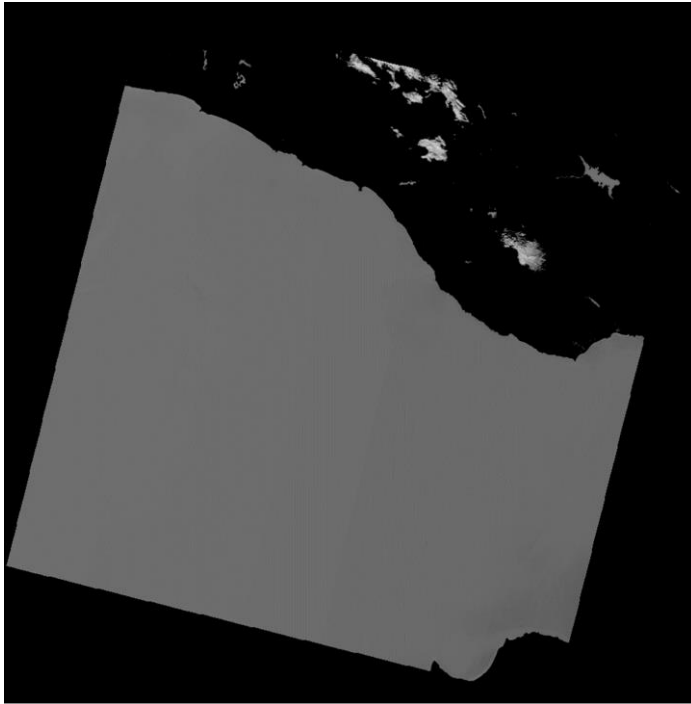


Figure 2.15 NDWI-XU Result (SWIR = B6) based on DN of Landsat 8 (LS8) Image
LC08_L1TP_177035_20180418_20180501_01_T1

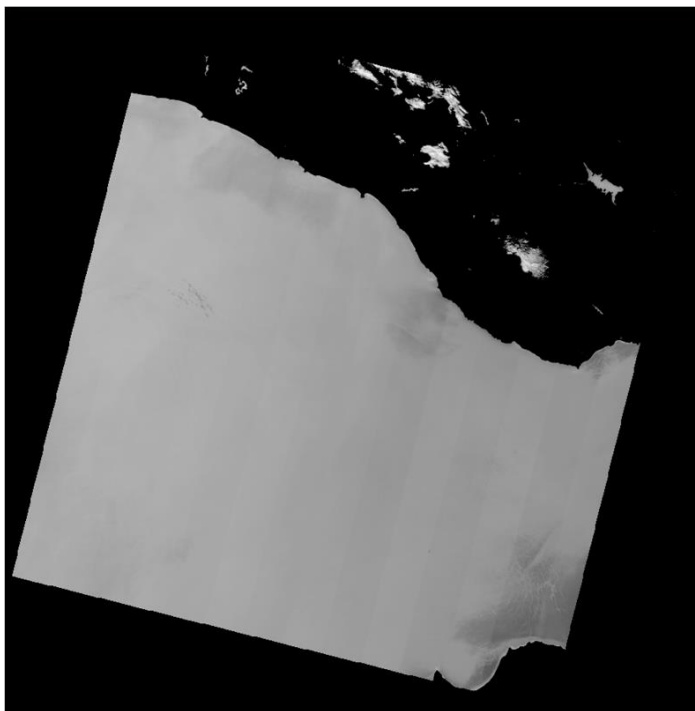


Figure 2.16 NDWI-XU Result (SWIR = B6) based on SR of LS8 Image
LC08_L1TP_177035_20180418_20180501_01_T1

2.5.3.3. TOA Reflectance, Radiance and Brightness Temperature Calculations

TOA reflectance calculation before acquisition of indices is performed with Eqn-3 proposed by the Data Manual of Landsat 8 (Department of the Interior U.S. Geological Survey, 2019). The selected application method included correction for solar angle and in order to apply correction for solar angle, reflectance coefficients were required. Those required reflectance coefficients were obtained from the MTL files related with the raster of interest and had been provided by the USGS.

$$\rho_{\lambda} = \frac{M_p * Q_{cal} * A_{\rho}}{\sin(\theta_{SE})} \quad (3)$$

where ρ_{λ} symbolizes TOA Spectral Reflectance with solar angle correction, M_p represents reflective multiplicative band scaling factor, Q_{cal} represents dynamic number regarding to the pixel of interest that belongs to a Level-1 data, A_{ρ} symbolizes reflectance additive band scaling factor and θ_{SE} represents Sun elevation angle. M_p , A_{ρ} and θ_{SE} values have been obtained from MTL files of the Landsat images, whereas the Q_{cal} values are obtained directly from the tif files regarding to the respective bands.

TOA radiance calculation of the DN values of the Landsat raster carried out using Eqn-4 proposed by the Data Manual of Landsat 8 (Department of the Interior U.S. Geological Survey, 2019) and the required radiance coefficients was obtained from the MTL files related with the raster of interest.

$$L_{\lambda} = M_L * Q_{cal} * A_L \quad (4)$$

where L_{λ} symbolizes TOA Spectral Radiance in terms of $W/(m^2 * sr * \mu m)$, M_L denotes radiance multiplicative band scaling factor, Q_{cal} denotes dynamic number regarding to the pixel of interest that belongs to a Level-1 data, A_L symbolizes radiance additive band scaling factor. M_L and A_L values have been obtained from MTL files of

the Landsat images, whereas the Q_{cal} values are obtained directly from the tif files regarding to the respective bands.

For BT calculations, the Eqn-5 provided by the Data Manual of Landsat 8 (Department of the Interior U.S. Geological Survey, 2019) has been used. Since this formula requires calculation of surface radiance a priori, surface radiance calculations were performed, and the obtained results have been used in the equation.

$$T = \frac{K_2}{\ln\left(\frac{K_1}{L_\lambda} + 1\right)} \quad (5)$$

where T denotes TOA BT in terms of Kelvin, L_λ symbolizes TOA Spectral Radiance in terms of $W/(m^2 * sr * \mu m)$, K_1 and K_2 represent thermal conversion constants that are band specific values. K_1 and K_2 values have been obtained from MTL files of the Landsat images.

2.6. Post-Processed Data

Landsat 8 images (i.e., different bands) are post processed with different combination to retrieve products that will be primarily used in the water-land detection algorithm as well as mask parts of the images that may not contain useful information and/or add high errors.

2.6.1. Selected Water Area Detection Indices

Different water detection indices have been utilized in this study to see the differences that based on formulation of indices. Selected indices are AWEI, NDPI, NDWI-MCF and WI2015.

2.6.1.1. AWEI

AWEI is a water detection index that requires cloud free observations. AWEI has two variants, AWEI-NS and AWEI-S, where the AWEI-NS (Eqn-6) is a robust method that eliminates the non-water pixels for images without shadow problem and AWEI-S (Eqn-7) is a refined version that considers shadows too (Feyisa et al., 2014). Both AWEI formulations are depended on radiometric resolution and hence their thresholds depend on the platform.

$$AWEI.S = BLUE + 2.5 * GREEN - 1.5 * (NIR + SWIR1) - 0.25 * SWIR2 \quad (6)$$

$$AWEI.NS = 4 * (GREEN - SWIR1) - (0.25 * NIR + 2.75 * SWIR1) \quad (7)$$

In this study AWEI-S variant is utilized to discriminate the water from the land.

2.6.1.2. 8 NDPI

NDPI is a water detection index, developed mainly for pond detection, aims to detect small water bodies correctly (Lacaux et al., 2007). The original formulation of NDPI uses a MIR band covering interval 1.58 – 1.75 μm (Lacaux et al., 2007) that is very similar to Landsat-8 SWIR-1 (Band-6) interval 1.57 – 1.65 μm (Department of the Interior U.S. Geological Survey, 2019). Accordingly, in this study the NDPI calculations were performed using below Eqn-8 using Landsat-8 Band-6 images. As can be seen from the formula, NDPI results can be negative when the DN of the Green Band is greater than the DN of the SWIR band, while it becomes positive when SWIR DN values are greater than SWIR DN values.

$$NDPI = (SWIR - GREEN) / (SWIR + GREEN) \quad (8)$$

2.6.1.3. NDWI

NDWI is a water detection index is based on NIR and Green bands in a way that it divides the difference between Green and NIR to sum of Green and NIR to find a ratio (McFeeters, 1996), while several different variations of NDWI has been

generated since its initial development (B. Gao, 1996; Xu, 2006). On contrast to AWEI, this index resulting interval does not depend on radiometric resolution of the platform. NDWI variation used in this study is the McFeeters' variation and calculations were done by using Eqn-9. As can be seen from the formula, Normalized Difference Water Index – Mcfeeter's Variation (NDWI.MCF) results can be negative (like the NDPI results) when the DN of the NIR Band is greater than the DN of the GREEN band and positive when vice versa.

$$NDWI.MCF = (GREEN - NIR) / (GREEN + NIR) \quad (9)$$

2.6.1.4. WI2015

WI2015 is a water detection index that its estimation is not based on ratio calculation (Fisher et al., 2016). Accordingly, its resulting interval depends on the radiometric resolution. In other words, result interval of WI2015 index will be different for an 8-bit image (DN range of 0-255) and 16-bit image (DN range of 0-65535), similar to AWEI. WI2015 calculations were done by using Eqn-10, provided below.

$$WI2015 = 1.7204 + 171 * GREEN + 3 * RED - 70 * NIR - 45 * SWIR1 - 71 * SWIR2 \quad (10)$$

2.6.2. Applied Buffers and Masks

2.6.2.1. Region of Interest Subset

Two buffer areas (initial subset and proximity mask) are defined and utilized in this study. An initial subset (Figure 2.17 and Figure 2.18) is used to reduce the raw Landsat image with ~35 million pixels (over an area larger than 34.000 km²) to ~1 million pixels (~900 km² area). This subset also reduces the computational time and also prevents the overestimation of F-Mask cloud detection algorithm.



Figure 2.17 Initial Subset Marked (with Red) over the Altunkaya RGB Image



Figure 2.18 Initial Subset Marked (with Red) over the Ermenek RGB Image

2.6.2.2. Proximity Mask

Initial iterations of the research model had shown that even after the initial cropping based on rectangular shape file that has been extracted from Google Earth Pro, there exist cases that the results include overestimation of water areas. Some of the overestimation is based on cloud, shadow and icy areas and those anomalies can be deducted by masks and introduction of additional indices. However, as it can be seen from the results section, research model tends to yield better results for hot seasons and worse ones for wet seasons. Therefore, some of the overestimation is based on soil moisture that cannot be deducted without an extensive and accurate modelling of soil moisture. Moreover, there exists some other natural or artificial water bodies in the proximity of areas of interest. Hence, a buffer zone is introduced to further eliminate the overestimation.

Proximity buffer area (Figure 2.19 and Figure 2.20) modelling is based on shape files of the dam areas. Shape files have been extracted from Google Earth Pro in kml format and transformed into shp files via QGIS. Those extracted points represent the boundary of water body and hence everything within those points are labeled as area of interest. The transformation of projection of shp file to UTM is performed by R-Programming Language's (R) "raster" library. When it comes to the outsider points, a proximity limit of 10 pixels (300 meters since each Landsat pixel is equal to 30 meters) is defined and every point that lays within that proximity limit is added to the area of interest. Distance measurement was done based on Euclidian distance formula and the reference point is defined as the point in area of interest such that it yields the smaller distance for the point that was being inspected.

Every pixel in the area of interest is labeled with a binary (0 or 1) value. Since the final step of this study includes multiplication of final binary image with to DEM image and then introducing a statistical model afterwards, this binary mask prevents overestimations due to false positive water markings in the areas that are far away from the area of interest.

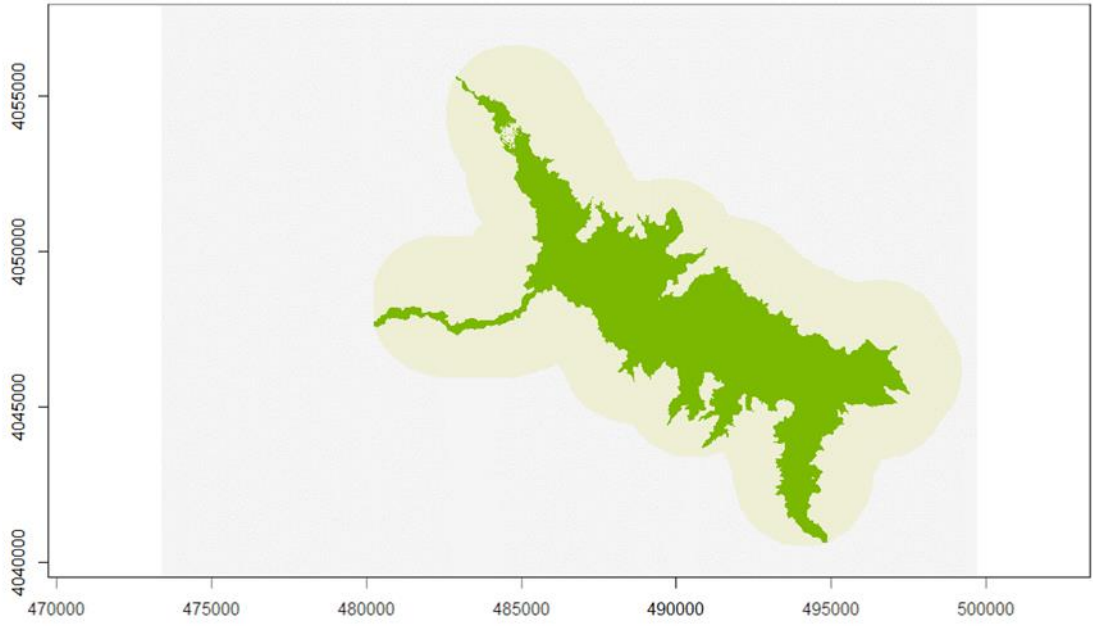


Figure 2.19 Proximity Buffer Area for Ermenek Dam

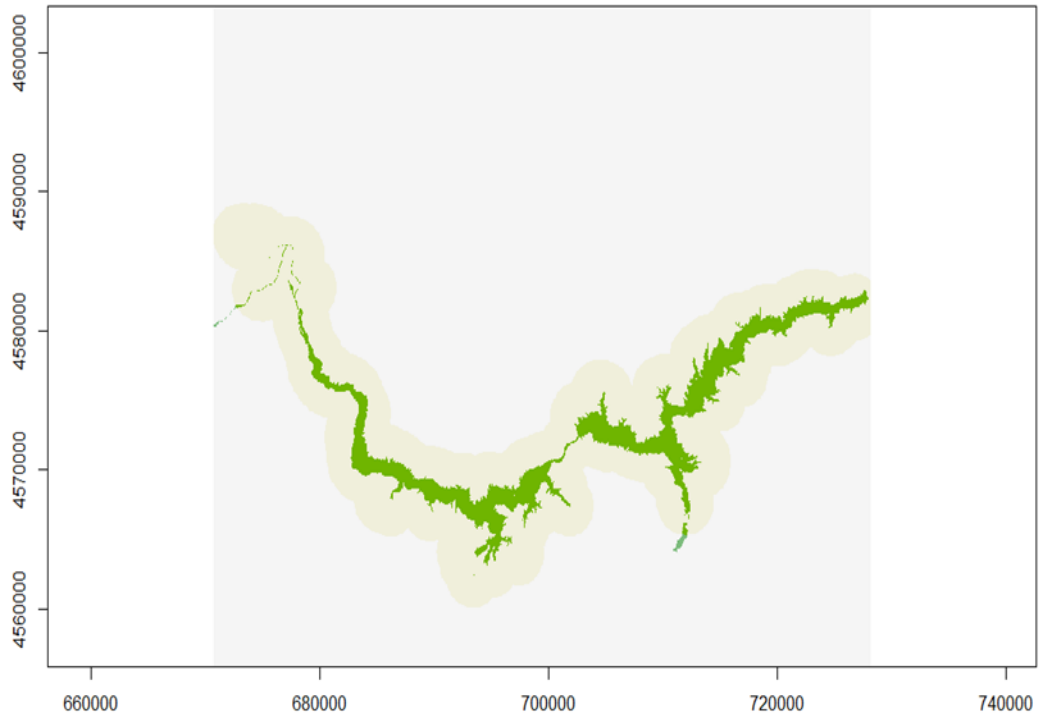


Figure 2.20 Proximity Buffer Area for Altinkaya Dam

2.6.2.3. Cloud Mask

Landsat 8 has been equipped with Band 9, named cirrus band, that covers the 1.36 - 1.38 μm (Department of the Interior U.S. Geological Survey, 2019). Accordingly, to prevent the cirrus clouds interfering the results, either a threshold should be selected and Band 9 mask should be applied (to cover some of the cirrus bands) or a mask should be calculated via different combinations of Band 9 data as well as whiteness, temperature anomalies and other bands datasets. Although the initial F-Mask cloud algorithm had been developed without the Landsat 8 data (Zhu & Woodcock, 2012), the improved iteration of F-Mask takes Band 9 into account to eliminate the computational intensity of the Potential Cloud Pixel (PCP) detection step (Zhu, Wang, & Woodcock, 2015).

A threshold needs to be defined in F-mask algorithm for the detection of the clouds. Although the threshold 0.01 selected in this study as suggested by a similar study (Wilson & Oreopoulos, 2013) is much smaller threshold than the 0.03 value used in a similar masking algorithm for MODIS (Ackerman et al., 2010), there still is a tendency of overestimation of F-Mask algorithm (Zhu et al., 2015). F-Mask algorithm's results seemed to be highly skewed towards overestimation over the Ermenek image that includes almost extensive Mediterranean pixels as well as high mountains. F-Mask uses average whiteness and temperature values and having unrelated pixels, affect the results in a way that increases errors.

In fact, since the effect of temperature difference on the final result can be considered as high, it is observed that the algorithm has a tendency of producing false positives (pixels marked as cloud whereas they are not) within the study area. The reasoning behind this is the effect of sea water's consistent temperature and the decrease in temperature with the increase in elevation. Landsat images of the study areas cover high mountains, valleys within mountains and plateaus between the mountainous area in addition to sea and shore that is included in the Landsat images covering Ermenek Dam's area. Even the border between land and water body of

interest was labeled as cloud for some of the images that had their cloud masks calculated with the F-Mask algorithm. An example for overestimation over the water boundary line has been provided for the Landsat 8 image LC08_L1TP_177035_20160802_20170322_01_T1 that covers Ermenek Dam area (Figure 2.21).

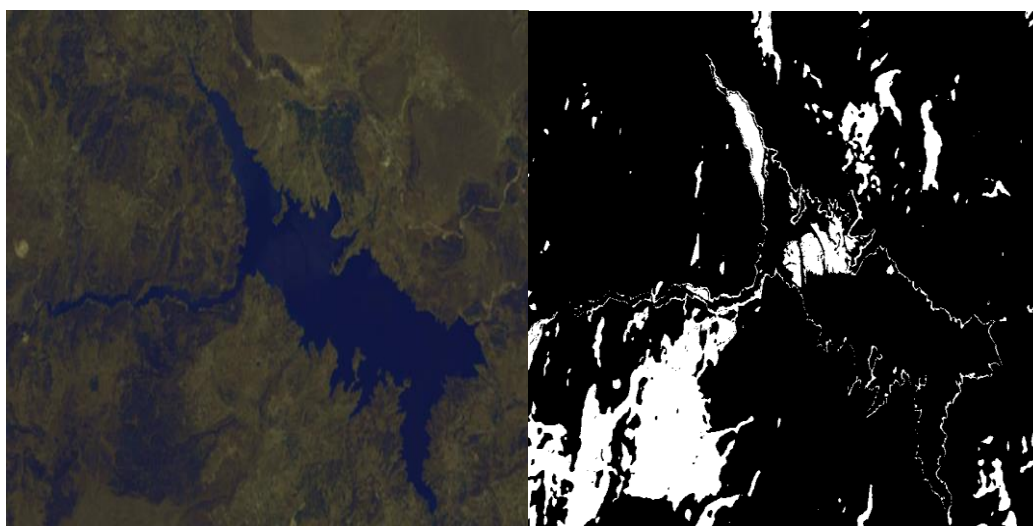


Figure 2.21 RGB Image (Left) and Related Cloud Mask Result (Right) of the LS8 Image LC08_L1TP_177035_20160802_20170322_01_T1

In order to cope with this problem, cropping with region of interest subset (See Section 2.6.2.1) step of the calculations had been performed before the final cloud mask was detected and the results were successful in terms of eliminating the false positives. This change of order has changed mask algorithm's adaptive statistical thresholds of whiteness and BT steps.

The final cloud mask still had overestimation based on bidirectional reflectance distribution function (BRDF) artifacts but since the further steps of methodology of this research calculates the boundary between water and land, the BRDF-based false positive cloud pixels over the water area have not affected the results.

The only change in F-mask algorithm that was made in this study is using a shapefile to cut the area of interest (Section 2.6.2.1) and hence getting rid of the unrelated pixels' effect on the results by skewing the statistical values. If this cutting

were not performed, than the geographically irrelevant pixels would skew the statistical computations of the F-Mask algorithm. All of the remaining calculations explained through this study are were performed based on the existing literature that introduced and improved the algorithm (Zhu et al., 2015; Zhu & Woodcock, 2012).

F-Mask algorithm's first step aims to determine the PCP coverage of the entire raster. Initial algorithm design had included complex calculations for this step (Zhu & Woodcock, 2012) but the refined algorithm relies on the Landsat-8's Band-9 that is called as Cirrus band and covers the 1.36 - 1.38 μm interval of the electromagnetic spectrum (Department of the Interior U.S. Geological Survey, 2019). PCP result is limited to binary values such that, 1 for probable cloud and 0 for not cloud (Figure 2.22 – Left).

After PCP calculation, a water mask is generated with a function that utilizes Band 4 (Red Band) and Band 5 (NIR) bands of Landsat 8. This function calculates Normalized Difference Vegetation Index (NDVI) and returns a binary mask with respect to the outcome of two initial tests that are based on the TOA reflectance Band-4 value and NDVI result. Returned result are in binary form (Figure 2.25 – Right).

Production of water mask enables clear sky water pixel mask generation. The function that is used to generate clear sky water pixel mask uses Band 7 (SWIR-2) band of Landsat 8 and incorporates this analysis into water mask matrix. Returned result is limited to binary values such that, 1 for probable cloud and 0 for not cloud (Figure 2.23).

BT mask is generated with Band-10 (TIR-1) and Band-11 (TIR-2) bands of Landsat-8. Final BT matrix has been returned as the simple average of two masks calculated with two different bands (Figure 2.24).

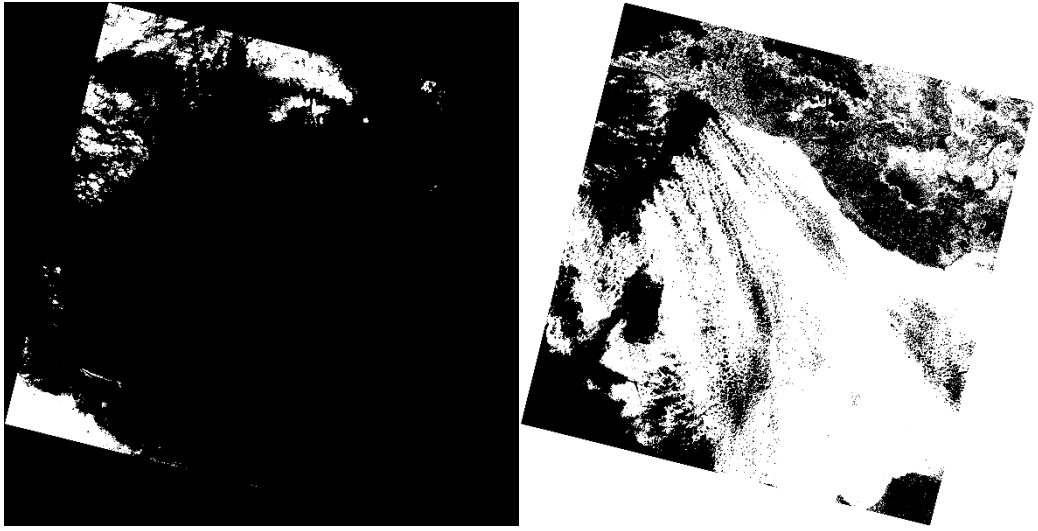


Figure 2.22 PCP (Left) and Water Mask (Right) results of LS8 Image
LC08_L1TP_177035_20180402_20180416_01_T1

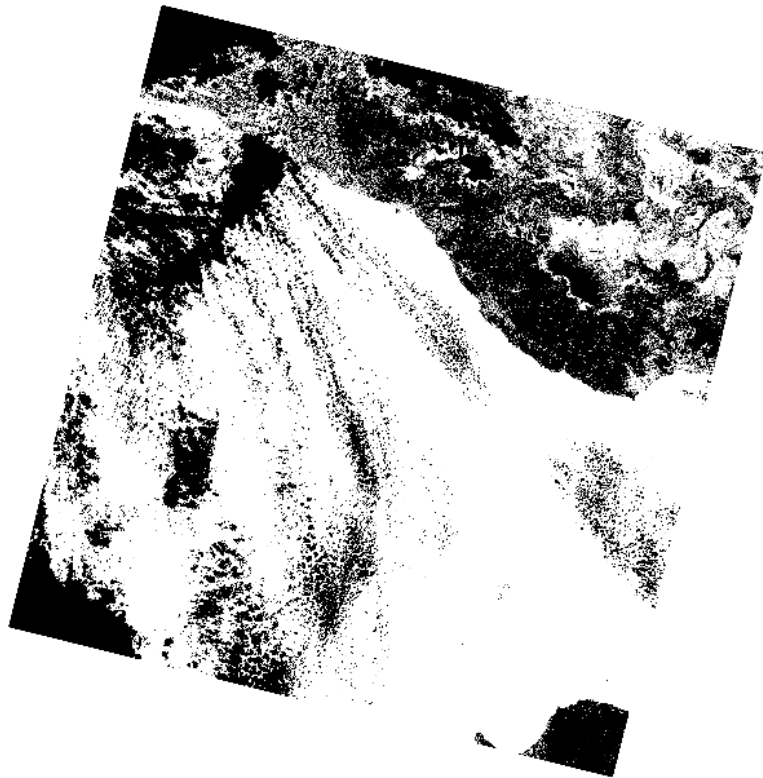


Figure 2.23 Clear Sky Water Mask results of LS8 Image
LC08_L1TP_177035_20180402_20180416_01_T1

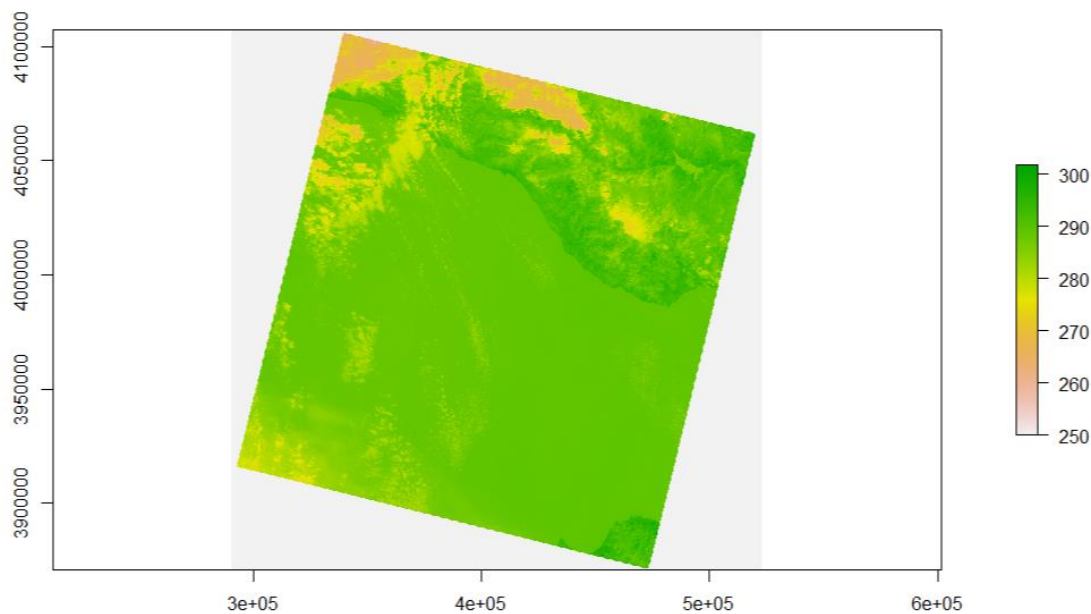


Figure 2.24 Brightness Temperature (Kelvin) Result of LS8 Image LC08_L1TP_177035_20180402_20180416_01_T1 (Axes Represent UTM Coordinates)

Generalized water temperature value is calculated by multiplying clear water mask with BT matrix. The returned value is the 0.825th quantile of the resultant matrix. The 0.825 value has been offered by both the original and the improved algorithms (Zhu et al., 2015; Zhu & Woodcock, 2012).

After calculating a temperature threshold for water pixels, one of the probability analysis calculations can be performed and temperature-based cloud probability mask for water areas based on temperature analysis has been generated. (Figure 2.25 – Left)

Before generating a final cloud mask for water areas, a second probability mask named as brightness probability mask, based on TOA reflectance values of Band-5 (NIR) of Landsat-8, has been generated. Returned result includes values limited with 1 for probable cloud and 0 for not cloud. (Figure 2.25 – Right)

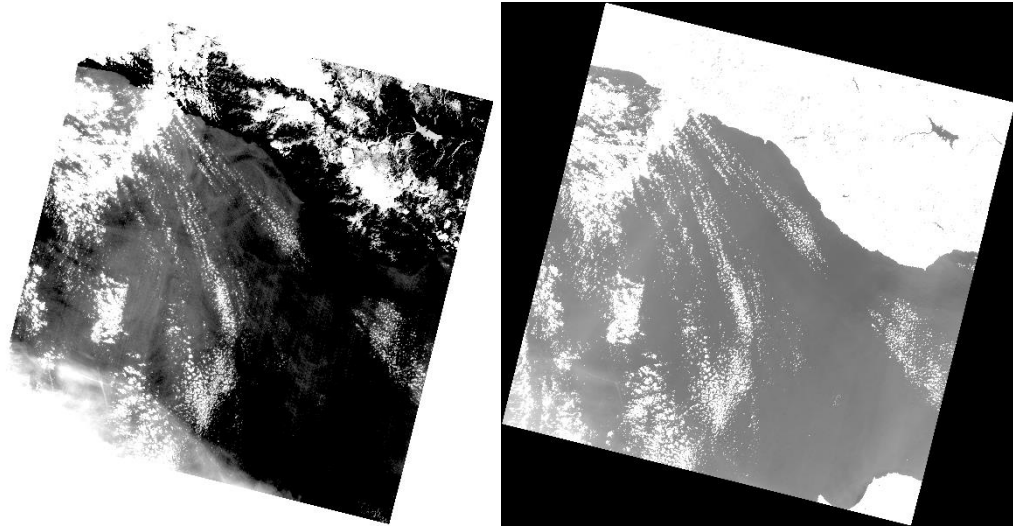


Figure 2.25 Temperature Based Water Probability Mask (Left) and Brightness based Probability Mask (Right) of LS8 Image LC08_L1TP_177035_20180402_20180416_01_T1

Finalized cloud mask over the water areas have been generated by incorporating temperature-based cloud probability mask and brightness probability mask. This result includes binary values such that 1 for probable cloud and 0 for not cloud.

In order to generate a cloud mask for the land areas too, a clear sky land pixels mask based on PCP and initial water mask, has been generated. However, calculation steps of this method do not just mark intersections of PCP's 0 (false) pixels with the water mask's 0 (false) ones. Calculation steps also take total number of pixels (regardless of being water or land and cloudy or clear sky) and if the number of clear sky land pixel count of the result candidate is lower than 1% of the total number of pixels of the raster, that result candidate is combined with the clear sky water mask, otherwise the result candidate is returned as it is. Returned result is a binary image (Figure 2.26 – Left).

After generating the clear sky land mask, a probability mask based on temperature has been generated for land pixels. Calculation of this mask includes BT values that had been defined previously and clear sky land pixels (Figure 2.26 – Right).

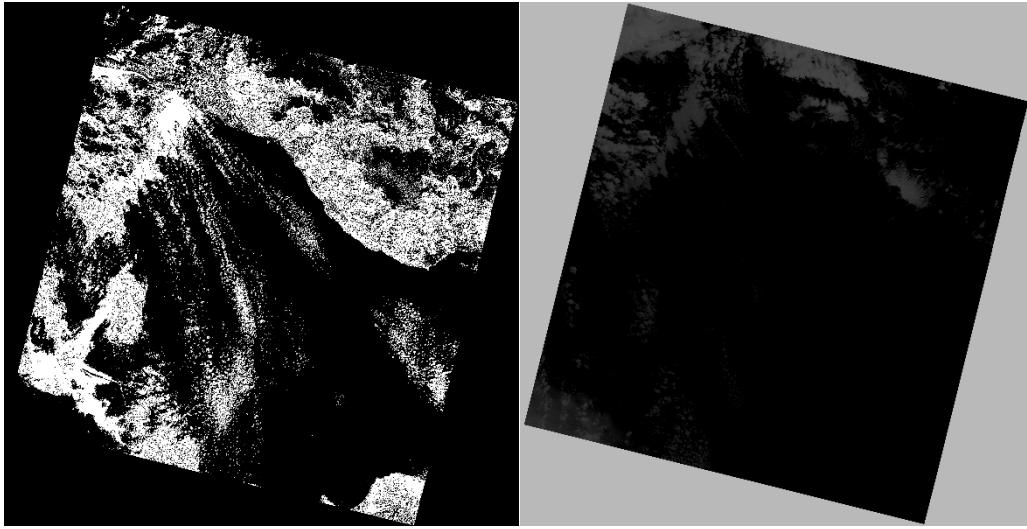


Figure 2.26 Clear Sky Land Mask (Left) and Temperature Based Cloud Probability Mask (Right) of LS8 Image LC08_L1TP_177035_20180402_20180416_01_T1

Another step to calculate is whiteness mask. Calculation of this mask includes calculating the mean visible matrix which is the arithmetic average of RGB (Band 2, Band 3 and Band 4 of Landsat 8) band values. After that differences between DN of each band and the mean visible matrix are calculated and returned as result.

Generating of Cloud Mask for land areas also includes another mask named as variability probability mask. This step utilizes Bands 3, 4, 5 and 6 of Landsat 8 and whiteness mask. Throughout the calculation, function calculates NDVI and NDPI (with Band 6 as SWIR) values and assigns binary values the resultant band based both those calculations and whiteness mask (Figure 2.27– Left).

After calculating clear sky land mask, temperature mask for land pixels, whiteness mask and variability probability mask, a second finalized cloud mask can be generated, and that new mask will define the cloudy areas for land pixels (Figure 2.27- Right).

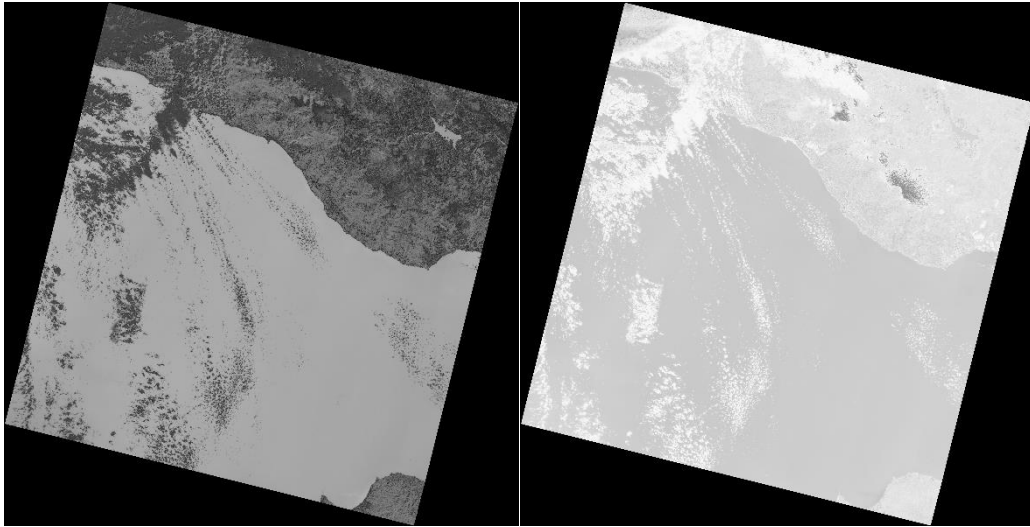


Figure 2.27 Whiteness Mask (Left) and Land Variance Mask (Right) calculations of the Cloud Mask of LS8 Image LC08_L1TP_177035_20180402_20180416_01_T1

The final cloud mask is generated by summing finalized cloud mask covering water areas and finalized cloud mask covering land areas and assigning 1 (cloud) or 0 (no cloud) to each pixel. This assignment is based on the result of the summation such that every pixel with a value greater than 0 is assigned to be 1 and the ones with a value smaller than 0 is assigned to be 0. Reason of the possibility of values being greater than one when both water and land masks have values either 0 or 1 is a precaution against an overlapping and having a value equal to 2. Since this final mask is used in a deductive manner at the water border detection step, having a value equal to 2 would result in having a value of -1 in the water border calculations. Those possible -1 values would skew the density distribution of the final elevation-candidates-matrix in an unpredictable and uncorrectable way.

Considering both the RGB image (Figure 2.28) and the final cloud mask (Figure 2.29) together, it can be observed that the cloud mask algorithm overestimates the cloud pixels when temperature distribution is skewed. Some of this overestimation may be due to occurrence of very thin clouds that cannot be detected during human inspection. However, it can also be observed that the algorithm performed better over

pixels belonging to Mediterranean Sea. In the light of the algorithm's general flow, reason of this accuracy is sea pixels' uniformity and that is the reason of proposing an initial cropping with respect to a shape file covering the area of interest.

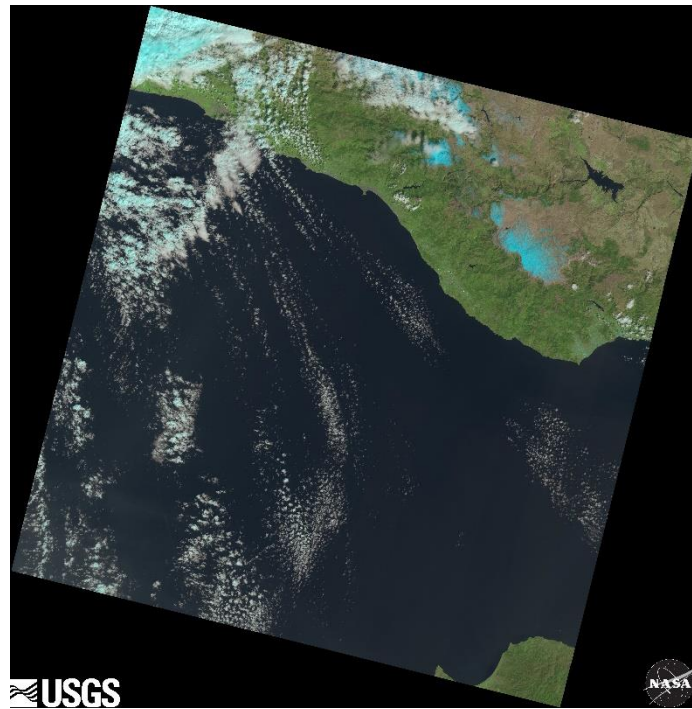


Figure 2.28 RGB image of LS8 Image LC08_L1TP_177035_20180402_20180416_01_T1

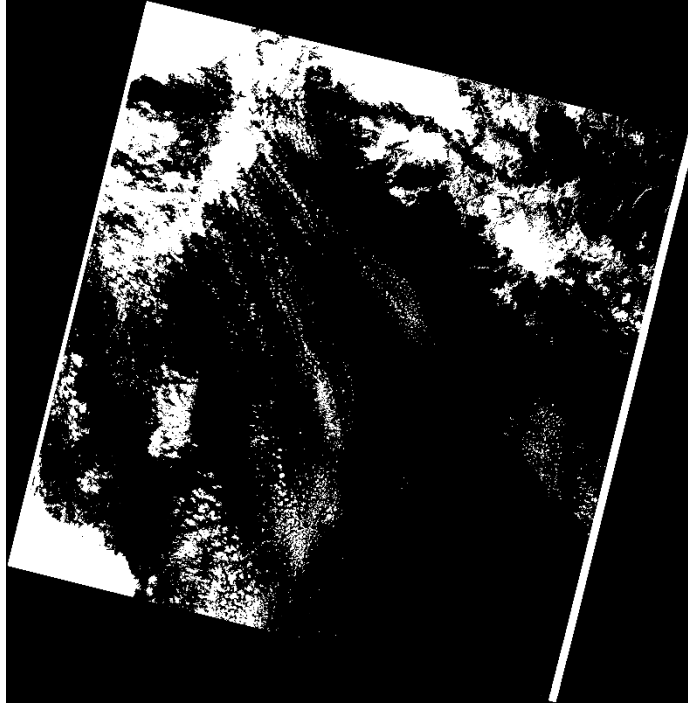


Figure 2.29 Final Cloud Mask of LS8 Image LC08_L1TP_177035_20180402_20180416_01_T1

2.6.2.4. Snow and Shadow Mask

In this study mTCW is used as snow and shadow mask. Tasseled Cap Transformations had been introduced in 1976 mainly for agricultural land cover classification (Kauth & Thomas, 1976) and derivations have been published to detect wet areas and vegetation. (Crist, 1985)

$$TCW_{Crist-LS8} = 0.0315 * B2 + 0.2021 * B3 + 0.3102 * B4 + 0.1594 * B5 - 0.6806 * B6 - 0.6109 * B7 \quad (11)$$

Although TCW method has been used as an input for water area detection (Ouma & Tateishi, 2006), its derivatives with different coefficients have also been utilized (Bhagat & Sonawane, 2011). A more recent study based on Australia also stated that the original TCW_{Crist} coefficients yield slightly worse performance when

it comes to detecting the water area and hence coefficient fine tuning should be performed with respect to the study area (Fisher et al., 2016).

Considering the TCW_{Crist} calculates the wetness of the surface and even the initially equation proposed by TCW_{Crist} (Eqn-12) was found out to be a good indicator of snowy areas, probably due to highness of its coefficients of SWIR bands with respect to VIS and NIR ones, a modified version of TCW_{Crist} has been generated (for details see Table 2:1) and used in this study as mTCW. Thermal bands have been utilized in mTCW when compared to TCW_{Crist} to generate a more separated set of values for ice and water. Resultant mTCW formula has been found to be useful for eliminating some of the false positive water area markings due to not only ice and snow pixels but also cloud shadow pixels.

$$mTCW = 0.03 * B2 + 0.20 * B3 + 0.41 * B4 + 0.16 * B5 - 0.54 * B7 - 0.36 * B11 \quad (12)$$

Table 2:1 Band Coefficients of TCW-Crist and mTCW

Band Number (Landsat 8)	TCW_{Crist}	mTCW
B2	0.0315	0.03
B3	0.2021	0.20
B4	0.3102	0.41
B5	0.1594	0.16
B6	-0.6806	NA
B7	-0.6109	-0.54
B11	NA	-0.36
$\frac{\sum(UV + VIS + NIR)}{\sum(SWIR + TIR)}$	1.84	0.89

The image (Figure 2.30 – Left) belongs to the result of AWEIS (best model for water level estimation over Altinkaya Dam, see Section 3.4) application over the Landsat 8 Level 1 raster image taken at 19.02.2017 with the name of LC08_L1TP_176031_20170219_20170301_01_T1, covering the Altinkaya Dam area. As it can be seen in the image (Figure 2.31) from the RGB plotting of the same

image that the NDPI application returns both water and icy areas as black. However, the image (Figure 2.30 – Right) indicates that the mTCW approach is more sensitive to icy areas and combining mTCW application with NDPI application have reduced the false positive water markings as it can be seen in the resultant image (Figure 2.32). It should also be noted on the upper left part of the resultant image that, unless the cloud masking is applied, the clouds' effect on false positiveness of water detection index results may persists through mTCW corrections.

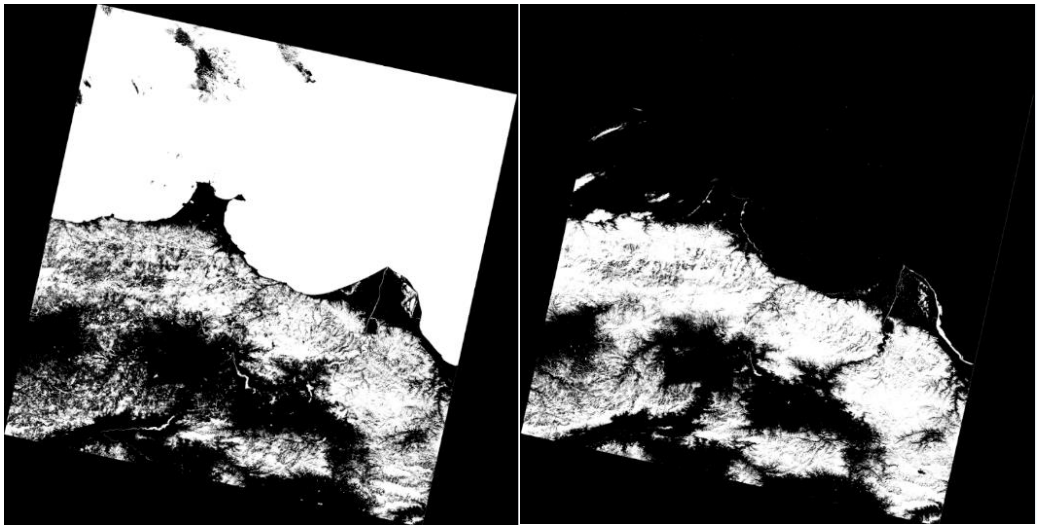


Figure 2.30 Results of AWEI-S (Left) and mTCW (Right) Calculations of Landsat-8 Image LC08_L1TP_173033_20180201_20180220_01_T1

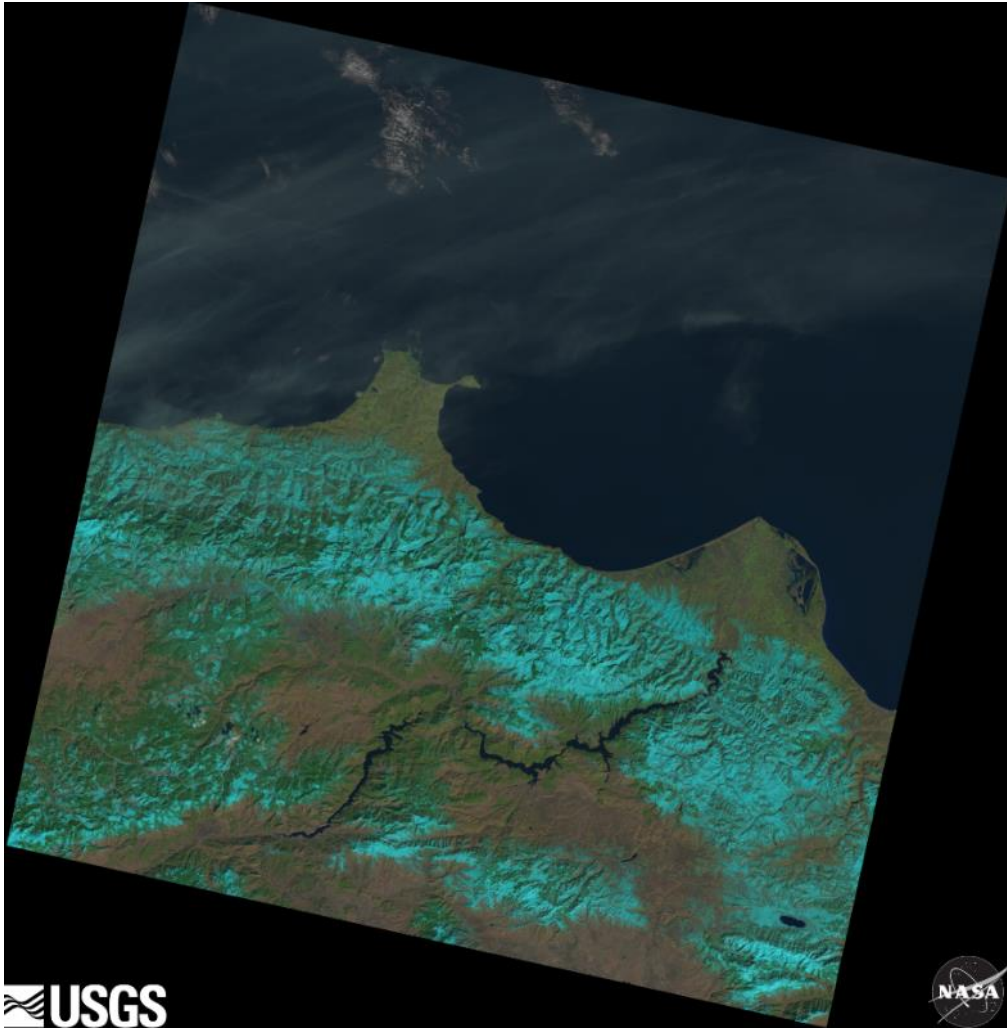


Figure 2.31 RGB Image of Landsat-8 Image LC08_L1TP_176031_20170219_20170301_01_T1
(Image obtained from USGS)

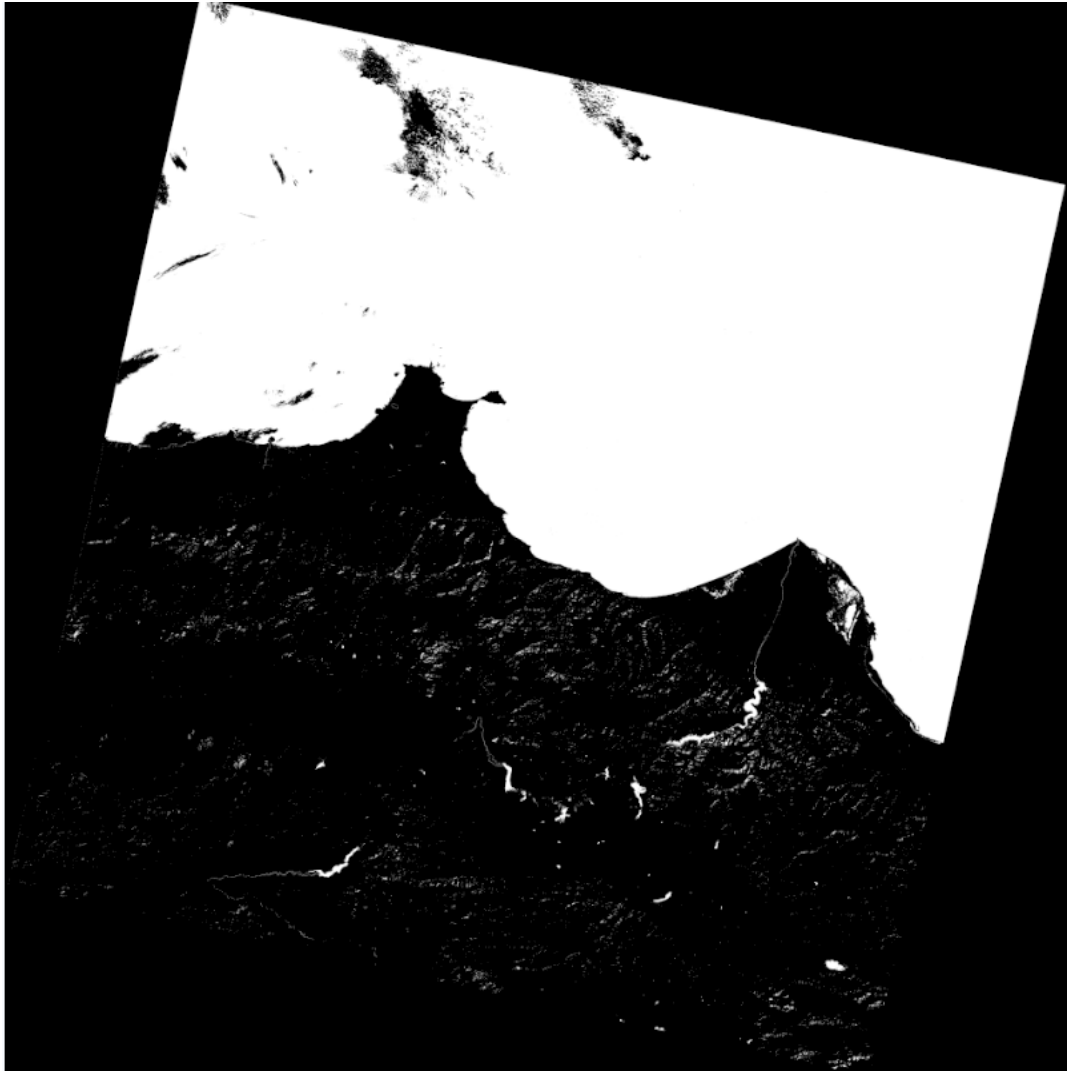


Figure 2.32 Resultant Image (Introduction of mTCW to Water Detection Index) of Landsat-8 Image LC08_L1TP_176031_20170219_20170301_01_T1

2.7. Optimization of Water Level Detection Estimations

2.7.1. Optimization Method and Design Decisions

There are numerous kinds of optimization methods and their variants. However, NMS method has been selected for optimization tasks of this study. However, to check for the difference between a generalized method and a method that

is tailored for a specific dam, another approach was also carried out that was based on some of Altinkaya Dam's data as training to model both Altinkaya and Ermenek Dam.

Initial results with the selected initial parameters have shown that the RMSE value changes with respect to time of the year. In order to achieve better results, the semiannual (winter and summer) variant and seasonal (winter, spring, summer and autumn) variant were tried and results were inspected manually. This manual inspection led the decision of using seasonal model with seasons of winter, spring, summer and autumn.

Inspection of the initial results and division of the year into four parts also led a requirement of four different thresholds for determining the elevation. NMS method starts with generating at least $n+1$ random candidates for n number of variables. Although division of the year into four equal parts that have their own water thresholds and elevation quantile thresholds makes 8 parameters that require an initial pool of at least 9 candidates, every season was independent from the others. Moreover, NMS algorithm includes finding the centroid of the best candidates and optimizing all parts of the year had a probability of undesired changes in unrelated parameters. Hence, every season was considered on its own and objective function was calculated only for the season-of-interest related data. This decision led to a result that have 3 parameters (water threshold, statistical outlier threshold and elevation quantile threshold) that require an initial pool of 4 candidates. However, in order to have an initial pool that has as much variety as it can, size of the initial candidate pool was set to be equal to 100. But one of the candidates in the initial candidate pool was entered manually with respect to inspection of the histogram and plotting would-be-detected-water-area based on different water thresholds. Reason of this manual entry is providing an anchorage for optimization algorithm to consider and speed up the convergence.

Parameters with respect to water area detection methods kept constant for different DEMs in order to observe the differences between DEMs under a constant

water body marking. Step sizes for elevation quantile threshold was set to be equal to 0.025 and step size for water thresholds of different water detection indices (Table 2:2) were set based on their initial values obtained from the histogram.

Minimum and maximum values for elevation quantile threshold were set to be equal to 0 and 1 respectively. Whereas, minimum and maximum values for water thresholds of water detection indices were set to be equal to minimum and maximum values of the histogram of each index. Statistical outlier threshold is not iterated like water area detection and water elevation detection parameters. It is hard coded in the NMS loop that NMS could decrease the statistical outlier threshold by 0.25 after every hundred iterations, as long as the current best model's RMSE value is larger than 7.50 m., which is the elevation change within a Landsat pixel over the Ermenek and Altinkaya Dams' areas (See Section 2.41 and Section 2.4.2).

Table 2:2 Predetermined Step Sizes of Applied Water Indices

Index Name	Step Size
AWELS	500
NDWI.MCF	0.01
NDPI	0.01
WI2015	5000

2.7.2. Initial Threshold Selection for Water Detection Indices

Each water detection index has results scattered among a range of values. Indices, like NDPI and NDWI.MCF, that calculates ratio of bands without any additional multiplier have result interval that is independent of radiometric resolution. Whereas the indices that includes coefficients have results scattered among intervals that are closely related with the radiometric resolution. Because Landsat-7, that has a radiometric resolution of 8 bits has its pixel values scattered among interval 0-255 but Landsat-8, which has a radiometric resolution of 16 bits has its pixel values scattered among interval 0-65,536. This difference affects the results greatly and thresholds

calculated for this kind of indices for Landsat-7 raster images are useless for Landsat 8 images.

Moreover, existing literature promotes the idea of calculating area specific thresholds for classification indices (Avisse et al., 2017; Coltin, McMichael, Smith, & Fong, 2016; Liu, Song, Peng, & Ye, 2012). Therefore, instead of using threshold values that have been defined in other articles, initial definition was done manual calibration by inspecting the histogram of the results (Figure 2.33) and initial plot (Figure 2.34) before plotting the resultant binary image based on various threshold candidates (Figure 2.35 and Figure 2.36).

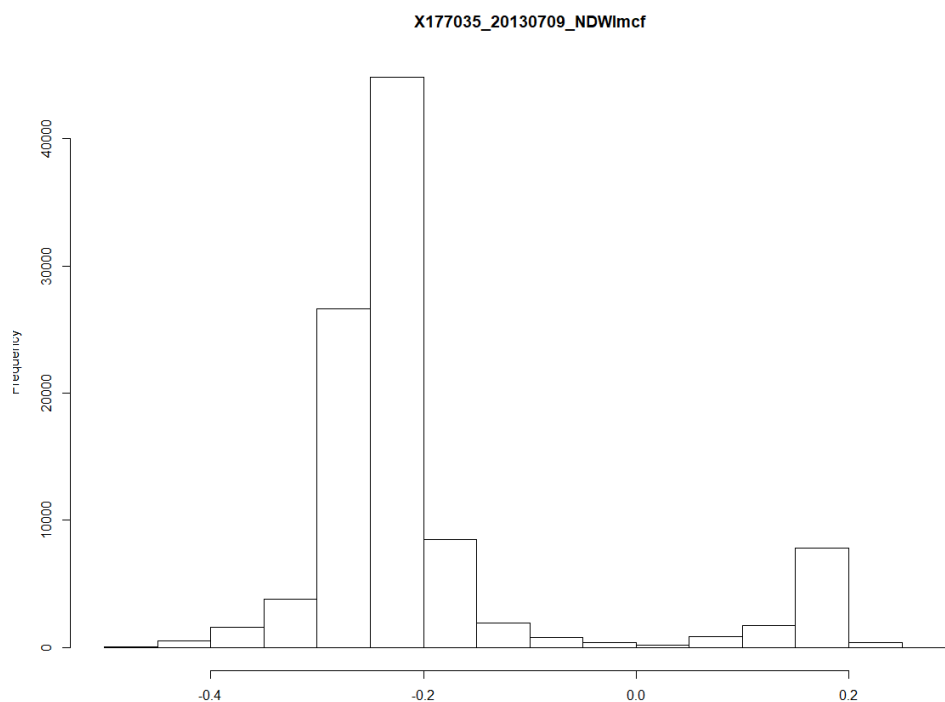


Figure 2.33 Histogram of NDWI.MCF Result of Ermenek Dam for Date 09.07.2013

(Y-Axis is Frequency and X-Axis is Calculated Index Values)

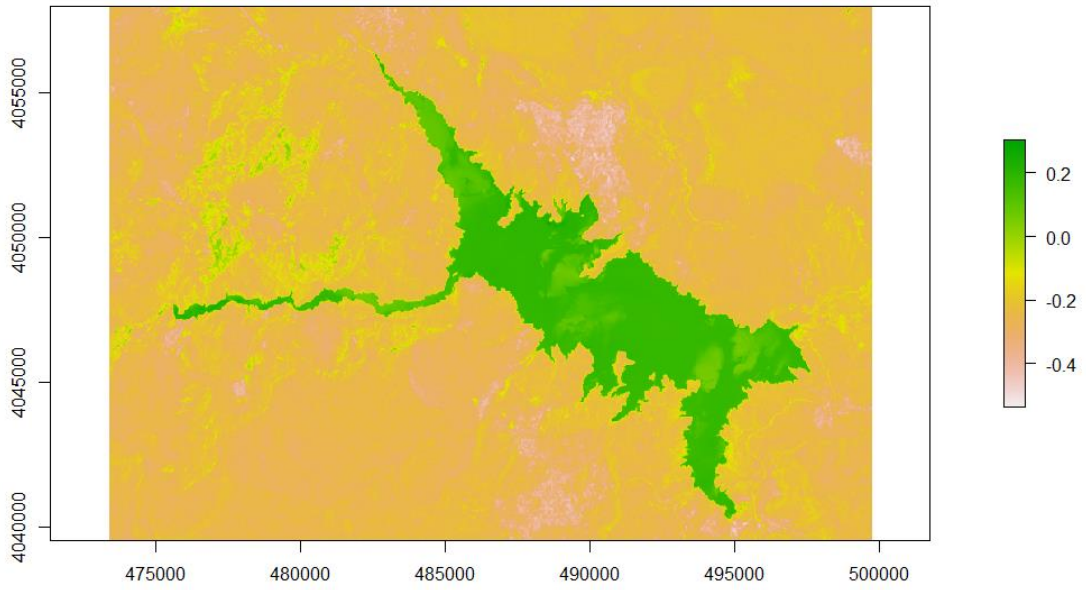


Figure 2.34 Plot of NDWI.MCF Result of Ermenek Dam for Date 09.07.2013

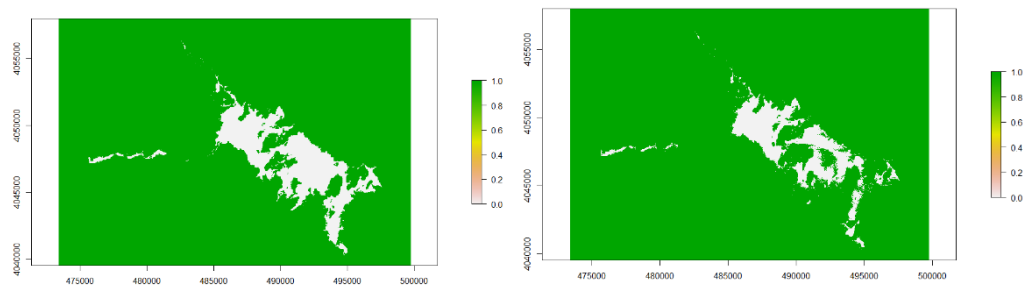


Figure 2.35 Result Plots of Ermenek Dam Area based on Different NDWI.MCF Thresholds
(0.16 on the Left and 0.18 on the Right)

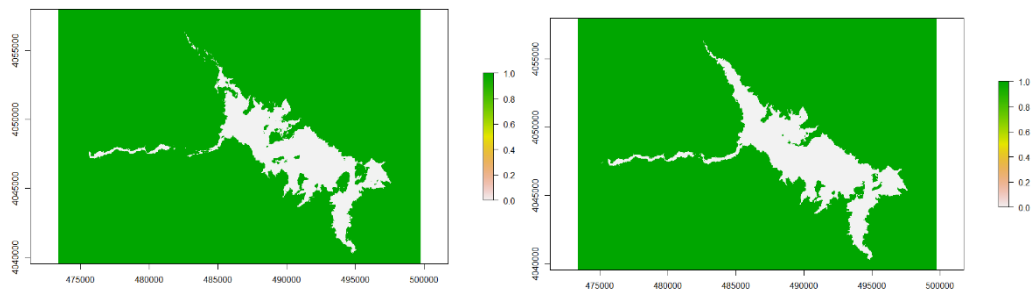


Figure 2.36 Result Plots of Ermenek Dam Area based on Different NDWI.MCF Thresholds
(0.10 on the Left and 0.05 on the Right)

2.7.3. Objective Function

Error measurement has been done in terms of coefficient of correlation, mean error, standard deviation of error and RMSE. The most viable approach would be minimizing the RMSE while introducing the mean error as a constant to the methodology. However, this would yield methods that are water body specific and hence require a bigger data set than the one that had been used in this study in order to distinguish the difference between a better model and the overfitted one.

Therefore, the objective function focused on minimizing the RMSE. Although the initial model tried minimizing the mean error, test results also shown that even when the mean error is minimized, there can still be worse performance in terms of error standard deviation and RMSE. In order to prevent this problem, minimization of absolute mean error could also be selected.

RMSE calculations that served as a basis for objective function and hence the optimization is calculated with Eqn-13. where N is count of both predicted and actual data points, P is the results of model and A is the ground control data points that had been obtained from DSI. All RMSE, P and A values' units are meters.

$$RMSE = \sqrt{\frac{\sum_{i=1}^N (P_i - A_i)^2}{N}} \quad (13)$$

Interpolation has been calculated by the Eqn-14 where VP is previous value, SOM is the count of days between the next value and 1st of that month, VN is next value, EOM is the count of days between the previous value and 1st of the next month and IRs is interpolated result. According to this equation if the day belonging to the Landsat Image Date is 1, no interpolation has been done and the result belonging to that image used directly.

$$IRs = \begin{cases} \text{Day Of Landsat Image Date} == 1 \Rightarrow \text{Do Not Interpolate} \\ \frac{VP * SOM + VN * EOM}{SOM + EOM + 1} \end{cases} \quad (14)$$

2.7.4. Training and Test Data

Each optimized parameter set is then tested with local (same dam) and remote (other dam) data. For the models that were based on both Ermenek and Altinkaya Dams data, ground data related with respective dam between 2013 May and 2019 May was used for optimization. Here, the use of entire time series for the calibration and validation over the same region overfits the results, while the use of entire datasets for calibration on one dam and implementation and validation over the other dam provides an independent and more realistic check of the methodology.

2.8. Alternative Statistical Methods to Retrieve Water Level Estimation

NMS methodology used in this study to distinguish the water and the land also provides an estimate for the ECDF methodology to acquire the water level estimate. Here, the same water-land border estimate obtained from NMS methodology could be used together with other statistical methods to obtain the water level estimate. In this study, four alternative methods are used (GEV, mean, median, and mode) to compare the success of different statistical approaches. Here, all statistical methods, including ECDF, use similar masks: cloud mask, snow and shadow mask and proximity buffer are applied to all of the alternative methods.

One alternative approach to ECDF is GEV distribution as a final step for elevation detection. This methodology was applied over Hoover Dam's water level detection and have a statistical outlier detection threshold of 2.0 (Tseng et al., 2016).

Another alternative is using frequency analysis that had been used (with further analyses) in the study about Jordan (Avisse et al., 2017). In order to apply this

methodology, more calculations were performed among the elevation arrays. Additionally, median and mean values are also checked for their ability to predict water level of the reservoir.

2.9. Used Software and Web Apps

In this study Google Earth Pro, Google Maps Web Site, USGS BDA, QGIS, R-Studio, Microsoft Excel, 7-Zip, Notepad, Notepad++ and Firefox software was used in addition to the USGS Earth Explorer Web Portal.

Google Earth Pro was utilized for extracting the shape files in terms of “kml” files. Both initial area of interest shape files and the narrower, proximity-based buffer zone shape file are drawn on Google Earth Pro and extracted as “kml” files.

USGS BDA is a software that lets user to download Landsat images in bulk. Normally, the USGS Earth Explorer Web Portal has a limitation of 6 concurrent downloads. This software has been officially supported and proposed by USGS. Dependency of USGS BDA software is the installment of Java language environment.

Landsat images and DEM files have been selected by using USGS Earth Explorer Web Portal and DEM files have been downloaded from this portal directly.

QGIS is an open source Geographic Information System (GIS) software and its use in this study was transforming “kml” files into “shp” format in addition to the conversion of CRS of the DEM files in a Landsat-compatible format.

R-Studio is used for utilization of R-Language in this study. All of the computations of this study were done by using R-Language and hence either R-Studio or R’s native terminal is essential and irreplaceable for the application of the model described in this study. Dependency of R-Studio software is the installment of R-Language environment. After the installation of the R-Language, those packages should also be installed since the methods used in the study depends on them; “sp”, “rgdal”, “fields”, “maps”, “magic”, “raster”.

CHAPTER 3

RESULTS AND DISCUSSION

The water level detection methodology introduced in this study relies on estimation of water-land border first using NMS methodology, then retrieval of DEM values at the calculated water-land border pixels, and then utilizing several different methods (ECDF, GEV, mean, median, or mode) to obtain the water level estimate using the DEM values at the border pixels. Below, first the optimized parameters obtained from the NMS methodology is given, then the water-land border based detection results are given, later the water level estimate results over Ermenek and Altinkaya dams are given.

3.1. Optimized Parameters

Optimized parameters obtained from the NMS methodology (Section 2.7) over Ermenek and Altinkaya Dams are provided in Table 3:1. Results of water elevation estimates in this study are calculated by using those parameters. Although these values can also be found by trial and error, using an optimization algorithm provides ability to automate the process of threshold calibration.

Table 3:1 Optimized parameters for training data based on Ermenek Dam and Altunkaya Dam

Dam	DEM	Area Index	Water Threshold Winter	Water Threshold Summer	Water Threshold Autumn	Water Threshold Spring	Water Is Higher/Lower Than Threshold	Statistical Outlier Threshold	Elevation Quantile Winter	Elevation Quantile Summer	Elevation Quantile Autumn	Elevation Quantile Spring
Ermenek												
ASTER												
		AWEIS	5000	10000	5000	7500	Higher	1.75	0.825	0.900	0.825	0.900
		NDPI	-0.10	-0.15	-0.15	-0.17	Higher	1.75	0.825	0.900	0.825	0.900
		NDWIMCF	0.10	0.16	0.10	0.12	Lower	1.75	0.850	0.900	0.850	0.900
		W12015	120000	275000	145000	285000	Lower	1.75	0.800	0.900	0.825	0.900
SRTM												
		AWEIS	5000	10000	5000	7500	Higher	1.75	0.850	0.900	0.900	0.900
		NDPI	-0.10	-0.15	-0.15	-0.17	Higher	1.75	0.850	0.900	0.850	0.900
		NDWIMCF	0.10	0.16	0.10	0.12	Lower	1.75	0.850	0.900	0.850	0.900
		W12015	120000	275000	145000	285000	Lower	1.75	0.650	0.650	0.675	0.850
Altunkaya												
ASTER												
		AWEIS	7500	5000	7500	5000	Higher	1.75	0.700	0.800	0.825	0.700
		NDPI	-0.10	-0.02	-0.15	-0.23	Higher	1.75	0.725	0.725	0.750	0.575
		NDWIMCF	-0.03	-0.01	0.10	0.05	Lower	1.75	0.700	0.775	0.800	0.800
		W12015	100000	275000	145000	100000	Lower	1.75	0.650	0.825	0.800	0.750
SRTM												
		AWEIS	7500	5000	7500	5000	Higher	1.75	0.750	0.675	0.750	0.650
		NDPI	-0.10	-0.02	-0.15	-0.23	Higher	1.75	0.750	0.675	0.750	0.650
		NDWIMCF	-0.03	-0.01	0.10	0.05	Lower	1.75	0.725	0.775	0.825	0.775
		W12015	100000	275000	145000	100000	Lower	1.75	0.700	0.775	0.750	0.700

3.2. Water-Land Border Detection

In order not to include the start of the water retention as a model parameter and be able to process all water bodies with the same statistical model, a design decision has been made. According to this design decision, only the border lines (Figure 3.2) between the water and land pixels have been considered instead of whole water area (Figure 3.1). Border line detection has been performed with R Programming Language's image processing functions.



Figure 3.1 Detected Water Area of Ermenek Dam for 18/08/2016 (Green areas are land pixels)

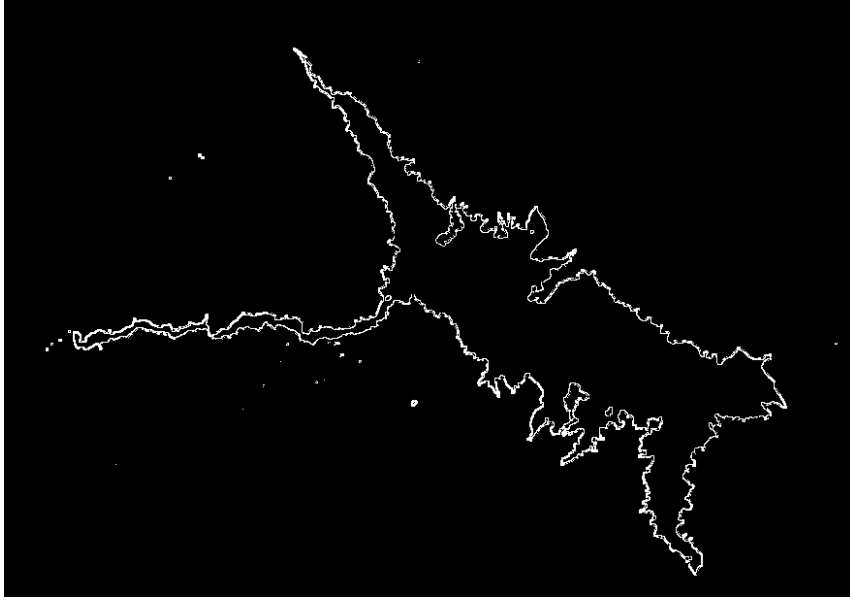


Figure 3.2 Detected Water Border of Ermenek Dam for 18/08/2016

Once the water-land border is retrieved via NMS methodology, the actual water level estimates of the dam can be obtained via five different methodologies (i.e., ECDF, GEV, mean, median, or mode). or via simple statistics using the histograms of the DEM values of the water-land border pixels. Even though the water-land border detection from NMS methodology is used in both NMS-based and simple statistic-based water level estimates, their performances change as these different methodologies utilize the histogram of the water-land border DEM differently. |

3.3. **Ermenek Dam Estimations**

Error statistics (bias, standard deviation and RMSE) and correlation coefficients for the water level estimates over Ermenek dam are given in Tables 3.2 – 3.5 below. In these tables, the best results for the local (Ermenek Dam) training data is shown in blue while the remote (Altinkaya Dam) training data is shown in purple. There are total 80 experiments (2 training datasets * 4 indices * 2 DEM * 5 Statistical Methodologies). Experiments are named as “Training-Indices-DEM-Test

Location” where “Training” refers to local/remote training case (i.e., Ermenek or Altinkaya dam), “Indices” refer to each utilized index name (AWEI, NDPI, NDWI, or WI2015), “DEM” refer to the utilized DEM image (ASTER or SRTM), and “Test Location” refers to the site where the water elevation errors are calculated (“E” for Ermenek or “A” for Altinkaya). For example, “ErmT-AWEI_S-SRTM-A” refers to the experiment utilizes Ermenek dam values to find the necessary parameters in NMS optimization, AWEI index, and SRTM DEM where the evaluations are validated over Altinkaya dam. Here, if the selected index (e.g., AWEI) has variants in literature, then the variant is defined with another substring separated by an underscore. For example, for the AWEI index shadow sensitive variant (AWEI_S) is used and for the NDWI index McFeeter’s variation (NDWI_MCF) is used.

Water level estimation error averages (i.e., zero mean error is regarded as unbiased) for 16 tested experiments belonging to ECDF statistical approach are shown in Table 3.2. Among the tested experiments, WI2015 index & ASTER DEM combination provided best results among the local models (0.31 m average error) and WI2015 index & SRTM DEM provided best results among the remote models (0.18 m average error). Overall, experiments utilized SRTM DEM yield smaller water level estimation bias than the ones utilized ASTER DEM. Additionally, local training outperforms remote training in terms of average water level error (0.65 m and -1.97 m for the water level average errors of local and remote training respectively). Overall, different months yield different bias values depending on the selected index, training dataset and DEM values (Table 3.2, Figure 3.5 and Figure 3.6). This may be researched with a larger dataset to check whether those differences can be utilized for decreasing RMSE values.

Water level estimation error standard deviations for 16 tested experiments belonging to ECDF are shown in Table 3.3. Among the tested experiments, AWEI_S & ASTER DEM combination provided best results (3.43 m error standard deviation) among the local models and NDPI & ASTER DEM among the remote models (5.31 m error standard deviation). Overall, experiments utilized ASTER DEM yield slightly

smaller water level estimation error standard deviation than the ones utilized SRTM DEM. Similar to the error average results, local training outperforms remote training in terms of water level estimation error standard deviation (on average 4.85 m and 8.52 m for the water level average errors of local and remote training respectively). Additionally, summer months (particularly July – September) yield smaller water level estimation error standard deviation (on average ~1.80 m) than winter months (on average > 5.0 m) regardless from the index, training location, and DEM selection (Table 3.3).

Water level estimation RMSE for 16 tested experiments belonging to ECDF are shown in Table 3.4. Among the tested experiments, NDPI & SRTM DEM combination provided best results (3.63 m RMSE) among the local models and NDPI & SRTM DEM among the remote models (5.13 m RMSE). Differences between remote and local training in terms of RMSE, error mean and error standard deviation values are understandable since parameter optimization is performed with one set of dam data and then applied to another dam. This enables local models (trained with data of dam of interest) to perform better than remote models. Overall, experiments utilized ASTER DEM yield marginally smaller RMSE than the ones utilized SRTM DEM. Similar to the error average and standard deviation results, local training clearly outperforms remote training in terms of water level estimation RMSE (on average 5.01 m and 9.51 m for the water level average errors of local and remote training respectively). Again, similar to water level estimation error averages, summer months (particularly July – August) yield smaller water level estimation error standard deviation (on average ~2.85 m) than winter months (on average ~8.0 m) regardless from the index, training location, and DEM selection (Table 3.4).

The linear relationship (i.e., correlation coefficient) between the monthly remotely sensed water level estimation and ground observations are given in Table 3.5. Overall, all local estimates are statistically significant considering the 0.26 threshold with respect to Fisher's Test. Among the experiments, ASTER DEM adds higher linear predictive capability (i.e., average correlation coefficient of 0.59) than

SRTM (i.e., average correlation coefficient of 0.48), while local training estimates clearly yield much better predictions (i.e., average correlation coefficient of 0.65) than remote training estimates (i.e., average correlation coefficient of 0.43).

Time series of the most successful model for water level estimation of Ermenek Dam is provided Figure 3.3 in and its scatter plot versus ground data is provided in Figure 3.4. Overall, the remote sensing-base estimations accurately estimate the timing of increasing and decreasing trends even though there are some large errors such as November 2017. Reason of error happened in November 2017 can be explained by looking into the details of that estimation. November 2017 estimation was calculated by interpolating two Landsat 8 images with dates of 24.10.2017 and 09.11.2017. Calculated water levels for these two dates are calculated as 659.58 m and 686.91 m, while the ground data is measured as 682.10 m at 01.11.2017. These findings indicate that the source of error is the water level calculation over the 24.10.2017 image. Further inspection shown that the main reason is the amount of cloud cover over the image, reservoir is almost invisible (Figure 3.7). Whereas an image belonging to a successful data estimation point show that the water area detection functions as expected (

Figure 3.8).

Comparison between the best models of each statistical approaches (ECDF, GEV, mean, mode and median) is provided in Table 3:6. Both best models for local trained and remote trained approaches are provided for ECDF and as can be observed from the table, best model for water elevation detection is local trained ECDF based approach. Detailed comparison for a selected date (01.03.2017) is provided in Figure 3.11. Where red line (674.29 m) is the result of best local trained model based on ECDF approach (NDPI + SRTM), green line (674.25 m) is the ground data, brown line (673.17 m) is the result of best remote trained model based on ECDF approach (NDPI + SRTM), magenta line (668.50 m) is the result of best median approach, light blue line (667.54 m) is the result of best mean approach, dark blue line (657.45 m) is

the result of best mode approach and the orange line (662.96 m) is the result of best GEV approach.

NDPI + SRTM [over Ermenek with Local Training Dataset]

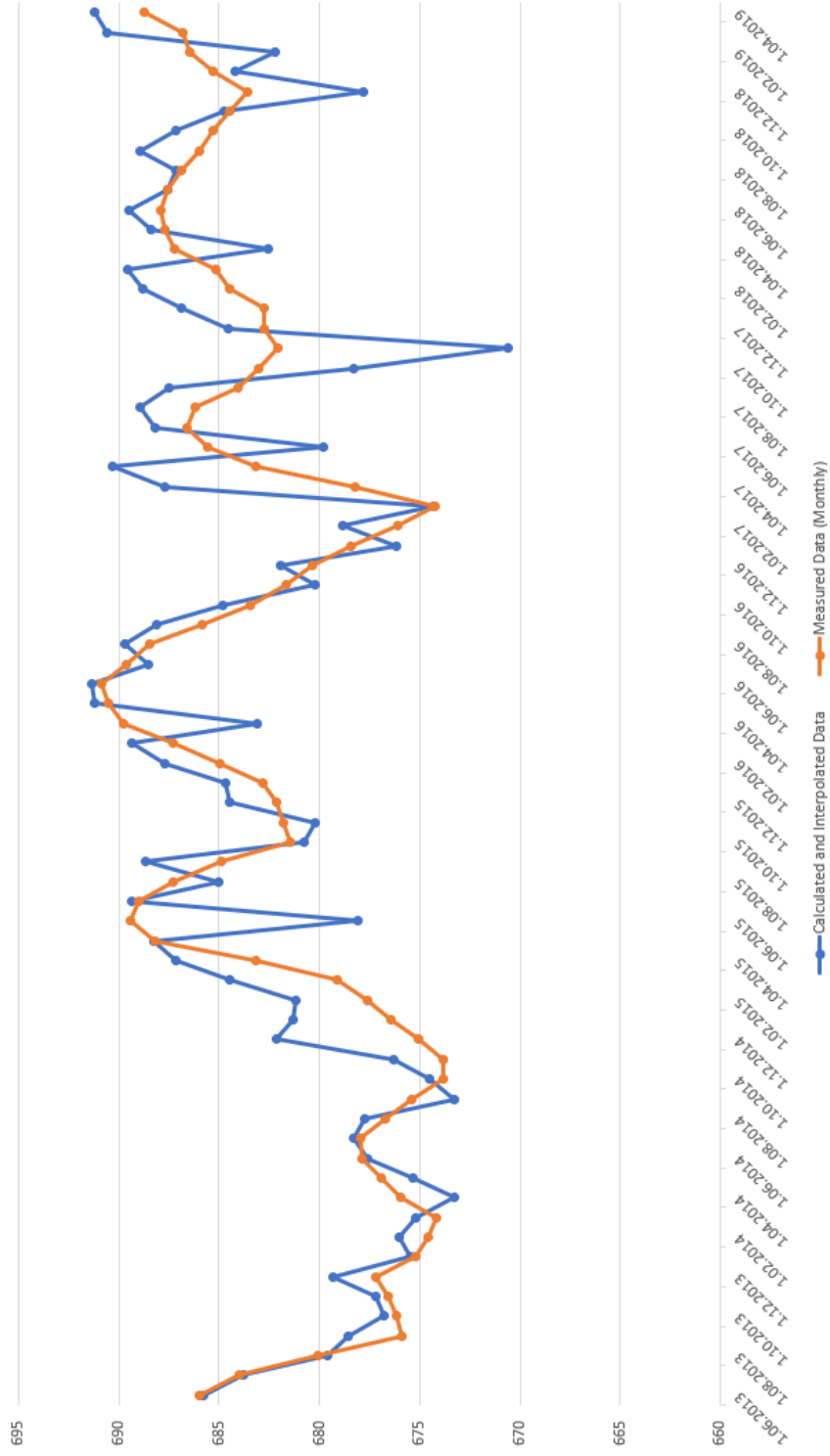


Figure 3.3 Time Series of Best (NDPI + SRTM) Model for Estimating Ermenek Dam's Water Level

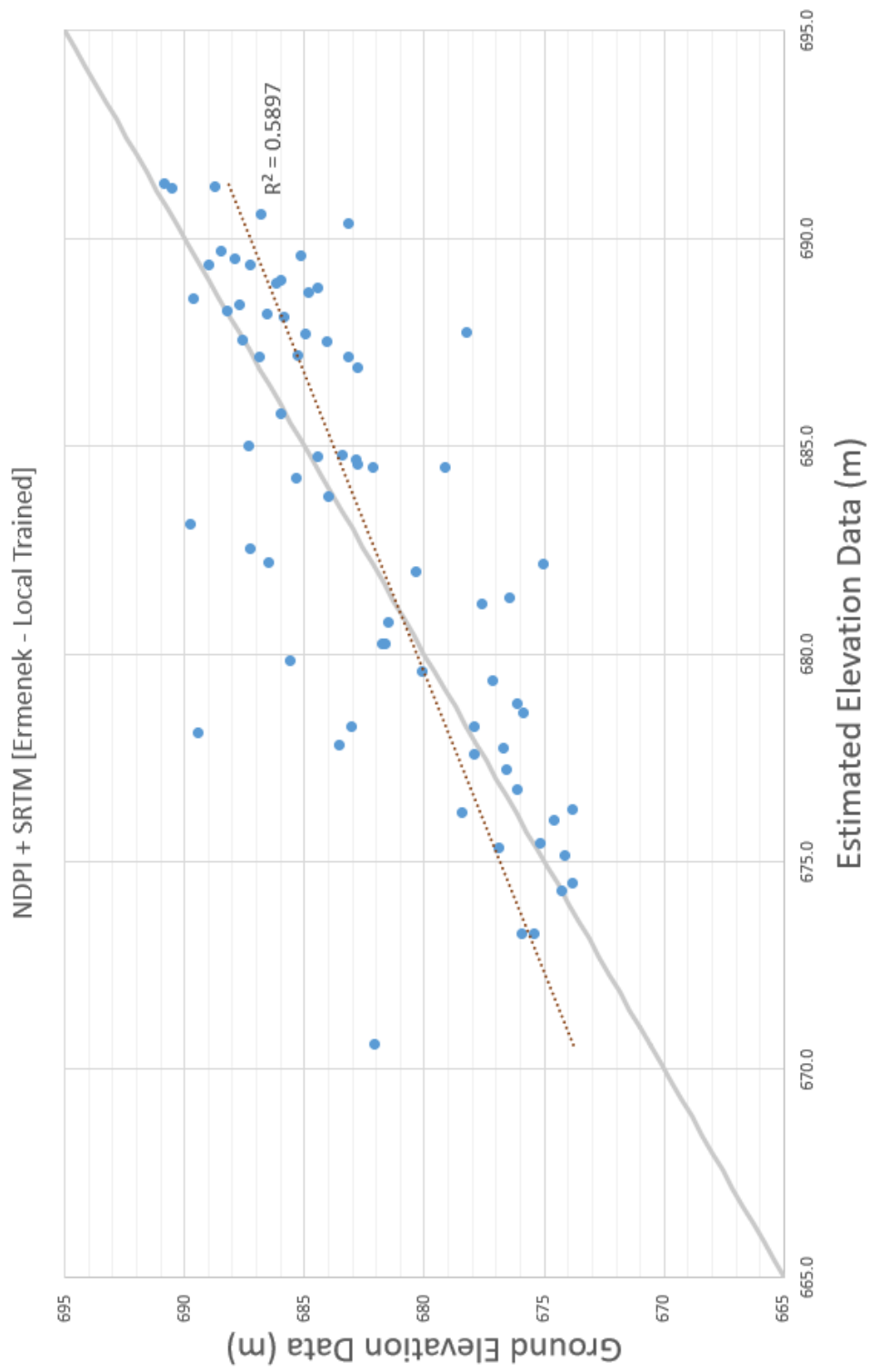


Figure 3.4 Ground Elevation vs Estimated Elevation Data Scatter Plot of Best Model for Ermenek Dam

Table 3:2 Average Error Values of Both Local and Remote Trained Models over Ermenek Dam (ErmT means Ermenek Trained and AltT means Altinkaya Trained; AWEL_S, NDPI, NDWI_MCF and W2015 are Water Detection Indices, ASTER and SRTM are DEMs, E means that model is estimating Ermenek Dam' s water level and A means model is estimating Altinkaya Dam' s water level)

	Jan.	Feb.	Mar.	Apr.	May	June	July	Aug.	Sep.	Oct.	Nov.	Dec.	Annual
ErmT-AWEL_S-ASTER-E	1.36	3.03	0.82	3.12	1.98	0.28	0.93	1.03	1.83	2.29	2.96	2.27	1.82
ErmT-NDPI-ASTER-E	2.63	1.86	3.21	0.40	2.36	-2.47	0.21	-0.20	1.43	-1.07	-1.51	2.87	0.79
ErmT-NDWI_MCF-ASTER-E	-1.77	-1.79	1.21	2.09	4.42	-3.20	1.53	0.32	5.64	0.97	0.23	-1.53	0.62
ErmT-W2015-ASTER-E	0.06	0.12	3.08	1.08	0.61	-1.09	1.03	1.57	2.00	0.16	-1.90	-3.54	0.31
ErmT-AWEL_S-SRTM-E	2.37	5.43	1.79	3.01	2.39	1.74	2.16	2.66	3.08	3.40	3.84	2.27	2.85
ErmT-NDPI-SRTM-E	1.29	1.75	2.78	0.31	1.40	-2.60	0.16	0.40	2.17	-0.16	-1.84	1.54	0.59
ErmT-NDWI_MCF-SRTM-E	-1.44	-0.53	0.70	2.00	3.47	-7.75	-1.14	-1.88	4.11	-0.66	-2.31	-3.99	-0.85
ErmT-W2015-SRTM-E	-2.40	-3.97	0.08	2.70	3.47	-5.40	1.68	0.71	2.92	0.86	-3.21	-7.28	-0.92
AltT-AWEL_S-ASTER-E	-8.16	-6.35	-9.03	-5.71	-10.27	-2.45	-1.18	-0.37	1.48	-0.96	-7.82	-16.56	-5.55
AltT-NDPI-ASTER-E	-4.48	-3.82	-5.46	-14.46	-6.58	-8.47	-3.95	-3.09	-2.20	-8.00	-9.78	-6.32	-6.38
AltT-NDWI_MCF-ASTER-E	0.07	-1.28	-1.80	-1.82	-13.60	-1.49	4.08	3.71	4.88	-1.48	-2.44	-2.52	-0.97
AltT-W2015-ASTER-E	-4.03	-4.73	-6.85	-1.38	-9.83	-3.46	2.76	1.63	3.89	1.10	-2.57	-6.22	-2.32
AltT-AWEL_S-SRTM-E	-2.48	-0.18	-4.18	-2.53	-5.32	1.38	1.97	2.93	5.05	3.22	-3.00	-10.83	-1.11
AltT-NDPI-SRTM-E	-0.02	0.84	-0.97	-6.93	-4.51	-5.15	-1.16	-0.04	1.70	-3.03	-5.07	-1.36	-2.11
AltT-NDWI_MCF-SRTM-E	4.27	3.00	0.98	-0.51	-12.65	2.09	7.19	7.12	8.53	3.39	1.99	2.13	2.51
AltT-W2015-SRTM-E	0.09	0.64	-4.16	-1.01	-9.48	-1.18	4.66	3.79	5.61	3.18	-0.29	-3.63	0.18
AVERAGE-AWEL_S	-1.73	0.48	-2.65	-0.53	-2.80	0.24	0.97	1.56	2.86	1.99	-1.00	-5.71	-0.50
AVERAGE-NDPI	-0.15	0.16	-0.11	-5.17	-1.83	-4.67	-1.18	-0.73	0.78	-3.06	-4.55	-0.82	-1.78
AVERAGE-NDWI	0.28	-0.15	0.27	0.44	-4.59	-2.59	2.91	2.32	5.79	0.55	-0.63	-1.48	0.33
AVERAGE-W2015	-1.57	-1.99	-1.96	0.35	-3.81	-2.79	2.53	1.93	3.61	1.33	-1.99	-5.17	-0.69
AVERAGE-ASTER	-1.79	-1.62	-1.85	-2.08	-3.86	-2.80	0.68	0.58	2.37	-0.87	-2.85	-3.94	-1.46
AVERAGE-SRTM	0.21	0.87	-0.37	-0.37	-2.65	-2.11	1.94	1.96	4.15	1.27	-1.24	-2.64	0.14
AVERAGE-LOCAL	0.26	0.74	1.71	1.84	2.51	-2.56	0.82	0.58	2.90	0.72	-0.47	-0.92	0.65
AVERAGE-REMOTE	-1.84	-1.49	-3.93	-4.29	-9.03	-2.34	1.80	1.96	3.62	-0.32	-3.62	-5.66	-1.97
AVERAGE-ALL	-0.79	-0.37	-1.11	-1.23	-3.26	-2.45	1.31	1.27	3.26	0.20	-2.04	-3.29	-0.66

Table 3:3 Average Error Standard Deviation Values of Both Local and Remote Trained Models over Ermenek Dam (ErmT means Ermenek Trained and AItT means Altnkaya Trained; AWEL_S, NDPI, NDWI_MCF and WI2015 are Water Detection Indices, ASTER and SRTM are DEMs, E means that model is estimating Ermenek Dam' s water level and A means model is estimating Altnkaya Dam' s water level)

	Jan.	Feb.	Mar.	Apr.	May	June	July	Aug.	Sep.	Oct.	Nov.	Dec.	Annual
ErmT-AWEL_S-ASTER-E	3.13	2.47	5.65	5.59	4.29	3.12	1.00	1.12	2.66	0.97	0.65	6.22	3.43
ErmT-NDPI-ASTER-E	2.86	1.32	4.70	7.38	6.11	4.55	1.72	1.69	2.14	1.86	4.21	3.96	4.05
ErmT-NDWI_MCF-ASTER-E	2.97	2.74	2.58	6.07	3.92	8.11	3.60	1.92	1.52	3.58	3.32	7.75	4.83
ErmT-WI2015-ASTER-E	2.15	2.51	3.77	7.34	5.31	3.16	0.89	0.92	1.67	2.35	5.37	4.71	3.87
ErmT-AWEL_S-SRTM-E	4.97	2.88	8.94	5.44	3.22	3.09	0.89	1.06	2.56	1.12	0.54	10.07	4.52
ErmT-NDPI-SRTM-E	2.85	3.13	2.08	6.08	3.34	4.98	0.87	1.71	2.20	2.42	4.95	4.15	3.61
ErmT-NDWI_MCF-SRTM-E	2.82	3.28	5.63	6.15	3.24	15.41	4.01	1.14	1.54	5.55	5.63	8.50	6.67
ErmT-WI2015-SRTM-E	6.93	12.17	3.76	7.48	4.60	10.52	2.23	2.50	3.33	4.35	9.74	13.12	7.82
AItT-AWEL_S-ASTER-E	4.47	1.27	8.72	9.25	15.95	2.45	1.42	1.48	0.44	2.22	6.01	21.85	9.50
AItT-NDPI-ASTER-E	3.57	2.50	0.81	7.42	3.30	5.72	1.73	1.78	0.28	3.92	7.07	7.24	5.31
AItT-NDWI_MCF-ASTER-E	6.93	13.46	8.86	8.09	34.23	3.42	1.77	1.58	1.48	4.19	3.81	4.28	10.85
AItT-WI2015-ASTER-E	6.30	4.25	8.98	8.67	23.24	4.30	2.66	2.77	2.95	2.76	6.17	6.08	8.04
AItT-AWEL_S-SRTM-E	4.73	1.51	10.01	9.52	14.87	2.35	1.30	1.51	0.57	2.05	5.61	20.49	8.93
AItT-NDPI-SRTM-E	3.75	3.65	2.47	5.80	2.44	4.36	1.78	1.91	0.43	3.82	6.85	7.33	4.71
AItT-NDWI_MCF-SRTM-E	6.86	13.21	10.80	8.65	36.68	3.12	1.67	1.41	1.36	3.66	3.07	4.75	11.64
AItT-WI2015-SRTM-E	5.14	5.67	12.71	9.24	27.36	4.92	2.10	2.14	2.59	3.19	7.09	9.77	9.17
AVERAGE-AWEL_S	4.33	2.03	8.33	7.45	9.58	2.75	1.15	1.29	1.56	1.59	3.20	14.66	6.59
AVERAGE-NDPI	3.26	2.65	2.52	6.67	3.80	4.90	1.53	1.77	1.26	3.01	5.77	5.67	4.42
AVERAGE-NDWI	4.90	8.17	6.97	7.24	19.52	7.51	2.76	1.51	1.48	4.25	3.96	6.32	8.50
AVERAGE-WI2015	5.13	6.15	7.30	8.18	15.13	5.72	1.97	2.08	2.64	3.16	7.09	8.42	7.23
AVERAGE-ASTER	4.05	3.81	5.51	7.48	12.04	4.36	1.85	1.66	1.64	2.73	4.57	7.76	6.24
AVERAGE-SRTM	4.76	5.69	7.05	7.29	11.97	6.09	1.86	1.67	1.82	3.27	5.43	9.77	7.13
AVERAGE-LOCAL	3.58	3.81	4.64	6.44	4.25	6.62	1.90	1.51	2.20	2.78	4.30	7.31	4.85
AVERAGE-REMOTE	5.22	5.69	7.92	8.33	19.76	3.83	1.80	1.82	1.26	3.23	5.71	10.22	8.52
AVERAGE-ALL	4.40	4.75	6.28	7.38	12.01	5.22	1.85	1.67	1.73	3.00	5.00	8.77	6.68

Table 3.4 Average RMSE Values of Both Local and Remote Trained Models over Ermenek Dam (ErmT means Ermenek Trained and AltT means Altinkaya Trained; AWEL_S, NDPI, NDWI_MCF and WI2015 are Water Detection Indices, ASTER and SRTM are DEMs, E means that model is estimating Ermenek Dam' s water level and A means model is estimating Altinkaya Dam' s water level)

	Jan.	Feb.	Mar.	Apr.	May	June	July	Aug.	Sep.	Oct.	Nov.	Dec.	Annual
ErmT-AWEL_S-ASTER-E	3.17	3.78	5.22	5.98	4.32	2.86	1.30	1.45	3.04	2.45	3.02	6.11	3.86
ErmT-NDPI-ASTER-E	3.70	2.22	5.36	6.75	5.95	4.84	1.58	1.55	2.42	2.01	4.13	4.61	4.10
ErmT-NDWI_MCF-ASTER-E	3.23	3.07	2.65	5.92	5.64	8.07	3.62	1.79	5.81	3.41	3.04	7.24	4.84
ErmT-WI2015-ASTER-E	2.01	2.29	4.62	6.79	4.64	3.09	1.32	1.78	2.51	2.15	5.26	5.50	3.85
ErmT-AWEL_S-SRTM-E	5.12	6.03	8.36	5.80	3.74	3.32	2.31	2.83	3.86	3.54	3.87	9.47	5.32
ErmT-NDPI-SRTM-E	2.90	3.35	3.37	5.56	3.30	5.24	0.81	1.62	2.96	2.22	4.88	4.09	3.63
ErmT-NDWI_MCF-SRTM-E	2.95	3.04	5.19	5.96	4.52	16.06	3.84	2.15	4.34	5.11	5.63	8.73	6.68
ErmT-WI2015-SRTM-E	6.91	11.79	3.43	7.34	5.29	11.02	2.64	2.39	4.22	4.06	9.45	13.81	7.82
AltT-AWEL_S-ASTER-E	9.12	6.46	12.04	10.20	17.58	3.32	1.75	1.40	1.53	2.24	9.55	25.92	10.95
AltT-NDPI-ASTER-E	5.54	4.45	5.51	15.96	7.21	9.95	4.26	3.49	2.21	8.76	11.71	9.14	8.28
AltT-NDWI_MCF-ASTER-E	6.33	12.35	8.28	7.61	33.50	3.46	4.39	3.98	5.06	4.10	4.25	4.65	10.81
AltT-WI2015-ASTER-E	7.14	6.12	10.68	8.04	22.40	5.23	3.68	3.01	4.74	2.75	6.19	8.27	8.31
AltT-AWEL_S-SRTM-E	4.98	1.39	10.05	9.05	14.32	2.55	2.30	3.24	5.08	3.72	5.94	21.61	8.94
AltT-NDPI-SRTM-E	3.42	3.44	2.46	8.72	5.01	6.50	2.00	1.75	1.75	4.62	8.05	6.82	5.13
AltT-NDWI_MCF-SRTM-E	7.58	12.43	9.91	7.92	35.16	3.53	7.35	7.24	8.62	4.76	3.44	4.83	11.82
AltT-WI2015-SRTM-E	4.81	5.22	12.32	8.49	25.52	4.65	5.04	4.26	6.09	4.31	6.47	9.46	11.82
AVERAGE-AWEL_S	5.60	4.41	8.92	7.76	9.99	3.01	1.91	2.23	3.38	2.99	5.60	15.78	7.27
AVERAGE-NDPI	3.89	3.36	4.17	9.25	5.37	6.63	2.16	2.10	2.33	4.40	7.19	6.17	5.28
AVERAGE-NDWI	5.02	7.72	6.51	6.85	19.71	7.78	4.80	3.79	5.96	4.35	4.09	6.36	8.54
AVERAGE-WI2015	5.22	6.36	7.76	7.66	14.46	6.00	3.17	2.86	4.39	3.32	6.84	9.26	7.95
AVERAGE-ASTER	5.03	5.09	6.79	8.41	12.66	5.10	2.74	2.31	3.42	3.49	5.89	8.93	6.88
AVERAGE-SRTM	4.83	5.84	6.88	7.35	12.11	6.61	3.29	3.18	4.62	4.04	5.97	9.85	7.64
AVERAGE-LOCAL	3.75	4.45	4.77	6.26	4.68	6.81	2.18	1.95	3.65	3.12	4.91	7.44	5.01
AVERAGE-REMOTE	6.12	6.48	8.91	9.50	20.09	4.90	3.84	3.55	4.38	4.41	6.95	11.34	9.51
AVERAGE-ALL	4.93	5.46	6.84	7.88	12.38	5.85	3.01	2.75	4.02	3.76	5.93	9.39	7.26

ERMENЕК TRAINED [LOCAL] ESTIMATION (ERMENЕК DAM)

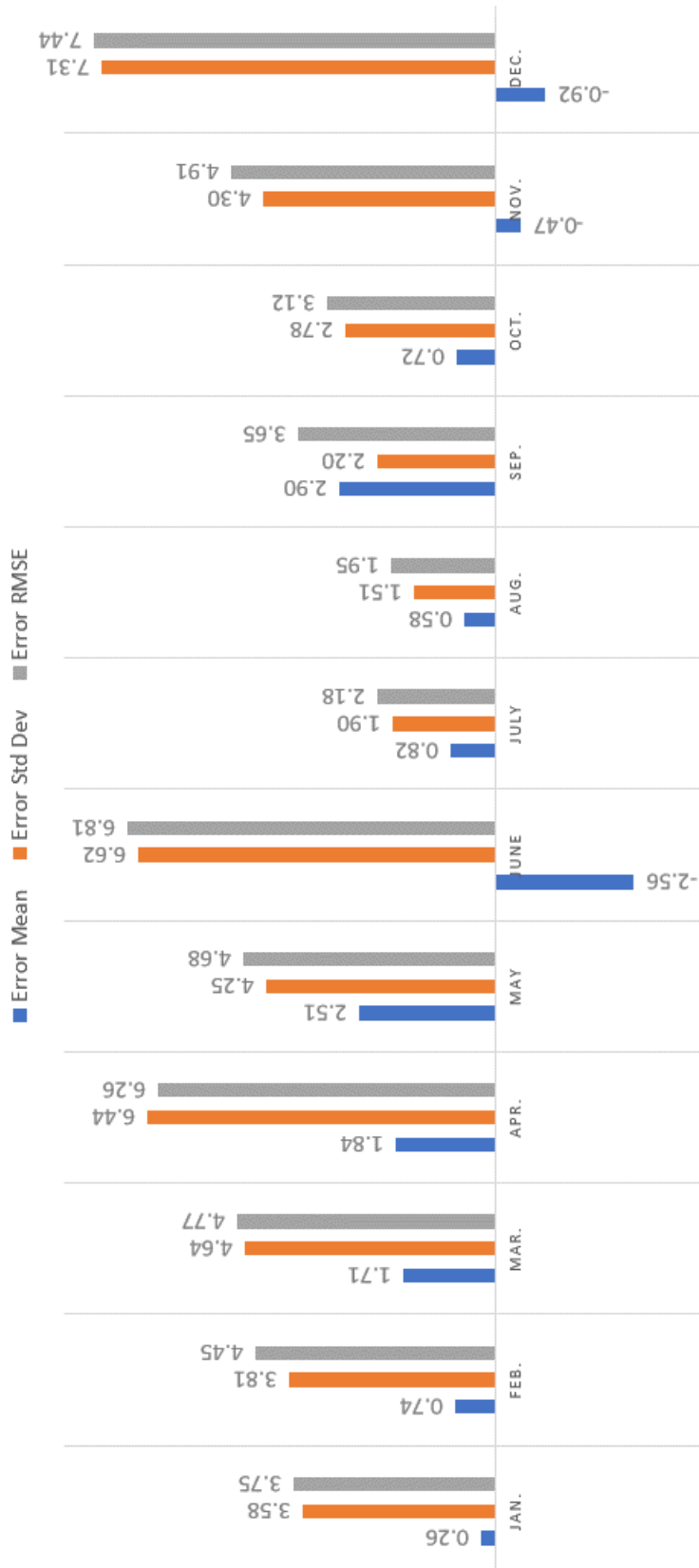


Figure 3.5 Average Statistics of Local Models ‘ Results over Ermenek Dam

ALTINKAYA TRAINED [REMOTE] ESTIMATION (ERMENEK DAM)

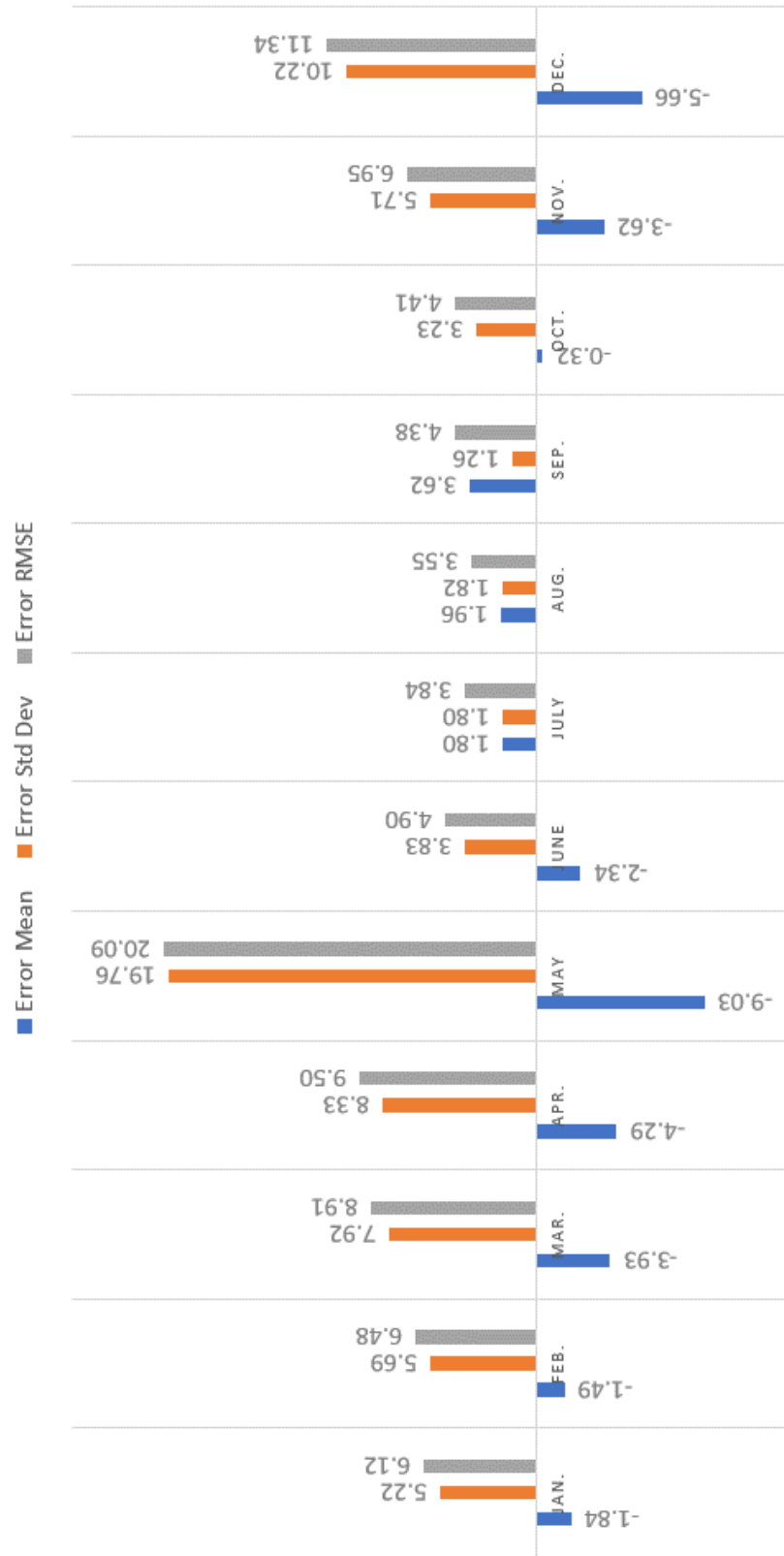


Figure 3.6 Average Statistics of Remote Models ‘ Results over Ermenek Dam

Table 3:5 Correlation Coefficient of Ermenek Dam Models

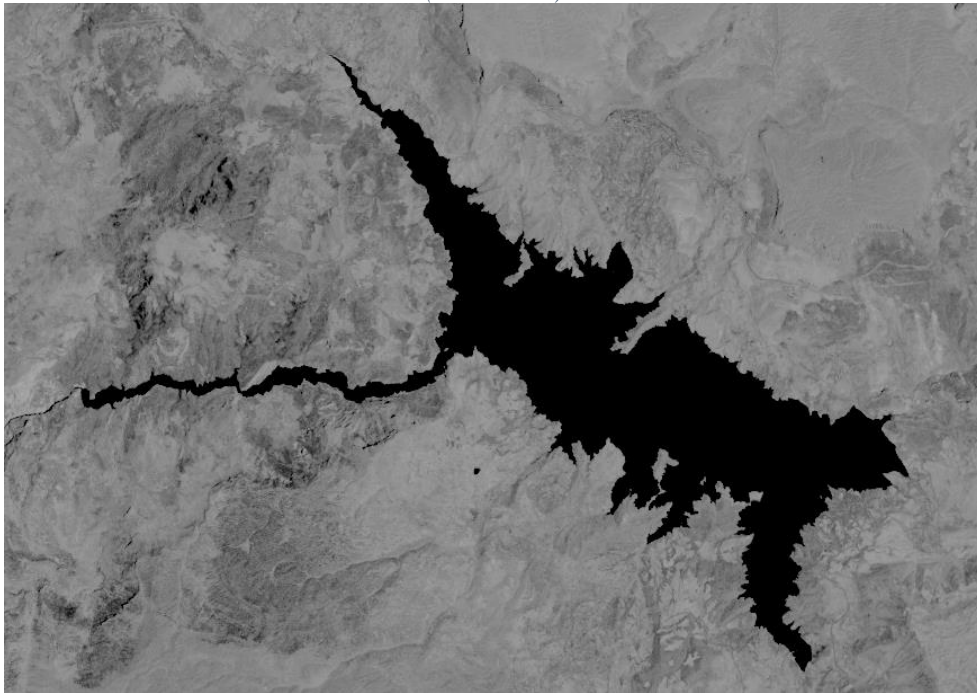
	Coefficient of Correlation
ErmT-AWEI_S-ASTER-E	0.77
ErmT-NDPI-ASTER-E	0.74
ErmT-NDWI_MCF-ASTER-E	0.63
ErmT-WI2015-ASTER-E	0.78
ErmT-AWEI_S-SRTM-E	0.64
ErmT-NDPI-SRTM-E	0.77
ErmT-NDWI_MCF-SRTM-E	0.44
ErmT-WI2015-SRTM-E	0.44
AltT-AWEI_S-ASTER-E	0.51
AltT-NDPI-ASTER-E	0.60
AltT-NDWI_MCF-ASTER-E	0.27
AltT-WI2015-ASTER-E	0.43
AltT-AWEI_S-SRTM-E	0.31
AltT-NDPI-SRTM-E	0.20
AltT-NDWI_MCF-SRTM-E	0.61
AltT-WI2015-SRTM-E	0.48
MEAN-ASTER	0.59
MEAN-SRTM	0.48
MEAN-LOCAL	0.65
MEAN-REMOTE	0.43
MEAN-ALL	0.54

Table 3:6 RMSE Results of Best Models based on Different Statistical Models for Estimation of Water Level of Ermenek Dam.

Statistical Methodology	Method Name	Jan.	Feb.	Mar.	Apr.	May	June	July	Aug.	Sep.	Oct.	Nov.	Dec.	Annual
ECDF	ErmT-NDPI-SRTM-E	2.90	3.35	3.37	5.56	3.30	5.24	0.81	1.62	2.96	2.22	4.88	4.09	3.63
ECDF	AltT-NDPI-SRTM-E	3.42	3.44	2.46	8.72	5.01	6.50	2.00	1.75	1.75	4.62	8.05	6.82	5.13
GEV	ErmT-NDPI-SRTM-E	24.28	24.81	21.69	36.25	25.90	24.52	19.91	21.31	25.24	18.53	24.44	39.71	26.25
Mean	ErmT-AWEI.S-SRTM-E	29.77	7.66	28.75	24.96	10.29	19.74	12.55	11.89	12.86	3.32	1.97	23.26	18.14
Mode	ErmT-AWEI.S-SRTM-E	43.12	19.74	37.20	43.51	21.41	36.15	26.55	18.21	22.33	7.50	4.52	39.06	29.58
Median	ErmT-AWEI.S-SRTM-E	29.05	6.53	29.47	23.54	9.06	18.44	10.50	10.06	11.02	2.69	1.68	23.14	17.43



*Figure 3.7 Water Area Detection based on NDPI Index over Ermenek Dam, Before Masking
(24.10.2017)*



*Figure 3.8 Water Area Detection based on NDPI Index over Ermenek Dam, Before Masking
(15.07.2017)*

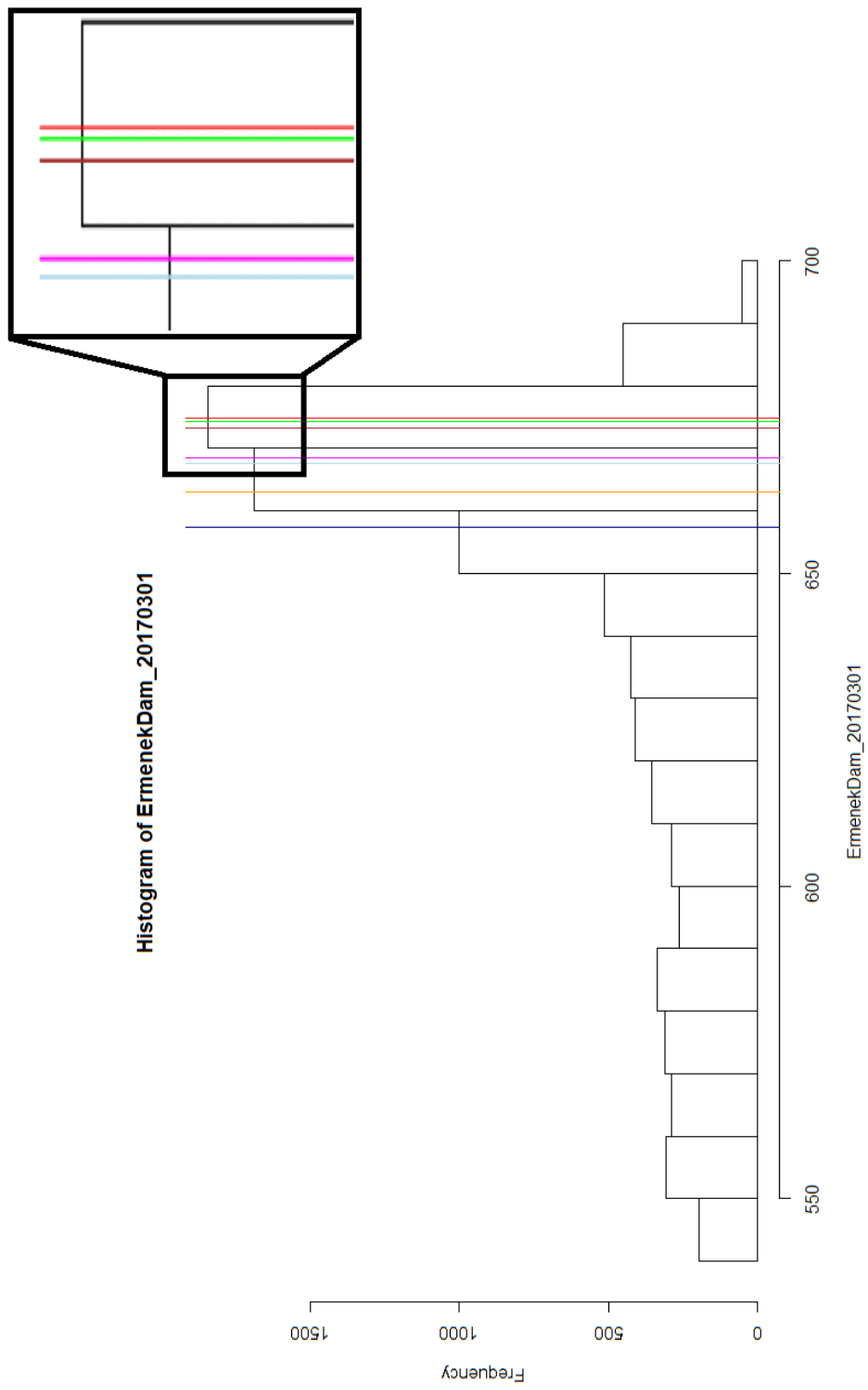


Figure 3.9 Elevation Histogram of Ermenek Dam showing Ground Data and Estimations of Different Statistical Approaches (01.03.2017)

3.4. Altinkaya Dam Estimations

Error statistics (bias, standard deviation and RMSE) and correlation coefficients for the water level estimates over Altinkaya dam are given in Table 3:7, Table 3:8, Table 3:9 and Table 3:10 below. In these tables, the best results for the local (Altinkaya Dam) training data is shown in blue while the remote (Ermenek Dam) training data is shown in purple. There are total 80 experiments (2 training datasets * 4 indices * 2 DEM * 5 Statistical Methodologies). Experiments are named as “Training-Indices-DEM-Test Location” where “Training” refers to local/remote training case (i.e., Ermenek or Altinkaya dam), “Indices” refer to each utilized index name (AWEI, NDPI, NDWI, or WI2015), “DEM” refer to the utilized DEM image (ASTER or SRTM), and “Test Location” refers to the site where the water elevation errors are calculated (“E” for Ermenek or “A” for Altinkaya). For example, “ErmT-AWEI_S-SRTM-A” refers to the experiment utilizes Ermenek dam values to find the necessary parameters in NMS optimization, AWEI index, and SRTM where the evaluations are validated over Altinkaya dam. Here, if the selected index (e.g., AWEI) has variants in literature, then the variant is defined with another substring separated by an underscore. For example, for the AWEI index shadow sensitive variant (AWEI_S) is used and for the NDWI index McFeeter’s variation (NDWI_MCF) is used.

Water level estimation error averages (i.e., zero mean error is regarded as unbiased) for 16 tested experiments belonging to ECDF statistical approach are shown in Table 3:7. Among the tested experiments, NDPI index & ASTER DEM and combination provided best results among the local models (-0.01 m average error) and WI2015 index & SRTM DEM provided best results among the remote models (-1.58 m average error). Overall, experiments utilized SRTM DEM yield smaller water level estimation bias than the ones utilized ASTER DEM. Additionally, local training clearly outperforms remote training in terms of average water level error (0.09 m and 2.84 m for the water level average errors of local and remote training respectively). Overall, autumn months (particularly September and October) and July

yield smaller water level estimation bias (~ 0.75 m error bias) than spring months (~ 2.5 m error bias) regardless from the index, training location, and DEM selection (Figure 3.12 and Figure 3.13). The best month in terms of bias is October with local training (0.27 m of bias).

Water level estimation error standard deviations for 16 tested experiments belonging to ECDF are shown in Table 3:8. Among the tested experiments, AWEI-S & ASTER DEM combination (just as the case of Ermenek Dam's water level estimation) provided best results (3.33 m error standard deviation) among the local models and NDPI & SRTM DEM among the remote models (3.84 m error standard deviation). Overall, experiments utilized ASTER DEM yield marginally smaller water level estimation error standard deviation than the ones utilized SRTM DEM. Similar to the error average results, local training is better than remote training in terms of water level estimation error standard deviation (on average 4.67 m and 4.97 m for the water level average errors of local and remote training respectively). The best month in terms of error standard deviation is a summer month, August (Error standard deviation of 2.52 m).

Water level estimation RMSE for 16 tested experiments belonging to ECDF are shown in Table 3:9. Among the tested experiments, AWEI_S & ASTER DEM combination provided best results (3.34 m RMSE) among the local models and AWEI_S & ASTER DEM among the remote models (5.09 m RMSE). Overall, experiments utilized SRTM DEM yield marginally smaller RMSE than the ones utilized ASTER DEM. Similar to the error average and standard deviation results, local training clearly outperforms remote training in terms of water level estimation RMSE (on average 4.65 m and 5.93 m for the water level average errors of local and remote training respectively). Overall, the best month in terms of RMSE is a summer month, August (RMSE of 3.38 m).

The linear relationship (i.e., correlation coefficient) between the monthly remotely sensed water level estimation and ground observations are given in

Table 3:10. Overall, all local and remote estimates are statistically significant considering the 0.26 threshold with respect to Fisher's Test. Among the experiments, ASTER DEM adds slightly higher linear predictive capability (i.e., average correlation coefficient of 0.53) than SRTM (i.e., average correlation coefficient of 0.49), while local training estimates yield much better predictions (i.e., average correlation coefficient of 0.54) than remote training estimates (i.e., average correlation coefficient of 0.48).

Time series of the most successful model for water level estimation of Altinkaya Dam is provided in Figure 3.10 in and its scatter plot versus ground data is provided in Figure 3.11. Overall, the remote sensing-base estimations accurately estimate the timing of increasing and decreasing trends. Higher error in 01.01.2019 estimation is due to lack of processable image for December 2018 and increased duration for interpolation.

Comparison between the best models of each statistical approaches (ECDF, GEV, mean, mode and median) is provided in Table 3:11. Both best models for local trained and remote trained approaches are provided for ECDF and as can be observed from the table, best model for water elevation detection is local trained ECDF based approach. Detailed comparison for a selected date (01.03.2017) is provided in Figure 3.14. Where red line (180.15 m) is the result of best local trained model based on ECDF approach (AWEI_S + ASTER), green line (179.67 m) is the ground data, brown line (182.68 m) is the result of best remote trained model based on ECDF approach (AWEI_S + SRTM), magenta line (169.95 m) is the result of best median approach, light blue line (168.97 m) is the result of best mean approach, dark blue line (160.0 m) is the result of best mode approach and the orange line (170.97 m) is the result of best GEV approach.

AWEI-S + ASTER [over Altinkaya with Local Training Dataset]

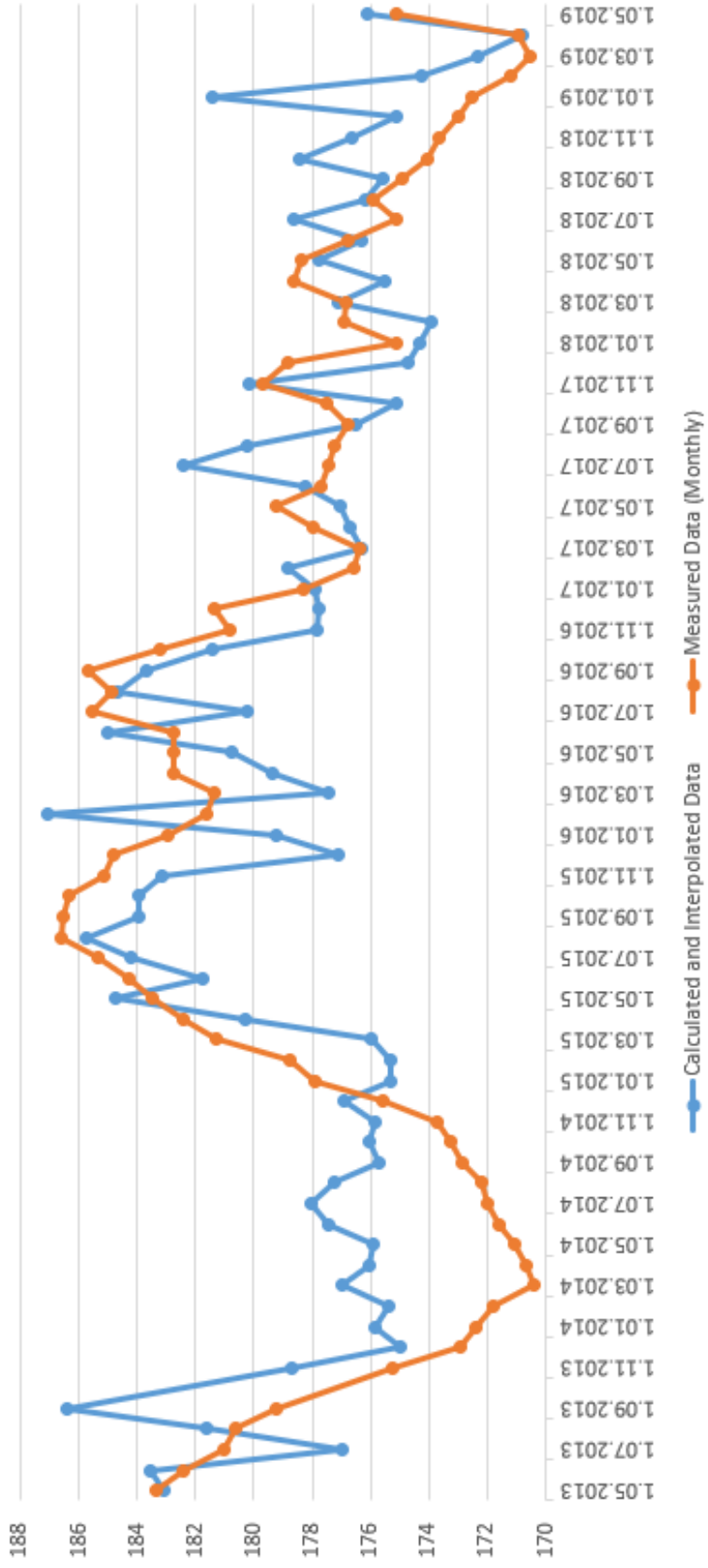


Figure 3.10 Time Series of Best (AWEI-S + ASTER) Model for Estimating Altinkaya Dam's Water Level

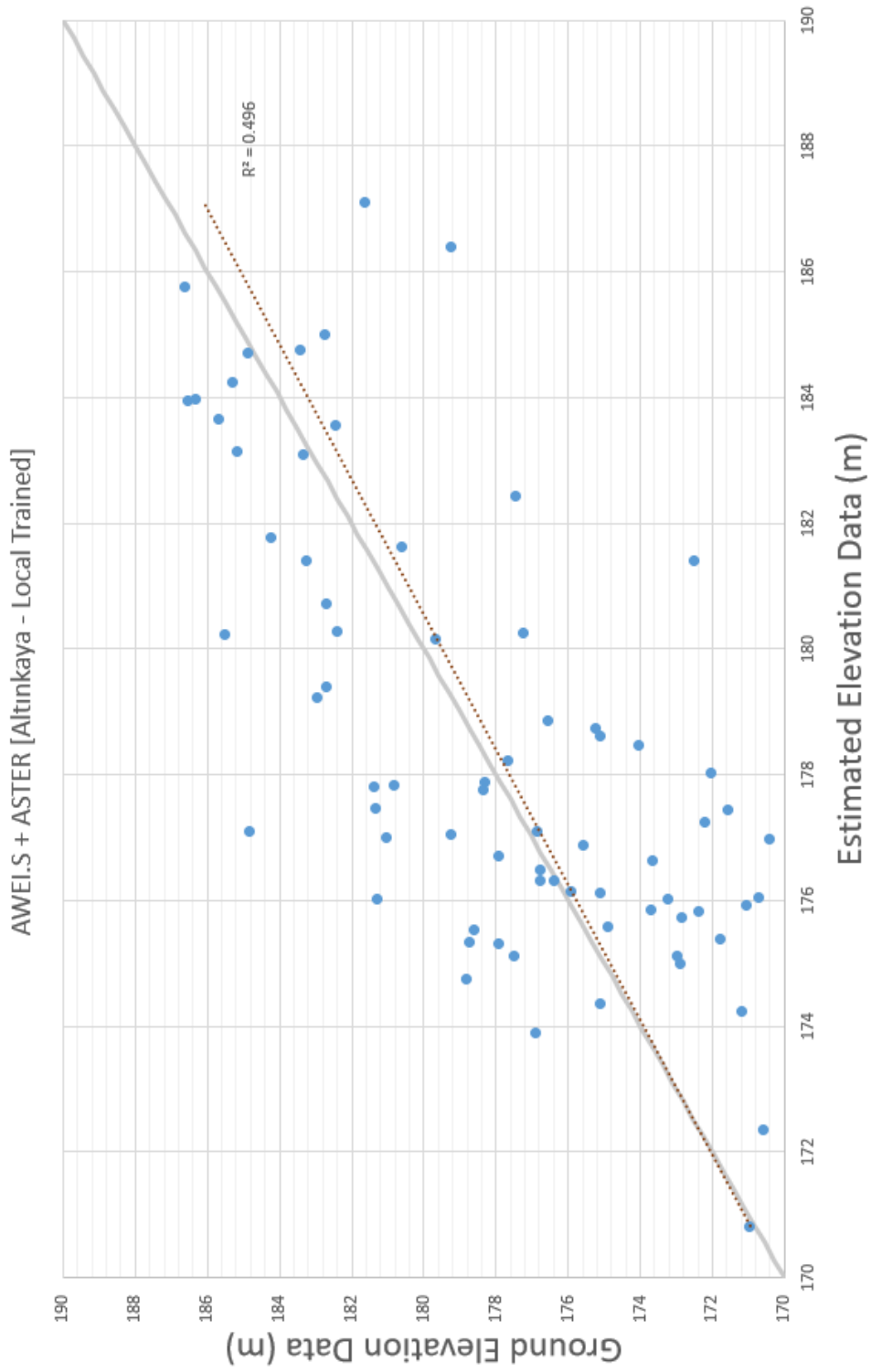


Figure 3.11 Ground Elevation vs Estimated Elevation Data Scatter Plot of Best Model for Altinkaya Dam

Table 3:7 Average Error Values of Both Local and Remote Trained Models over Altnkaya Dam (ErmT means Ermenek Trained and AItT means Altnkaya Trained; AWEL_S, NDPI, NDWI_MCF and Wl2015 are Water Detection Indices, ASTER and SRTM are DEMs, E means that model is estimating Ermenek Dam' s water level and A means model is estimating Altnkaya Dam' s water level)

	Jan.	Feb.	Mar.	Apr.	May	June	July	Aug.	Sep.	Oct.	Nov.	Dec.	Annual
AItT-AWEL_S-ASTER-A	0.81	1.33	-0.11	-0.76	0.30	0.85	0.68	1.38	0.97	0.13	0.67	-1.65	0.40
AItT-NDPI-ASTER-A	0.30	2.30	1.83	0.41	-1.45	1.65	-1.08	-0.22	-1.00	-0.33	0.52	-3.17	-0.01
AItT-NDWI_MCF-ASTER-A	1.19	-0.64	-2.56	0.29	1.48	-0.39	-1.36	0.84	0.29	-1.03	0.47	-0.97	-0.17
AItT-Wl2015-ASTER-A	0.21	-2.02	-0.12	-0.63	1.29	-0.04	-0.17	0.46	0.88	0.00	0.32	1.31	0.14
AItT-AWEL_S-SRTM-A	2.89	1.75	1.12	-2.01	1.83	-2.45	1.23	3.15	0.54	1.33	0.47	-1.57	0.65
AItT-NDPI-SRTM-A	0.86	2.75	3.35	1.92	-1.70	1.13	-2.49	-0.33	0.03	0.00	0.77	-2.82	0.28
AItT-NDWI_MCF-SRTM-A	1.29	-1.37	-1.98	-1.10	2.76	-0.74	0.14	2.95	0.70	0.47	1.43	-0.98	0.31
AItT-Wl2015-SRTM-A	0.58	-1.88	0.15	-3.19	1.62	-2.71	-0.38	0.88	-0.70	-0.80	-1.42	0.32	-0.62
ErmT-AWEL_S-ASTER-A	4.31	3.41	3.79	4.02	6.04	3.12	3.01	1.37	3.11	1.67	2.59	2.74	3.26
ErmT-NDPI-ASTER-A	5.01	6.34	6.29	8.85	8.47	3.84	3.97	3.60	4.61	5.02	6.91	2.23	5.43
ErmT-NDWI_MCF-ASTER-A	7.90	7.40	8.19	6.17	5.13	3.11	3.13	5.16	4.10	0.96	2.51	3.25	4.75
ErmT-Wl2015-ASTER-A	4.12	4.48	6.54	5.68	5.18	3.16	3.21	3.48	3.02	0.85	1.12	3.04	3.66
ErmT-AWEL_S-SRTM-A	3.87	1.98	2.43	2.18	5.73	2.35	2.70	1.07	1.13	-0.39	-0.90	-0.95	1.85
ErmT-NDPI-SRTM-A	1.75	3.30	3.48	7.24	6.04	6.67	2.50	3.26	3.28	2.92	3.59	-1.44	3.59
ErmT-NDWI_MCF-SRTM-A	6.92	4.28	5.79	3.19	4.36	1.68	0.11	1.54	-1.24	-2.89	-2.18	-1.55	1.77
ErmT-Wl2015-SRTM-A	-3.31	-1.29	1.61	3.03	4.80	1.08	-5.21	-4.60	-4.76	-3.66	-4.40	-3.69	-1.58
AVERAGE-AWEL_S	2.97	2.12	1.81	0.86	3.48	0.97	1.91	1.74	1.44	0.69	0.71	-0.36	1.54
AVERAGE-NDPI	1.98	3.67	3.74	4.61	2.84	3.32	0.73	1.58	1.73	1.90	2.95	-1.30	2.32
AVERAGE-NDWI	4.33	2.42	2.36	2.14	3.43	0.91	0.50	2.62	0.96	-0.62	0.56	-0.06	1.67
AVERAGE-Wl2015	0.40	-0.18	2.04	1.22	3.22	0.37	-0.64	0.06	-0.39	-0.90	-1.09	0.25	0.40
AVERAGE-ASTER	2.98	2.83	2.98	3.00	3.31	1.91	1.43	2.01	2.00	0.91	1.89	0.85	2.18
AVERAGE-SRTM	1.86	1.19	2.00	1.41	3.18	0.88	-0.18	0.99	-0.13	-0.38	-0.33	-1.58	0.78
AVERAGE-LOCAL	1.02	0.28	0.21	-0.63	0.77	-0.34	-0.43	1.14	0.22	-0.03	0.41	-1.19	0.12
AVERAGE-REMOTE	3.82	3.74	4.77	5.04	5.72	3.13	1.68	1.86	1.66	0.56	1.15	0.45	2.84
AVERAGE-ALL	2.42	2.01	2.49	2.21	3.24	1.39	0.62	1.50	0.94	0.27	0.78	-0.37	1.48

Table 3:8 Average Error Standard Deviation Values of Both Local and Remote Trained Models over Altminkaya Dam (ErmT means Ermenek Trained and AItT means Altminkaya Trained; AWEL_S, NDPI, NDWI_MCF and WI2015 are Water Detection Indices, ASTER and SRTM are DEMs, E means that model is estimating Ermenek Dam' s water level and A means model is estimating Altminkaya Dam' s water level)

	Jan.	Feb.	Mar.	Apr.	May	June	July	Aug.	Sep.	Oct.	Nov.	Dec.	Annual
AItT-AWEL_S-ASTER-A	4.66	3.67	4.23	3.21	2.41	2.43	4.81	2.23	3.61	3.22	2.69	4.08	3.33
AItT-NDPI-ASTER-A	4.92	3.93	5.04	4.79	6.16	3.03	2.95	2.97	5.42	5.63	2.78	5.93	4.51
AItT-NDWI_MCF-ASTER-A	4.72	4.87	8.85	3.61	2.84	4.38	4.17	2.51	4.52	4.67	3.84	8.27	4.81
AItT-WI2015-ASTER-A	6.00	5.44	5.23	3.50	2.48	5.37	4.35	2.40	4.04	3.33	4.51	6.10	4.29
AItT-AWEL_S-SRTM-A	3.05	3.16	5.65	4.85	2.99	10.71	5.41	1.89	3.77	3.56	2.97	3.12	4.89
AItT-NDPI-SRTM-A	3.78	2.96	4.77	3.30	3.06	5.21	5.17	2.80	4.33	5.21	2.53	4.94	4.22
AItT-NDWI_MCF-SRTM-A	5.01	4.95	10.15	5.56	3.42	5.15	5.72	2.61	4.68	4.55	3.58	8.30	5.43
AItT-WI2015-SRTM-A	5.56	4.88	6.69	5.16	3.11	8.15	5.19	1.98	4.37	4.15	5.54	6.48	5.16
ErmT-AWEL_S-ASTER-A	4.55	2.58	5.16	3.54	2.07	7.06	4.51	2.35	3.55	3.88	3.38	6.33	4.39
ErmT-NDPI-ASTER-A	3.79	3.55	5.26	3.46	5.44	7.01	4.80	2.31	4.33	3.69	2.58	5.00	5.08
ErmT-NDWI_MCF-ASTER-A	5.61	3.67	5.78	2.63	2.87	6.80	3.82	3.73	5.09	4.78	3.47	9.16	5.45
ErmT-WI2015-ASTER-A	5.06	4.08	5.50	2.82	2.49	6.79	4.01	2.42	3.47	3.24	4.48	5.39	4.88
ErmT-AWEL_S-SRTM-A	4.84	2.74	5.24	4.51	2.29	6.67	4.39	1.38	3.83	4.80	5.65	7.42	4.77
ErmT-NDPI-SRTM-A	3.75	3.30	4.63	2.86	2.05	2.53	3.22	2.31	3.51	4.46	2.22	4.70	3.84
ErmT-NDWI_MCF-SRTM-A	5.57	4.00	6.53	2.58	3.35	6.26	4.40	3.73	5.12	4.54	3.79	9.48	5.74
ErmT-WI2015-SRTM-A	5.00	4.47	5.21	2.71	3.13	6.36	5.43	2.68	5.70	4.65	5.37	6.34	5.64
AVERAGE-AWEL_S	4.27	3.04	5.07	4.03	2.44	6.72	4.78	1.96	3.69	3.87	3.67	5.24	4.34
AVERAGE-NDPI	4.06	3.43	4.92	3.60	4.18	4.45	4.04	2.60	4.40	4.75	2.52	5.14	4.41
AVERAGE-NDWI	5.23	4.37	7.83	3.59	3.12	5.65	4.53	3.15	4.85	4.63	3.67	8.80	5.36
AVERAGE-WI2015	5.41	4.72	5.66	3.55	2.80	6.67	4.75	2.37	4.39	3.84	4.97	6.08	4.99
AVERAGE-ASTER	4.91	3.97	5.63	3.44	3.34	5.36	4.18	2.62	4.25	4.06	3.47	6.28	4.59
AVERAGE-SRTM	4.57	3.81	6.11	3.94	2.92	6.38	4.87	2.42	4.41	4.49	3.95	6.35	4.96
AVERAGE-LOCAL	4.71	4.23	6.33	4.25	3.31	5.55	4.72	2.42	4.34	4.29	3.55	5.90	4.58
AVERAGE-REMOTE	4.77	3.55	5.41	3.14	2.96	6.19	4.32	2.62	4.32	4.25	3.87	6.73	4.97
AVERAGE-ALL	4.74	3.89	5.87	3.69	3.13	5.87	4.52	2.52	4.33	4.27	3.71	6.31	4.78

Table 3:9 Average RMSE Values of Both Local and Remote Trained Models over Altnkaya Dam (ErmT means Ermenek Trained and Alft means Altnkaya Trained; AWEL_S, NDPI, NDWI_MCF and WI2015 are Water Detection Indices, ASTER and SRTM are DEMs, E means that model is estimating Ermenek Dam' s water level and A means model is estimating Altnkaya Dam' s water level)

	Jan.	Feb.	Mar.	Apr.	May	June	July	Aug.	Sep.	Oct.	Nov.	Dec.	Annual
Alft-AWEL_S-ASTER-A	4.33	3.61	3.86	3.03	2.25	2.43	4.44	2.46	3.44	2.88	2.54	4.08	3.34
Alft-NDPI-ASTER-A	4.50	4.26	4.95	4.39	5.88	3.25	2.90	2.72	5.05	5.05	2.59	6.27	4.47
Alft-NDWI_MCF-ASTER-A	4.46	4.50	8.47	3.30	3.02	4.08	4.04	2.44	4.14	4.30	3.54	7.61	4.78
Alft-WI2015-ASTER-A	5.48	5.36	4.77	3.26	2.63	4.97	3.98	2.24	3.79	2.98	4.13	5.72	4.27
Alft-AWEL_S-SRTM-A	4.01	3.37	5.28	4.86	3.32	10.21	5.09	3.59	3.49	3.45	2.75	3.25	4.90
Alft-NDPI-SRTM-A	3.55	3.85	5.50	3.57	3.30	4.96	5.34	2.58	3.96	4.66	2.43	5.32	4.20
Alft-NDWI_MCF-SRTM-A	4.75	4.72	9.48	5.19	4.20	4.82	5.23	3.80	4.33	4.09	3.57	7.64	5.40
Alft-WI2015-SRTM-A	5.11	4.84	6.11	5.69	3.31	8.02	4.76	2.01	4.05	3.79	5.25	5.93	5.17
ErmT-AWEL_S-ASTER-A	5.98	4.15	6.04	5.15	6.33	7.24	5.11	2.54	4.49	3.86	4.03	6.39	5.27
ErmT-NDPI-ASTER-A	6.09	7.12	7.91	9.39	9.86	7.32	5.91	4.18	6.07	6.01	7.30	5.08	7.03
ErmT-NDWI_MCF-ASTER-A	9.42	9.59	11.25	5.93	6.45	6.89	4.75	6.95	6.39	4.33	4.94	8.69	7.42
ErmT-WI2015-ASTER-A	6.19	5.83	8.24	6.24	5.67	7.01	4.87	4.12	4.37	3.02	4.24	5.79	5.63
ErmT-AWEL_S-SRTM-A	5.88	3.19	5.37	4.66	6.11	6.53	4.84	1.65	3.68	4.31	5.23	6.84	5.09
ErmT-NDPI-SRTM-A	3.84	4.47	5.48	7.70	6.34	7.06	3.86	3.88	4.59	4.94	4.12	4.52	5.24
ErmT-NDWI_MCF-SRTM-A	8.59	5.62	8.31	3.96	5.35	5.96	4.02	3.74	4.83	4.98	4.09	8.79	5.97
ErmT-WI2015-SRTM-A	5.64	4.28	5.03	3.91	5.61	5.91	7.19	5.21	7.06	5.54	6.58	6.86	5.82
AVERAGE-AWEL_S	5.05	3.58	5.14	4.43	4.50	6.60	4.87	2.56	3.77	3.63	3.64	5.14	4.65
AVERAGE-NDPI	4.50	4.93	5.96	6.26	6.35	5.65	4.50	3.34	4.91	5.16	4.11	5.30	5.24
AVERAGE-NDWI	6.81	6.11	9.38	4.60	4.75	5.44	4.51	4.23	4.92	4.43	4.03	8.18	5.89
AVERAGE-WI2015	5.61	5.08	6.04	4.77	4.30	6.48	5.20	3.39	4.82	3.83	5.05	6.07	5.22
AVERAGE-ASTER	5.81	5.55	6.94	5.09	5.26	5.40	4.50	3.46	4.72	4.05	4.16	6.20	5.28
AVERAGE-SRTM	5.17	4.29	6.32	4.94	4.69	6.68	5.04	3.31	4.50	4.47	4.25	6.14	5.22
AVERAGE-LOCAL	4.53	4.31	6.05	4.16	3.49	5.34	4.47	2.73	4.03	3.90	3.35	5.73	4.57
AVERAGE-REMOTE	6.45	5.53	7.20	5.87	6.46	6.74	5.07	4.03	5.18	4.62	5.07	6.62	5.93
AVERAGE-ALL	5.49	4.92	6.63	5.01	4.98	6.04	4.77	3.38	4.61	4.26	4.21	6.17	5.25

ALTINKAYA TRAINED [LOCAL] ESTIMATION (ALTINKAYA DAM)

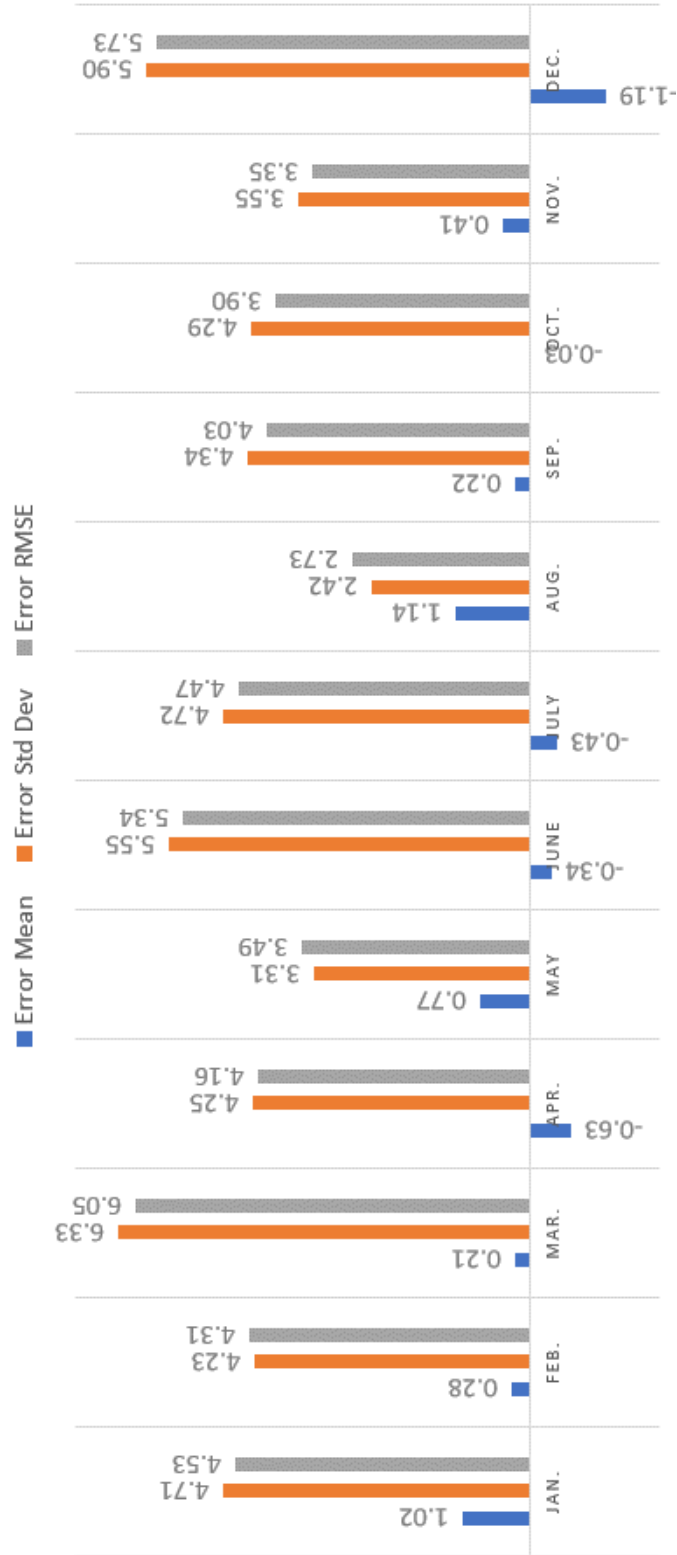


Figure 3.12 Average Statistics of Local Models ‘ Results over Altinkaya Dam

ERMENEK TRAINED [REMOTE] ESTIMATION (ALTINKAYA DAM)

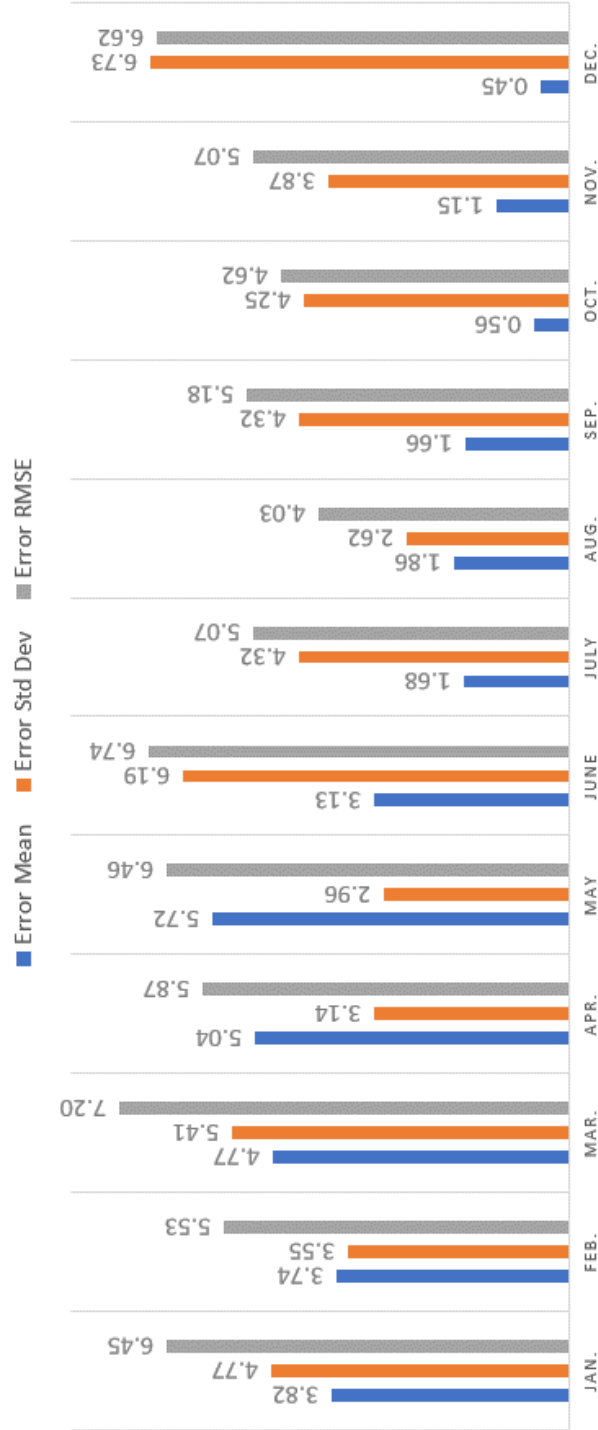


Figure 3.13 Average Statistics of Remote Models ‘ Results over Altinkaya Dam

Table 3:10 Correlation Coefficient of Altinkaya Dam Models

	Coefficient of Correlation
AltT-AWEI_S-ASTER-A	0.70
AltT-NDPI-ASTER-A	0.54
AltT-NDWI_MCF-ASTER-A	0.48
AltT-WI2015-ASTER-A	0.54
AltT-AWEI_S-SRTM-A	0.51
AltT-NDPI-SRTM-A	0.61
AltT-NDWI_MCF-SRTM-A	0.49
AltT-WI2015-SRTM-A	0.47
ErmT-AWEI_S-ASTER-A	0.56
ErmT-NDPI-ASTER-A	0.55
ErmT-NDWI_MCF-ASTER-A	0.38
ErmT-WI2015-ASTER-A	0.50
ErmT-AWEI_S-SRTM-A	0.48
ErmT-NDPI-SRTM-A	0.66
ErmT-NDWI_MCF-SRTM-A	0.26
ErmT-WI2015-SRTM-A	0.42
MEAN-ASTER	0.53
MEAN-SRTM	0.49
MEAN-LOCAL	0.54
MEAN-REMOTE	0.48
MEAN-ALL	0.51

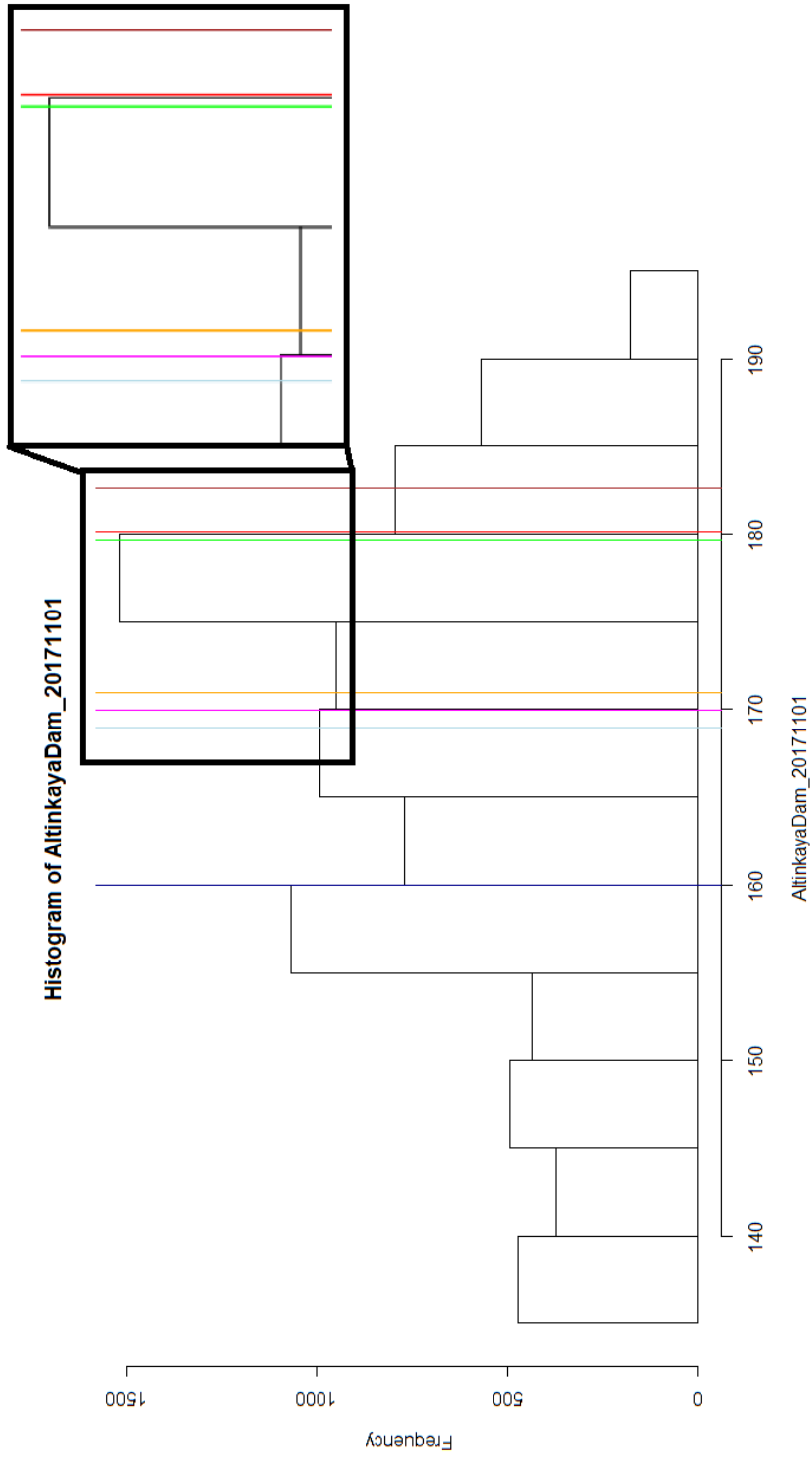


Figure 3.14 Elevation Histogram of Altinkaya Dam showing Ground Data and Estimations of Different Statistical Approaches (01.11.2017)

Table 3:11 RMSE Results of Best Models based on Different Statistical Models for Estimation of Water Level of Altmkaya Dam.

Statistical Methodology	Method Name	Jan.	Feb.	Mar.	Apr.	May	June	July	Aug.	Sep.	Oct.	Nov.	Dec.	Annual
ECDF	AItT-AWEI_S-ASTER-A	4.33	3.61	3.86	3.03	2.25	2.43	4.44	2.46	3.44	2.88	2.54	4.08	3.34
ECDF	ErmT-AWEI_S-SRTM-A	5.88	3.19	5.37	4.66	6.11	6.53	4.84	1.65	3.68	4.31	5.23	6.84	5.09
GEV	AItT-NDPI-ASTER-A	9.53	11.27	18.16	7.66	10.90	9.75	13.42	16.03	12.42	16.92	17.45	13.56	13.37
Mean	AItT-NDPI-ASTER-A	12.27	11.49	5.86	5.46	6.93	8.83	15.69	9.91	14.11	12.09	10.99	19.18	11.64
Mode	AItT-NDPI-ASTER-A	11.76	20.38	9.26	6.66	8.83	6.60	13.47	6.69	7.98	13.65	11.11	13.07	11.34
Median	ErmT-AWEI.S-SRTM-E	11.42	11.68	5.53	6.20	7.98	7.91	15.12	8.02	12.75	11.49	10.97	17.90	11.06

CHAPTER 4

SUMMARY AND CONCLUSION

In this study, Landsat 8 images are used to estimate the water levels of Ermenek and Altinkaya dam reservoirs between May 2013 and May 2019. Total around 269 images are used for both dams. Water levels estimations based on 16-day periods are performed using remote sensing datasets and validated using monthly DSI observations. Estimation errors (i.e., performances) of four different indices, 2 different DEM images, and 2 different training datasets and 5 different statistical modelling approaches are studied.

On average, the water level estimate RMSE values are found as 3.63 m and 3.34 m over Ermenek and Altinkaya dams, respectively, while correlation coefficient values of the best models are found as 0.78 and 0.77 over Ermenek and Altinkaya dams, respectively. Even though these statistics imply the estimates are reasonable, there still exists room for improvements. Bias could be very easily eliminated in case ground observations of the region of interest could be found; elimination of bias would also reduce the RMSE to the levels of error standard deviation values.

Average slope over the Ermenek Dam is calculated as 14.99 degrees when ASTER DEM is utilized and 14.54 degrees when SRTM DEM is utilized. Considering the spatial resolution of a Landsat pixel is 30 m (Department of the Interior U.S. Geological Survey, 2019), this slope implies there is elevation difference of 7.53 or 7.79 m (for SRTM or ASTER, respectively) within a single Landsat pixel. Around the land-water borders, if half of the Landsat pixel contains water and the other half contains land, then on average ~1.9 m (quarter of 7.53 or 7.79) error will occur regardless from the classification of this pixel as water or land. While 1.9m error is the upper limit for the errors for the land-water mixed pixels, steep slopes behave as

source of added uncertainty in the water elevation level estimation where the land-water border does not generally overlap with the Landsat pixel border. Considering this upper limit, the RMSE value of 3.63 m for the NDPI & SRTM combination is a reasonable accuracy, implying the model performance can be considered as useful. Although Landsat has the advantage of large historical data availability, same model can be applied to Sentinel platform which has spatial resolution of 10m (ESA, n.d.-d); however, an independent parameter tuning step is necessary for this implementation as the spectral windows of Landsat 8 and Sentinel images are different. Accordingly, above mentioned spatial resolution-based error is expected to decrease when 10m resolution Sentinel images are used (i.e., for a product with 10m spatial resolution this added error upper limit becomes about 0.60 m).

Overall, the error statistics show a strong seasonality that errors are lower during the summer months than winter months over both Ermenek dam (Figures 3.3 and 3.4) and Altinkaya dam (Figures 3.10 and 3.11). The reason for this behavior is probably due to the fact that the summer months are less cloudy than the winter months, where the haze of thin cloud layers contribute considerably to the errors of the estimated water levels. Moreover, it should also be noted that ice and snow cover increase in winter months. In addition to these, April is a special month for Ermenek Dam since it has higher RMSE values than the months before and after it. Reason of this can be explained with the limnology report of the Ermenek Dam that concludes that, due to melting of snow cover, algae population increases in April (Çevlik, 2013) and this affects the results of Green Band of Landsat 8.

Overall, DEM dataset source (i.e., ASTER or SRTM) selection does not make a consistent impact over the water level estimation errors; some estimates benefit from ASTER images better than SRTM and some vice versa. Hence, it is not possible to make a general conclusion about the added utility of the DEM images used in this study. On the other hand, among the four indices used in this study, NDPI performed marginally better than other indices over Ermenek dam, while AWEI_S performed better than other indices over Altinkaya dam.

On the other hand, DEM rasters have zero valued pixels for existing water bodies that persist throughout the production of the DEM model. In addition to this, SRTM also have problems for mountainous areas. In order to cope with these problems an old topographic map is incorporated with DEMs but a bathymetry model based on Hyperion images may be developed and utilized too.

About the different between the local and the remote training data selection, models based on local training data are found to be much better (i.e., smaller error average, standard deviation, and RMSE). Among the error statistics, the error average could be handled by adding/removing a constant in case ground observations are available for a limited time period. However, the random errors occur in time and contribute to the error standard deviation cannot be handled as easy as the error averages. For practical point of view, the temporal variability of the water level estimates is more important; accordingly, the local training also considerably reduce the error standard deviations. Therefore, consistent with the existing literature, it is advised that water level estimation models should be trained for each dam of interest with its own historical data.

Another source of error is conflict between the data periods provided by governmental institutions and Landsat's temporal resolution. DSI observations are representative for the beginning of each month, while Landsat 8 images are only available biweekly and are available on various days of the month. This conflict required this research to utilize a linear interpolation method based on inverse weights assigned with respect to the number of days between the image acquisition date and governmental data measurement date. Alternatively, MODIS images could be also utilized to reduce the errors added via such linear interpolation. Even though MODIS image have much lower spatial resolution (500m) than Landsat 8 image spatial resolution (30m), some algorithms can be used to fill in the temporal gap between the Landsat images via using MODIS datasets (F. Gao, Masek, Schwaller, & Hall, 2006).

This study should be extended using higher resolution satellite images (i.e. Sentinel) over various locations including more lakes and dams (i.e., entire Turkey), perhaps using much longer datasets (i.e., using entire Landsat archive), where the training should be carried out using local datasets if available. |

REFERENCES

- Ackerman, S., Strabala, K., Menzel, P., Frey, R., Moeller, C., Gumley, L., ... Zhang, H. (2010). Discriminating clear-sky from cloud with MODIS algorithm theoretical basis document (MOD35).
- Ataol, M. (2010). Burdur Gölü'nde Seviye Değişimleri. *Coğrafi Bilimler Dergisi*, 8(1), 077–092. https://doi.org/10.1501/cogbil_0000000105
- Avisse, N., Tilmant, A., François Müller, M., & Zhang, H. (2017). Monitoring small reservoirs' storage with satellite remote sensing in inaccessible areas. *Hydrology and Earth System Sciences*, 21(12), 6445–6459. <https://doi.org/10.5194/hess-21-6445-2017>
- Bahadır, M. (2013). Akşehir Gölü'nde Alansal Değişimlerin Uzaktan Algılama Teknikleri İle Belirlenmesi. *Marmara Coğrafya Dergisi*, (28), 246–275.
- Berthier, E., Arnaud, Y., Vincent, C., & Rémy, F. (2006). Biases of SRTM in high-mountain areas: Implications for the monitoring of glacier volume changes. *Geophysical Research Letters*, 33(8). <https://doi.org/10.1029/2006GL025862>
- Bhagat, V. S., & Sonawane, K. R. (2011). Use of Landsat ETM + data for delineation of water bodies in hilly zones. *Journal of Hydroinformatics*, 661–671. <https://doi.org/10.2166/hydro.2010.018>
- Cambridge University Press. (2013). *Cambridge Advanced Learner's Dictionary* (4th ed.). Cambridge University Press.
- Çevlik, H. (2013). *Ermenek Baraj Gölü Limnolojisi*. Ankara.
- Coltin, B., McMichael, S., Smith, T., & Fong, T. (2016). Automatic boosted flood mapping from satellite data. *International Journal of Remote Sensing*, 37(5), 993–1015. <https://doi.org/10.1080/01431161.2016.1145366>

- Crist, E. P. (1985). A TM Tasseled Cap Equivalent Transformation for Reflectance Factor Data. *Remote Sensing Of Environment*, (17), 301–306.
- Danaher, T., & Collett, L. (2006). Development, optimisation and multi-temporal application of a simple Landsat based water index. In *13th Australasian Remote Sensing and Photogrammetry Conference*. Canberra, Australia (Vol.29).
- Demirkesen, A. C. (2003). Sayısal Yükseklik Modellerinin Analizi ve Sel Basman Alanlarının Belirlenmesi. In *TUJK 2003 Yılı Bilimsel Toplantısı, Coğrafi Bilgi Sistemleri ve Jeodezik Ağlar Çalıştayı*. Konya.
- Department of the Interior U.S. Geological Survey. (2019). LANDSAT 8 (L8) DATA USERS HANDBOOK Version 4.0 April 2019. Retrieved May 15, 2019, from https://prd-wret.s3-us-west-2.amazonaws.com/assets/palladium/production/atoms/files/LSDS-1574_L8_Data_Users_Handbook_v4.0.pdf
- Du, Y., Zhang, Y., Ling, F., Wang, Q., Li, W., & Li, X. (2016). Water bodies' mapping from Sentinel-2 imagery with Modified Normalized Difference Water Index at 10-m spatial resolution produced by sharpening the swir band. *Remote Sensing*, 8(4). <https://doi.org/10.3390/rs8040354>
- Elkhrachy, I. (2018). Vertical accuracy assessment for SRTM and ASTER Digital Elevation Models: A case study of Najran city, Saudi Arabia. *Ain Shams Engineering Journal*, 9(4), 1807–1817. <https://doi.org/10.1016/j.asej.2017.01.007>
- ESA. (n.d.-a). JASON-2/OSTM. Retrieved July 29, 2019, from <https://directory.eoportal.org/web/eoportal/satellite-missions/j/jason-2>
- ESA. (n.d.-b). SAR Instrument. Retrieved July 29, 2019, from <https://sentinel.esa.int/web/sentinel/technical-guides/sentinel-1-sar/sar-instrument>
- ESA. (n.d.-c). Sentinel-1 Operations. Retrieved July 29, 2019, from

https://m.esa.int/Our_Activities/Operations/Sentinel-1_operations

ESA. (n.d.-d). Sentinel-2 Mission Details. Retrieved August 25, 2019, from <https://earth.esa.int/web/guest/missions/esa-operational-eo-missions/sentinel-2>

Feyisa, G. L., Meilby, H., Fensholt, R., & Proud, S. R. (2014). Automated Water Extraction Index: A new technique for surface water mapping using Landsat imagery. *Remote Sensing of Environment*, 140, 23–35. <https://doi.org/10.1016/j.rse.2013.08.029>

Fisher, A., Flood, N., & Danaher, T. (2016). Comparing Landsat water index methods for automated water classification in eastern Australia. *Remote Sensing of Environment*, 175, 167–182. <https://doi.org/10.1016/j.rse.2015.12.055>

Gao, B. (1996). NDWI - A Normalized Difference Water Index for Remote Sensing of Vegetation Liquid Water From Space. *Remote Sensing of Environment*, 58(257), 257–266.

Gao, F., Masek, J., Schwaller, M., & Hall, F. (2006). On the blending of the landsat and MODIS surface reflectance: Predicting daily landsat surface reflectance. *IEEE Transactions on Geoscience and Remote Sensing*, 44(8), 2207–2218. <https://doi.org/10.1109/TGRS.2006.872081>

Geymen, A. (2017). Coğrafi Bilgi Sistemi Kullanılarak Su Havzalarındaki Arazi Kullanım Değişikliği ve Çevresel Etkilerin İzlenmesi : Elmalı Havzası Örneği Monitoring of Environmental Impacts and Land-Use Changes in Water Basin Using Geographical Information Systems : Elmalı. *Iğdır Üni. Fen Bilimleri Enst. Der.*, 7(1), 171–181.

Google. (n.d.-a). Altınkaya Dam and Its Reservoir. Retrieved July 23, 2019, from <https://www.google.com/maps/place/Tepebaşı,+Altınkaya+Barajı,+55400+Bafra%2FSamsun/@41.3476287,35.2893921,45500m/data=!3m1!1e3!4m5!3m4!1s0x4086248c7991a785:0x1e5f4e67980e2138!8m2!3d41.3667686!4d35.7245146>

Google. (n.d.-b). Ermenek Dam and Its Reservoir. Retrieved July 23, 2019, from

<https://www.google.com/maps/place/Ermenek+Dam,+70402+Ağaççatı%2FErmenek%2FKaraman/@36.572723,32.8124111,28942m/data=!3m1!1e3!4m5!3m4!1s0x14dbe45ff494b3b1:0xb4778dbfa526f865!8m2!3d36.5682!4d32.965>

Huang, C., Nguyen, B. D., Zhang, S., Cao, S., & Wagner, W. (2017). A Comparison of Terrain Indices toward Their Ability in Assisting Surface Water Mapping from Sentinel-1 Data. *ISPRS International Journal of Geo-Information*, 6(5), 140. <https://doi.org/10.3390/ijgi6050140>

Jain, A. O., Thaker, T., Chaurasia, A., Patel, P., & Singh, A. K. (2018). *Vertical accuracy evaluation of SRTM-GL1, GDEM-V2, AW3D30 and CartoDEM-V3.1 of 30-m resolution with dual frequency GNSS for lower Tapi Basin India. Geocarto International* (Vol. 33). Taylor & Francis. <https://doi.org/10.1080/10106049.2017.1343392>

Karabulut, M. (2015). Farklı Uzaktan Algılama Teknikleri Kullanılarak Göksu Deltası Göllerinde Zamansal Değişimlerin İncelenmesi. *The Journal of International Social Research*, 8(37).

Karaman, M., Özelkan, E., & Taşdelen, S. (2018). Dar Nehirlerin Sentinel2-A Uydu Görüntüleri ile Belirlenebilirliğinde Havza Hidrojeolojisinin Etkisi: Karamenderes (Çanakkale) Örneği. *Doğal Afetler ve Çevre Dergisi*, 90(532), 140–155. <https://doi.org/10.21324/dacd.416514>

Kauth, R. J., & Thomas, G. S. (1976). The Tasseled Cap -- A Graphic Description of the Spectral-Temporal Development of Agricultural Crops as Seen by LANDSAT. In *Symposium on Machine Processing of Remotely Sensed Data June*. Indiana: The Institute of Electrical and Electronics Engineers, Inc. Copyright.

Kolecka, N., & Kozak, J. (2014). Assessment of the Accuracy of SRTM C- and X-Band High Mountain Elevation Data: A Case Study of the Polish Tatra Mountains. *Pure and Applied Geophysics*, 171(6), 897–912.

<https://doi.org/10.1007/s00024-013-0695-5>

Kramer, H. J. (2002). JERS-1. Retrieved July 29, 2019, from <https://directory.eoportal.org/web/eoportal/satellite-missions/j/jers-1>

Lacaux, J. P., Tourre, Y. M., Vignolles, C., Ndione, J. A., & Lafaye, M. (2007). Classification of ponds from high-spatial resolution remote sensing: Application to Rift Valley Fever epidemics in Senegal. *Remote Sensing of Environment*, 106(1), 66–74. <https://doi.org/10.1016/j.rse.2006.07.012>

Liu, Y., Song, P., Peng, J., & Ye, C. (2012). A physical explanation of the variation in threshold for delineating terrestrial water surfaces from multi-temporal images: Effects of radiometric correction. *International Journal of Remote Sensing*, 33(18), 5862–5875. <https://doi.org/10.1080/01431161.2012.675452>

McFeeters, S. K. (1996). The use of the Normalized Difference Water Index (NDWI) in the delineation of open water features. *International Journal of Remote Sensing*, 17(7), 1425–1432. <https://doi.org/10.1016/j.epsl.2004.10.018>

METI, NASA, & ERSDAC. (2011). *Aster Gdem 2 Readme Advanced Spaceborne Thermal Emission And Reflection Radiometer (Aster) Global Digital Elevation Model (Gdem) Version 2 October 2011*. METI, NASA, ERSDAC.

MGM. (2010). No Title. Retrieved July 23, 2019, from <https://www.mgm.gov.tr/veridegerlendirme/il-ve-ilceler-istatistik.aspx?k=A&m=SAMSUN>

NASA. (n.d.). SRTM Turkey Images. Retrieved August 16, 2019, from <https://www2.jpl.nasa.gov/srtm/turkey.html>

NASA. (2011). Landsat 7 Handbook, 186. Retrieved from http://landsat.gsfc.nasa.gov/wp-content/uploads/2016/08/Landsat7_Handbook.pdf

Okeowo, M. A., Lee, H., Hossain, F., & Getirana, A. (2017). Automated Generation

- of Lakes and Reservoirs Water Elevation Changes from Satellite Radar Altimetry. *IEEE Journal of Selected Topics in Applied Earth Observations and Remote Sensing*, 10(8), 3465–3481. <https://doi.org/10.1109/JSTARS.2017.2684081>
- Ouma, Y. O., & Tateishi, R. (2006). A water index for rapid mapping of shoreline changes of five East African Rift Valley lakes : an empirical analysis using Landsat TM and ETM + data. *International Journal of Remote Sensing*, 27(15), 3153–3181. <https://doi.org/10.1080/01431160500309934>
- Ozdemir, A., & Leloglu, U. M. (2014). Bathymetry and water quality measurement of shallow waters using hyperion: Serçin lake. *2014 22nd Signal Processing and Communications Applications Conference, SIU 2014 - Proceedings*, (Siu), 2023–2026. <https://doi.org/10.1109/SIU.2014.6830656>
- Özdemir, H. (2008). Taşkınların Tahmini ve Risk Analizinde CBS-UZAL ve Hidrolik Modellemenin Entegrasyonu. In *5. Dünya Su Forumu İSTANBUL 2009, Taşkın Konferansı* (pp. 131–143). Edirne.
- Öztan, A. F. (2011). *Altinkaya Barajı ve HES Jeoteknik Çalışmaları*. Ankara.
- Peker, E. A. (2019). *Spatio-Temporal Changes Of Lake Water Extents In Lakes Region (Turkey) Using Remote Sensing*. Middle East Technical University.
- Şener, E., Davraz, A., & İsmailov, T. (2005). Burdur Gölü Seviye Değişimlerinin Çok Zamanlı Uydu Görüntüleri ile İzlenmesi. *Türkiye Kuvaterner Sempozyumu (TURQUA-V)*, 148–156.
- T.R. Ministry of Energy and Natural Resources. (2018). Hydraulic. Retrieved July 29, 2019, from <https://www.enerji.gov.tr/tr-TR/Sayfalar/Hidrolik>
- Tachikawa, T., Kaku, M., & Iwasaki, A. (2011). ASTER GDEM Version 2 Validation Report. *International Geoscience and Remote Sensing Symposium (IGARSS)*, 1–24.

- Tseng, K. H., Shum, C. K., Kim, J. W., Wang, X., Zhu, K., & Cheng, X. (2016). Integrating Landsat Imageries and Digital Elevation Models to Infer Water Level Change in Hoover Dam. *IEEE Journal of Selected Topics in Applied Earth Observations and Remote Sensing*, 9(4), 1696–1709. <https://doi.org/10.1109/JSTARS.2015.2500599>
- U.S. Geological Survey. (2019). *Landsat 9*. Reston, VA. <https://doi.org/https://doi.org/10.3133/fs20193008>
- Usgs.gov. (2013). USGS Completes Decommissioning of Landsat 5. Retrieved May 20, 2019, from https://www.usgs.gov/land-resources/nli/landsat/usgs-completes-decommissioning-landsat-5?qt-science_support_page_related_con=4#qt-science_support_page_related_con
- USGS. (2003). 2003 Landsat Updates.
- USGS. (2008). The U.S. House of Representatives honors Landsat on Earth Day. Retrieved from <https://www.usgs.gov/land-resources/nli/landsat/april-22-2008-us-house-representatives-honors-landsat-earth-day>
- Viets, P. W. (1995, March 10). Landsat 6 Failure Attributed To Ruptured Manifold. *NOAA*.
- Wdowinski, S., Kim, S. W., Amelung, F., Dixon, T. H., Miralles-Wilhelm, F., & Sonenshein, R. (2008). Space-based detection of wetlands' surface water level changes from L-band SAR interferometry. *Remote Sensing of Environment*, 112(3), 681–696. <https://doi.org/10.1016/j.rse.2007.06.008>
- Wilson, M. J., & Oreopoulos, L. (2013). Enhancing a Simple MODIS Cloud Mask Algorithm for the Landsat Data Continuity Mission. *IEEE Transactions on Geoscience and Remote Sensing*, 51(2), 723–731.
- Xu, H. (2006). Modification of normalised difference water index (NDWI) to enhance open water features in remotely sensed imagery. *International Journal of Remote Sensing*, 27(14), 3025–3033. <https://doi.org/10.1080/01431160600589179>

Zhu, Z., Wang, S., & Woodcock, C. E. (2015). Improvement and expansion of the Fmask algorithm: cloud, cloud shadow, and snow detection for Landsats 4–7, 8, and Sentinel 2 images. *Remote Sensing of Environment*, *159*, 269–277. <https://doi.org/10.1016/j.rse.2014.12.014>

Zhu, Z., & Woodcock, C. E. (2012). Object-based cloud and cloud shadow detection in Landsat imagery. *Remote Sensing of Environment*, *118*, 83–94. <https://doi.org/10.1016/j.rse.2011.10.028>

|

APPENDICES

A. Results Other Statistical Models

Results of GEV Application:

	μ	σ	RMSE		μ	σ	RMSE
All Months Combined	-23.66	11.46	26.25	All Months Combined	-23.85	12.56	26.91
Month Based				Month Based			
January	-23.92	4.55	24.28	January	-19.97	7.71	21.17
February	-23.86	7.46	24.81	February	-18.09	8.04	19.52
March	-19.42	10.59	21.69	March	-22.85	7.81	23.93
April	-32.49	17.60	36.25	April	-38.32	18.70	41.95
May	-24.19	10.35	25.90	May	-22.07	5.40	22.60
June	-23.91	5.95	24.52	June	-23.63	2.49	23.74
July	-18.50	8.06	19.91	July	-24.96	15.31	28.61
August	-19.99	8.07	21.31	August	-22.33	6.76	23.17
September	-22.01	13.52	25.24	September	-27.69	14.31	30.62
October	-17.56	6.48	18.53	October	-17.23	5.78	18.02
November	-24.24	3.38	24.44	November	-19.75	5.01	20.28
December	-33.88	22.71	39.71	December	-28.99	25.71	37.30
MODEL INFO				MODEL INFO			
Water Index	GEV+SRTM (Ermenek)			Water Index	GEV+ASTER (Ermenek)		
Correlation Coefficient	0.16			Correlation Coefficient	0.08		
	μ	σ	RMSE		μ	σ	RMSE
All Months Combined	-11.60	7.82	13.96	All Months Combined	-11.18	7.39	13.37
Month Based				Month Based			
January	-7.46	6.82	9.72	January	-7.55	6.37	9.53
February	-9.93	6.79	11.70	February	-9.62	6.43	11.27
March	-14.39	14.22	19.38	March	-13.48	13.32	18.16
April	-7.25	4.05	8.14	April	-6.99	3.43	7.66
May	-11.42	3.44	11.85	May	-9.89	4.97	10.90
June	-8.68	5.82	10.22	June	-8.31	5.52	9.75
July	-12.66	4.78	13.40	July	-12.82	4.35	13.42
August	-16.68	5.99	17.55	August	-15.68	3.64	16.03
September	-12.03	3.80	12.52	September	-11.77	4.35	12.42
October	-15.63	9.91	17.97	October	-15.02	8.72	16.92
November	-13.56	11.83	17.33	November	-13.72	11.81	17.45
December	-10.75	9.99	14.10	December	-10.59	9.28	13.56
MODEL INFO				MODEL INFO			
Water Index	GEV+SRTM (Altunkaya)			Water Index	GEV+ASTER (Altunkaya)		
Correlation Coefficient	0.39			Correlation Coefficient	0.40		

Ermenek Trained Mean Approach Over Altinkaya Dam with ASTER DEM:

	μ	σ	RMSE		μ	σ	RMSE
All Months Combined	-15.08	9.78	17.93	All Months Combined	-10.53	7.24	12.75
Month Based				Month Based			
January	-11.55	8.42	13.88	January	-11.65	4.21	12.27
February	-14.09	7.61	15.70	February	-9.58	7.69	11.87
March	-15.86	10.01	18.30	March	-10.42	4.30	11.13
April	-19.27	11.12	21.78	April	-5.07	5.50	7.13
May	-8.36	3.66	9.02	May	-6.71	6.07	8.75
June	-17.01	19.41	24.75	June	-3.35	4.75	5.53
July	-16.49	8.60	18.26	July	-18.03	11.13	20.70
August	-20.33	4.32	20.71	August	-11.60	4.27	12.24
September	-14.29	7.18	15.72	September	-12.63	6.91	14.12
October	-15.34	11.19	18.31	October	-11.02	5.57	12.09
November	-14.37	8.93	16.52	November	-10.64	3.03	10.99
December	-14.79	9.43	17.12	December	-17.64	8.26	19.18
MODEL INFO				MODEL INFO			
Water Index	AWEI.S			Water Index	NDPI		
Correlation Coefficient	0.22			Correlation Coefficient	0.49		
	μ	σ	RMSE		μ	σ	RMSE
All Months Combined	-13.73	9.52	16.67	All Months Combined	-13.46	8.11	15.69
Month Based				Month Based			
January	-3.58	7.86	8.01	January	-11.18	6.74	12.76
February	-9.28	8.75	12.24	February	-9.54	8.04	12.03
March	-8.03	8.90	11.42	March	-9.53	8.55	12.32
April	-17.11	5.13	17.74	April	-15.42	4.96	16.08
May	-12.17	3.62	12.62	May	-11.43	4.10	12.05
June	-15.98	12.88	19.94	June	-14.86	13.36	19.34
July	-15.14	6.66	16.31	July	-15.86	8.15	17.52
August	-12.16	7.09	13.78	August	-13.31	5.13	14.11
September	-16.70	9.95	19.01	September	-15.32	9.52	17.61
October	-20.53	7.41	21.58	October	-17.15	9.18	19.02
November	-18.14	6.41	19.06	November	-16.37	10.67	19.04
December	-17.00	16.10	22.47	December	-12.33	6.93	13.85
MODEL INFO				MODEL INFO			
Water Index	NDWLMCF			Water Index	WI2015		
Correlation Coefficient	0.11			Correlation Coefficient	0.29		

Ermenek Trained Mean Approach Over Altinkaya Dam with SRTM DEM:

	μ	σ	RMSE		μ	σ	RMSE
All Months Combined	-16.48	10.28	19.39	All Months Combined	-11.35	7.32	13.48
Month Based				Month Based			
January	-13.23	8.94	15.55	January	-12.98	4.16	13.52
February	-16.40	7.17	17.66	February	-11.19	7.35	13.05
March	-17.32	10.77	19.92	March	-10.71	4.11	11.35
April	-20.77	11.41	23.23	April	-5.51	5.21	7.28
May	-9.10	4.24	9.91	May	-8.41	4.55	9.41
June	-18.55	20.87	26.79	June	-3.27	5.38	5.96
July	-17.24	9.23	19.18	July	-18.71	12.17	21.76
August	-20.81	4.36	21.19	August	-11.90	4.41	12.57
September	-15.84	7.02	17.09	September	-13.68	6.56	14.94
October	-16.82	12.07	19.99	October	-11.92	6.10	13.11
November	-15.88	9.79	18.22	November	-11.12	2.57	11.37
December	-16.80	9.61	18.95	December	-18.73	7.97	20.09
MODEL INFO				MODEL INFO			
Water Index	AWEI.S			Water Index	NDPI		
Correlation Coefficient	0.22			Correlation Coefficient	0.52		
	μ	σ	RMSE		μ	σ	RMSE
All Months Combined	-15.30	9.88	18.18	All Months Combined	-15.00	8.77	17.35
Month Based				Month Based			
January	-4.81	6.30	7.49	January	-13.47	6.24	14.63
February	-11.39	8.42	13.74	February	-12.13	8.16	14.23
March	-9.44	8.70	12.33	March	-10.94	9.29	13.84
April	-19.05	5.59	19.72	April	-17.34	5.72	18.11
May	-13.33	4.40	13.94	May	-12.18	4.63	12.92
June	-18.04	14.78	22.64	June	-16.46	15.19	21.65
July	-16.17	7.12	17.43	July	-16.76	8.74	18.56
August	-12.90	7.88	14.78	August	-13.88	5.38	14.72
September	-18.64	9.89	20.71	September	-17.35	9.31	19.32
October	-22.50	8.47	23.74	October	-18.32	9.89	20.35
November	-19.74	6.82	20.70	November	-18.04	12.01	21.11
December	-18.69	15.90	23.66	December	-13.96	8.81	16.11
MODEL INFO				MODEL INFO			
Water Index	NDWLMCF			Water Index	WI2015		
Correlation Coefficient	0.13			Correlation Coefficient	0.29		

Ermenek Trained Mode Approach Over Altinkaya Dam with ASTER DEM:

	μ	σ	RMSE		μ	σ	RMSE
All Months Combined	-8.10	11.62	14.10	All Months Combined	-7.92	8.03	11.24
Month Based				Month Based			
January	-3.59	5.05	5.84	January	-9.88	6.98	11.76
February	-4.00	6.93	7.48	February	-13.46	17.37	20.80
March	-11.26	12.63	16.11	March	-13.19	3.20	13.51
April	-11.58	14.68	17.71	April	-2.47	4.78	5.01
May	-4.95	5.24	6.93	May	-1.63	4.69	4.64
June	-17.26	27.42	30.70	June	-2.50	3.10	3.81
July	-7.64	5.42	9.11	July	-7.50	5.26	8.90
August	-7.38	5.02	8.68	August	-7.23	9.28	11.14
September	-10.88	11.63	15.20	September	-6.61	4.89	7.98
October	-3.87	5.73	6.42	October	-12.63	5.78	13.65
November	-8.00	6.85	10.16	November	-9.71	5.91	11.11
December	-5.09	7.58	8.59	December	-10.94	7.84	13.07
MODEL INFO				MODEL INFO			
Water Index	AWELIS			Water Index	NDPI		
Correlation Coefficient	0.17			Correlation Coefficient	0.49		
	μ	σ	RMSE		μ	σ	RMSE
All Months Combined	-8.40	9.61	12.71	All Months Combined	-5.29	7.59	9.21
Month Based				Month Based			
January	-4.03	9.91	9.91	January	-3.19	7.76	7.77
February	-6.55	8.55	10.19	February	-0.56	4.27	3.93
March	-8.24	7.10	10.48	March	-6.12	7.31	9.05
April	-9.96	12.01	14.81	April	-9.21	11.07	13.67
May	-5.63	6.56	8.28	May	-3.75	4.46	5.58
June	-3.64	5.02	5.90	June	-5.27	6.48	7.99
July	-4.51	5.16	6.52	July	-4.41	5.51	6.69
August	-12.33	9.78	15.22	August	-7.08	5.13	8.49
September	-10.81	13.51	16.40	September	-9.72	15.44	17.13
October	-12.29	16.89	19.47	October	-3.87	5.73	6.42
November	-11.77	5.96	12.97	November	-7.66	5.77	9.30
December	-12.93	12.01	16.95	December	-2.67	6.75	6.71
MODEL INFO				MODEL INFO			
Water Index	NDWLMCF			Water Index	WI2015		
Correlation Coefficient	0.31			Correlation Coefficient	0.25		

Ermenek Trained Mode Approach Over Altinkaya Dam with SRTM DEM:

	μ	σ	RMSE		μ	σ	RMSE
All Months Combined	-15.14	13.38	20.14	All Months Combined	-11.73	8.37	14.38
Month Based				Month Based			
January	-13.31	9.06	15.67	January	-13.35	5.57	14.29
February	-8.96	8.23	11.70	February	-17.28	14.42	21.72
March	-15.53	12.99	19.54	March	-12.85	3.61	13.27
April	-16.88	11.47	19.86	April	-5.92	3.24	6.61
May	-10.64	4.80	11.53	May	-4.87	6.76	7.93
June	-18.39	26.76	30.86	June	-3.35	4.41	5.28
July	-11.39	8.43	13.74	July	-14.21	8.91	16.38
August	-14.10	6.68	15.36	August	-13.55	7.82	15.32
September	-13.17	11.48	16.83	September	-12.97	6.54	14.28
October	-9.82	5.24	10.89	October	-14.14	6.70	15.36
November	-25.73	18.03	30.54	November	-14.57	8.66	16.57
December	-23.06	16.97	27.78	December	-16.66	8.32	18.31
MODEL INFO				MODEL INFO			
Water Index	AWEI.S			Water Index	NDPI		
Correlation Coefficient	0.17			Correlation Coefficient	0.55		
	μ	σ	RMSE		μ	σ	RMSE
All Months Combined	-15.23	13.87	20.54	All Months Combined	-12.82	10.58	16.58
Month Based				Month Based			
January	-6.24	10.80	11.67	January	-11.15	6.04	12.44
February	-11.89	13.25	16.97	February	-5.46	7.60	8.83
March	-10.46	5.40	11.57	March	-8.58	8.49	11.56
April	-18.31	22.24	27.34	April	-15.12	7.65	16.65
May	-10.02	5.31	11.16	May	-11.95	5.97	13.16
June	-22.02	23.72	31.10	June	-21.72	23.84	30.97
July	-13.28	4.49	13.90	July	-12.54	3.36	12.90
August	-12.76	8.74	15.05	August	-12.58	7.11	14.16
September	-17.07	12.08	20.32	September	-14.68	14.94	20.04
October	-20.65	17.86	26.11	October	-12.32	6.97	13.81
November	-21.76	11.06	23.99	November	-14.27	3.94	14.72
December	-18.96	16.16	24.03	December	-12.09	10.29	15.31
MODEL INFO				MODEL INFO			
Water Index	NDWI.MCF			Water Index	WI2015		
Correlation Coefficient	0.20			Correlation Coefficient	0.35		

Ermenek Trained Median Approach Over Altinkaya Dam with ASTER DEM:

	μ	σ	RMSE		μ	σ	RMSE
All Months Combined	-13.73	10.28	17.11	All Months Combined	-9.43	6.86	11.63
Month Based				Month Based			
January	-10.35	7.84	12.59	January	-11.00	3.36	11.42
February	-13.35	6.71	14.68	February	-9.12	8.60	12.03
March	-13.77	10.08	16.56	March	-9.73	5.06	10.77
April	-17.38	11.64	20.38	April	-4.40	5.46	6.64
May	-6.82	3.75	7.66	May	-5.43	6.23	7.92
June	-17.07	21.73	26.38	June	-2.55	4.42	4.82
July	-15.88	8.89	17.83	July	-14.82	9.93	17.38
August	-18.07	5.69	18.80	August	-9.24	3.44	9.76
September	-12.86	6.80	14.28	September	-11.19	6.73	12.76
October	-13.60	13.05	17.92	October	-10.64	4.84	11.49
November	-12.83	9.04	15.25	November	-10.64	2.93	10.97
December	-13.33	8.79	15.56	December	-16.44	7.74	17.90
MODEL INFO				MODEL INFO			
Water Index	AWEI.S			Water Index	NDPI		
Correlation Coefficient	0.22			Correlation Coefficient	0.54		
	μ	σ	RMSE		μ	σ	RMSE
All Months Combined	-12.74	8.85	15.47	All Months Combined	-12.32	8.14	14.74
Month Based				Month Based			
January	-3.34	7.20	7.37	January	-9.87	6.43	11.49
February	-8.98	7.92	11.53	February	-8.12	6.58	10.10
March	-7.16	8.12	10.31	March	-7.33	7.64	10.12
April	-15.87	4.93	16.49	April	-14.87	4.89	15.53
May	-10.96	4.46	11.72	May	-10.45	4.83	11.37
June	-14.89	12.45	18.83	June	-14.05	13.02	18.51
July	-13.13	7.18	14.67	July	-14.23	9.19	16.52
August	-11.57	7.30	13.35	August	-11.83	6.19	13.11
September	-15.92	9.30	18.04	September	-14.71	8.84	16.78
October	-18.38	7.82	19.67	October	-15.83	11.03	18.65
November	-17.67	5.12	18.28	November	-15.40	10.24	18.01
December	-15.84	13.28	19.94	December	-11.75	6.52	13.18
MODEL INFO				MODEL INFO			
Water Index	NDWI.MCF			Water Index	WI2015		
Correlation Coefficient	0.19			Correlation Coefficient	0.32		

Ermenek Trained Median Approach Over Altinkaya Dam with SRTM DEM:

	μ	σ	RMSE		μ	σ	RMSE
All Months Combined	-15.35	10.99	18.84	All Months Combined	-10.36	7.09	12.53
Month Based				Month Based			
January	-11.89	8.65	14.27	January	-12.42	3.48	12.82
February	-15.78	7.76	17.30	February	-10.74	8.57	13.28
March	-15.79	11.22	18.82	March	-10.25	4.58	11.07
April	-18.76	11.76	21.61	April	-5.15	5.36	7.10
May	-7.83	3.98	8.65	May	-7.58	4.38	8.60
June	-19.12	23.66	29.07	June	-2.32	5.21	5.36
July	-16.52	9.52	18.67	July	-15.98	11.41	19.08
August	-18.79	5.22	19.38	August	-9.47	3.37	9.96
September	-14.41	7.45	15.93	September	-12.11	7.50	13.91
October	-15.48	13.35	19.55	October	-11.46	5.88	12.61
November	-14.92	9.94	17.46	November	-11.03	2.52	11.27
December	-15.58	9.48	17.82	December	-17.84	7.08	18.97
MODEL INFO				MODEL INFO			
Water Index	AWEI.S			Water Index	NDPI		
Correlation Coefficient	0.20			Correlation Coefficient	0.55		
	μ	σ	RMSE		μ	σ	RMSE
All Months Combined	-13.97	9.67	16.96	All Months Combined	-13.84	9.13	16.54
Month Based				Month Based			
January	-3.55	6.86	7.19	January	-11.67	7.02	13.31
February	-10.10	8.07	12.51	February	-10.26	8.18	12.69
March	-8.01	8.75	11.31	March	-9.65	8.59	12.43
April	-17.19	5.53	17.92	April	-17.20	5.81	18.00
May	-11.94	4.31	12.59	May	-10.97	4.66	11.79
June	-16.47	14.48	21.24	June	-15.68	15.11	21.01
July	-14.30	7.18	15.73	July	-15.43	9.57	17.73
August	-12.02	6.96	13.60	August	-12.45	6.01	13.60
September	-17.40	9.82	19.58	September	-16.00	9.90	18.38
October	-20.90	9.45	22.55	October	-17.42	11.54	20.25
November	-19.43	6.28	20.26	November	-17.21	11.79	20.30
December	-17.42	14.55	21.90	December	-12.86	9.73	15.63
MODEL INFO				MODEL INFO			
Water Index	NDWI.MCF			Water Index	WI2015		
Correlation Coefficient	0.19			Correlation Coefficient	0.30		

Ermenek Trained Mean Approach Over Ermenek Dam with ASTER DEM:

	μ	σ	RMSE		μ	σ	RMSE
All Months Combined	-18.39	15.09	23.72	All Months Combined	-25.50	14.74	29.40
Month Based				Month Based			
January	-25.80	22.98	33.26	January	-23.58	15.97	27.73
February	-11.96	8.55	14.28	February	-16.86	10.10	19.22
March	-20.98	25.16	31.11	March	-17.90	5.66	18.63
April	-25.55	16.63	29.72	April	-38.66	24.10	44.48
May	-17.36	6.66	18.35	May	-26.18	9.19	27.44
June	-25.17	14.12	28.28	June	-37.98	17.09	41.06
July	-23.72	8.41	24.93	July	-28.49	7.98	29.41
August	-23.66	6.01	24.29	August	-27.65	10.24	29.19
September	-14.07	14.32	19.21	September	-14.31	8.73	16.37
October	-9.29	5.59	10.60	October	-24.13	11.82	26.43
November	-7.81	2.23	8.07	November	-26.77	11.10	28.62
December	-15.08	22.69	25.62	December	-23.63	21.66	30.81
MODEL INFO				MODEL INFO			
Water Index	AWEL.S			Water Index	NDPI		
Correlation Coefficient	0.02			Correlation Coefficient	0.08		
	μ	σ	RMSE		μ	σ	RMSE
All Months Combined	-29.03	18.53	34.37	All Months Combined	-18.77	16.63	25.00
Month Based				Month Based			
January	-34.92	17.59	38.43	January	-16.94	17.75	23.72
February	-29.07	15.20	32.21	February	-18.31	17.93	24.56
March	-29.53	24.04	36.79	March	-25.42	21.55	32.14
April	-34.32	19.65	38.72	April	-32.17	17.97	36.12
May	-20.18	5.61	20.80	May	-19.74	14.62	23.45
June	-46.70	24.68	51.85	June	-30.95	20.50	36.16
July	-31.75	16.87	35.28	July	-8.16	4.35	9.07
August	-28.29	4.17	28.55	August	-11.00	7.51	12.96
September	-12.18	6.72	13.64	September	-8.26	9.42	11.92
October	-19.51	17.42	25.17	October	-10.80	9.47	13.83
November	-22.19	19.64	28.53	November	-15.68	14.98	20.80
December	-38.24	22.05	43.22	December	-23.33	23.08	31.15
MODEL INFO				MODEL INFO			
Water Index	NDWI.MCF			Water Index	WI2015		
Correlation Coefficient	-0.12			Correlation Coefficient	0.11		

Ermenek Trained Mean Approach Over Ermenek Dam with SRTM DEM:

	μ	σ	RMSE		μ	σ	RMSE
All Months Combined	-10.75	14.71	18.14	All Months Combined	-15.90	14.08	21.17
Month Based				Month Based			
January	-20.34	23.81	29.77	January	-16.13	16.36	21.98
February	-4.51	6.78	7.66	February	-9.32	9.64	12.81
March	-15.30	26.66	28.75	March	-9.45	4.05	10.14
April	-19.13	17.57	24.96	April	-30.19	24.10	37.36
May	-9.10	5.38	10.29	May	-14.93	7.13	16.23
June	-15.33	13.62	19.74	June	-26.44	19.18	31.71
July	-11.89	4.40	12.55	July	-15.39	4.14	15.85
August	-11.54	3.15	11.89	August	-15.21	7.92	16.85
September	-7.40	11.52	12.86	September	-7.23	5.53	8.82
October	-2.46	2.44	3.32	October	-13.88	8.61	15.95
November	-1.80	0.87	1.97	November	-16.88	12.33	20.29
December	-9.93	23.04	23.26	December	-15.59	22.18	25.56
MODEL INFO				MODEL INFO			
Water Index	AWEI.S			Water Index	NDPI		
Correlation Coefficient	0.09			Correlation Coefficient	0.10		
	μ	σ	RMSE		μ	σ	RMSE
All Months Combined	-20.35	18.35	27.31	All Months Combined	-11.57	16.05	19.69
Month Based				Month Based			
January	-27.00	18.35	31.78	January	-10.58	15.34	17.83
February	-19.64	13.37	23.12	February	-11.18	18.60	20.33
March	-22.18	24.84	31.72	March	-18.73	22.08	27.51
April	-26.72	18.61	31.67	April	-23.43	19.21	29.27
May	-10.71	5.51	11.79	May	-11.15	10.97	14.65
June	-36.11	28.90	44.72	June	-21.37	20.95	28.68
July	-21.59	14.75	25.44	July	-2.10	2.75	3.27
August	-17.72	3.68	18.03	August	-3.69	3.85	5.10
September	-4.56	3.96	5.82	September	-1.71	5.36	5.18
October	-13.17	16.01	19.67	October	-5.20	8.75	9.53
November	-15.44	18.70	23.02	November	-9.89	15.06	16.94
December	-27.76	23.62	35.15	December	-17.10	23.17	26.86
MODEL INFO				MODEL INFO			
Water Index	NDWI.MCF			Water Index	WI2015		
Correlation Coefficient	-0.09			Correlation Coefficient	0.11		

Ermenek Trained Mode Approach Over Ermenek Dam with ASTER DEM:

	μ	σ	RMSE		μ	σ	RMSE
All Months Combined	-54.88	35.19	65.06	All Months Combined	-69.45	40.52	80.26
Month Based				Month Based			
January	-58.53	29.33	64.36	January	-67.33	44.78	78.77
February	-54.00	29.21	60.22	February	-59.29	26.44	64.02
March	-48.03	47.02	64.41	March	-65.51	48.74	79.19
April	-69.61	40.28	78.72	April	-93.73	47.22	103.17
May	-55.23	43.13	67.36	May	-94.96	57.54	108.01
June	-72.98	39.02	81.21	June	-78.96	57.11	94.62
July	-71.53	27.48	75.80	July	-84.66	35.85	90.77
August	-79.80	38.49	87.19	August	-76.53	28.16	80.73
September	-27.94	5.50	28.39	September	-31.26	6.06	31.74
October	-35.30	25.11	42.09	October	-60.07	34.91	68.00
November	-31.79	5.43	32.17	November	-61.88	19.22	64.32
December	-53.89	45.60	68.09	December	-63.45	46.26	76.22
MODEL INFO				MODEL INFO			
Water Index	AWEI.S			Water Index	NDPI		
Correlation Coefficient	-0.30			Correlation Coefficient	-0.27		
	μ	σ	RMSE		μ	σ	RMSE
All Months Combined	-72.72	39.82	82.78	All Months Combined	-58.26	41.65	71.44
Month Based				Month Based			
January	-84.71	43.19	93.44	January	-55.91	60.85	79.78
February	-74.44	27.86	78.66	February	-62.35	44.99	74.66
March	-69.91	55.98	86.60	March	-67.94	50.03	81.87
April	-85.26	40.86	93.06	April	-92.69	44.49	101.20
May	-88.38	34.56	93.64	May	-79.54	46.39	89.11
June	-94.86	51.02	105.68	June	-88.60	43.57	97.12
July	-80.95	40.08	88.83	July	-29.82	14.54	32.64
August	-71.88	29.08	76.62	August	-43.79	29.23	51.28
September	-38.47	8.36	39.22	September	-28.71	6.98	29.41
October	-43.26	26.86	49.72	October	-40.19	24.24	45.87
November	-53.73	24.23	58.11	November	-42.44	21.09	46.60
December	-89.41	53.51	101.88	December	-55.08	49.02	70.40
MODEL INFO				MODEL INFO			
Water Index	NDWLMCF			Water Index	WI2015		
Correlation Coefficient	-0.34			Correlation Coefficient	-0.15		

Ermenek Trained Mode Approach Over Ermenek Dam with SRTM DEM:

	μ	σ	RMSE		μ	σ	RMSE
All Months Combined	-18.17	23.50	29.58	All Months Combined	-27.22	23.32	35.74
Month Based				Month Based			
January	-26.58	37.19	43.12	January	-29.55	31.62	41.31
February	-11.13	17.86	19.74	February	-16.26	19.76	24.29
March	-23.39	31.69	37.20	March	-22.70	12.78	25.52
April	-35.93	26.87	43.51	April	-45.83	24.66	51.06
May	-18.69	11.66	21.41	May	-29.26	18.96	33.82
June	-26.96	26.38	36.15	June	-47.06	25.02	52.31
July	-22.09	16.14	26.55	July	-23.83	15.78	27.84
August	-15.43	10.61	18.21	August	-27.39	19.68	32.76
September	-13.79	19.24	22.33	September	-12.07	12.42	16.56
October	-5.15	5.98	7.50	October	-19.64	15.45	24.18
November	-2.89	3.81	4.52	November	-24.61	18.73	29.97
December	-16.12	38.97	39.06	December	-28.78	41.49	47.57
MODEL INFO				MODEL INFO			
Water Index	AWELIS			Water Index	NDPI		
Correlation Coefficient	-0.02			Correlation Coefficient	0.05		
	μ	σ	RMSE		μ	σ	RMSE
All Months Combined	-36.75	31.05	47.96	All Months Combined	-22.26	27.75	35.42
Month Based				Month Based			
January	-47.08	37.03	57.96	January	-22.17	33.84	38.65
February	-36.83	33.96	48.14	February	-22.05	37.75	40.91
March	-35.10	44.86	53.94	March	-35.22	37.00	48.80
April	-47.13	26.34	52.91	April	-45.00	26.33	51.02
May	-23.27	10.31	25.03	May	-23.79	21.22	30.07
June	-63.26	39.31	72.73	June	-35.19	35.47	47.82
July	-42.02	23.13	47.03	July	-7.46	2.82	7.89
August	-30.97	11.35	32.65	August	-9.07	5.68	10.45
September	-11.51	8.59	13.93	September	-8.27	10.80	12.86
October	-21.99	25.80	32.22	October	-10.80	14.56	17.12
November	-25.13	30.30	37.37	November	-14.78	20.82	24.08
December	-54.41	37.30	64.18	December	-27.28	39.88	44.91
MODEL INFO				MODEL INFO			
Water Index	NDWLMCF			Water Index	WI2015		
Correlation Coefficient	-0.13			Correlation Coefficient	0.01		

Ermenek Trained Median Approach Over Ermenek Dam with ASTER DEM:

	μ	σ	RMSE		μ	σ	RMSE
All Months Combined	-14.50	13.49	19.74	All Months Combined	-18.88	13.47	23.14
Month Based				Month Based			
January	-22.98	20.85	29.84	January	-17.85	13.44	21.66
February	-8.43	5.13	9.64	February	-12.97	8.16	14.96
March	-19.97	26.09	31.08	March	-11.02	3.87	11.58
April	-21.18	16.07	25.76	April	-32.02	25.26	39.46
May	-11.85	4.04	12.38	May	-15.07	6.99	16.31
June	-19.09	12.58	22.28	June	-29.10	18.99	33.87
July	-15.20	3.24	15.49	July	-18.03	3.06	18.25
August	-15.11	2.81	15.33	August	-18.27	6.05	19.08
September	-11.52	9.54	14.44	September	-11.84	4.69	12.59
October	-7.29	1.84	7.48	October	-18.23	8.56	19.83
November	-6.68	0.69	6.71	November	-21.66	12.70	24.57
December	-14.28	21.54	24.30	December	-19.85	20.08	27.02
MODEL INFO				MODEL INFO			
Water Index	AWEL.S			Water Index	NDPI		
Correlation Coefficient	-0.30			Correlation Coefficient	0.15		
	μ	σ	RMSE		μ	σ	RMSE
All Months Combined	-22.92	17.42	28.71	All Months Combined	-15.02	15.13	21.25
Month Based				Month Based			
January	-28.86	16.41	32.52	January	-11.36	13.68	17.11
February	-21.88	11.55	24.29	February	-14.81	16.58	21.18
March	-25.34	22.98	32.90	March	-22.13	20.19	28.80
April	-28.32	18.92	33.17	April	-24.84	20.46	31.08
May	-12.90	4.99	13.65	May	-13.24	8.56	15.17
June	-38.51	29.59	47.04	June	-25.21	20.17	31.22
July	-23.64	13.53	26.67	July	-6.31	3.40	7.03
August	-20.50	2.98	20.68	August	-7.86	4.02	8.68
September	-8.46	3.62	9.08	September	-5.64	4.99	7.25
October	-16.70	14.37	21.23	October	-9.54	8.03	12.03
November	-19.21	16.86	24.62	November	-14.86	15.35	20.42
December	-29.06	22.85	35.77	December	-21.09	21.86	28.76
MODEL INFO				MODEL INFO			
Water Index	NDWI.MCF			Water Index	WI2015		
Correlation Coefficient	-0.06			Correlation Coefficient	0.12		

Ermenek Trained Median Approach Over Ermenek Dam with SRTM DEM:

	μ	σ	RMSE		μ	σ	RMSE
All Months Combined	-9.92	14.44	17.43	All Months Combined	-14.34	13.89	19.90
Month Based				Month Based			
January	-19.73	23.35	29.05	January	-14.84	15.88	20.75
February	-3.75	5.85	6.53	February	-8.30	9.29	11.87
March	-15.31	27.58	29.47	March	-7.71	3.14	8.23
April	-17.79	16.88	23.54	April	-28.45	25.13	36.55
May	-8.11	4.53	9.06	May	-12.45	6.34	13.68
June	-14.22	12.86	18.44	June	-24.53	19.45	30.28
July	-10.09	3.21	10.50	July	-12.95	2.97	13.23
August	-9.75	2.72	10.06	August	-12.73	5.76	13.78
September	-6.50	9.74	11.02	September	-6.61	4.61	7.83
October	-2.09	1.85	2.69	October	-12.53	8.07	14.54
November	-1.56	0.67	1.68	November	-16.05	13.14	20.04
December	-9.79	22.97	23.14	December	-14.63	21.50	24.48
MODEL INFO				MODEL INFO			
Water Index	AWEI.S			Water Index	NDPI		
Correlation Coefficient	0.11			Correlation Coefficient	0.12		
	μ	σ	RMSE		μ	σ	RMSE
All Months Combined	-18.80	18.11	26.02	All Months Combined	-10.75	15.71	18.94
Month Based				Month Based			
January	-24.82	17.73	29.63	January	-8.89	14.01	15.83
February	-17.30	12.16	20.55	February	-10.25	17.99	19.36
March	-21.16	24.62	30.87	March	-17.99	21.84	26.85
April	-25.23	18.75	30.49	April	-22.05	19.44	28.30
May	-9.87	5.65	11.09	May	-9.58	8.68	12.18
June	-34.61	30.29	44.30	June	-20.54	20.82	27.98
July	-19.18	13.46	22.78	July	-1.79	2.67	3.03
August	-15.74	3.07	15.98	August	-3.11	3.39	4.39
September	-3.82	3.33	4.88	September	-1.17	4.58	4.34
October	-12.25	15.02	18.38	October	-4.84	8.34	9.02
November	-14.66	18.06	22.06	November	-9.78	15.36	17.09
December	-25.52	24.24	33.78	December	-16.64	23.30	26.67
MODEL INFO				MODEL INFO			
Water Index	NDWI.MCF			Water Index	WI2015		
Correlation Coefficient	-0.08			Correlation Coefficient	0.11		

Altinkaya Trained Mean Approach Over Altinkaya Dam with ASTER DEM:

	μ	σ	RMSE		μ	σ	RMSE
All Months Combined	-12.68	8.14	15.04	All Months Combined	-9.04	7.38	11.64
Month Based				Month Based			
January	-9.11	3.41	9.62	January	-11.65	4.21	12.27
February	-9.51	6.48	11.20	February	-8.85	8.04	11.49
March	-9.50	5.67	10.82	March	-2.29	5.91	5.86
April	-13.71	6.85	15.07	April	-2.24	5.45	5.46
May	-6.81	3.14	7.41	May	-4.55	5.65	6.93
June	-14.15	17.66	21.63	June	-5.49	7.47	8.83
July	-12.97	7.74	14.77	July	-13.65	8.47	15.69
August	-10.83	4.03	11.44	August	-9.60	2.67	9.91
September	-15.48	8.26	17.22	September	-12.52	7.13	14.11
October	-17.41	7.27	18.58	October	-11.02	5.57	12.09
November	-17.22	7.46	18.52	November	-10.64	3.03	10.99
December	-16.96	4.31	17.41	December	-17.64	8.26	19.18
MODEL INFO				MODEL INFO			
Water Index	AWEL.S			Water Index	NDPI		
Correlation Coefficient	0.11			Correlation Coefficient	0.48		
	μ	σ	RMSE		μ	σ	RMSE
All Months Combined	-15.37	10.23	18.42	All Months Combined	-13.28	8.58	15.78
Month Based				Month Based			
January	-10.00	6.34	11.55	January	-9.78	8.48	12.47
February	-14.15	10.07	16.87	February	-12.74	6.79	14.17
March	-19.15	18.81	25.72	March	-10.49	7.37	12.46
April	-17.68	10.48	20.10	April	-15.31	8.05	16.98
May	-10.51	4.21	11.21	May	-7.89	3.26	8.44
June	-14.90	13.36	19.37	June	-15.23	15.09	20.67
July	-15.62	9.23	17.75	July	-15.86	8.15	17.52
August	-11.63	5.71	12.75	August	-13.31	5.13	14.11
September	-15.48	8.61	17.36	September	-15.32	9.52	17.61
October	-20.53	7.41	21.58	October	-17.15	9.18	19.02
November	-18.14	6.41	19.06	November	-16.37	10.67	19.04
December	-18.45	15.19	23.08	December	-11.15	7.21	12.95
MODEL INFO				MODEL INFO			
Water Index	NDWI.MCF			Water Index	WI2015		
Correlation Coefficient	0.34			Correlation Coefficient	0.33		

Altinkaya Trained Mean Approach Over Altinkaya Dam with SRTM DEM:

	μ	σ	RMSE		μ	σ	RMSE
All Months Combined	-13.97	8.87	16.52	All Months Combined	-10.34	7.21	12.58
Month Based				Month Based			
January	-10.73	3.12	11.11	January	-12.98	4.16	13.52
February	-11.52	6.07	12.78	February	-10.55	7.74	12.70
March	-10.70	6.26	12.13	March	-3.74	5.56	6.31
April	-15.47	7.19	16.80	April	-3.53	4.77	5.60
May	-7.26	3.95	8.13	May	-7.37	3.42	8.02
June	-15.20	19.67	23.72	June	-6.47	8.22	9.99
July	-14.23	8.45	16.19	July	-14.81	9.73	17.27
August	-11.36	4.50	12.07	August	-10.65	3.09	11.01
September	-17.39	8.15	18.91	September	-13.61	6.69	14.92
October	-18.56	8.34	20.00	October	-11.92	6.10	13.11
November	-18.55	8.96	20.28	November	-11.12	2.57	11.37
December	-18.33	5.22	18.94	December	-18.73	7.97	20.09
MODEL INFO				MODEL INFO			
Water Index	AWEI.S			Water Index	NDPI		
Correlation Coefficient	0.37			Correlation Coefficient	0.52		
	μ	σ	RMSE		μ	σ	RMSE
All Months Combined	-16.98	10.80	20.08	All Months Combined	-14.72	9.24	17.35
Month Based				Month Based			
January	-12.20	7.18	13.85	January	-11.67	8.23	13.88
February	-16.95	10.29	19.38	February	-14.84	6.26	15.90
March	-20.92	19.33	27.36	March	-11.94	8.68	14.33
April	-19.25	10.67	21.58	April	-16.90	8.38	18.55
May	-11.37	4.67	12.16	May	-8.61	3.88	9.33
June	-16.59	15.45	21.90	June	-16.76	16.64	22.77
July	-16.42	10.03	18.80	July	-16.76	8.74	18.56
August	-12.21	6.11	13.42	August	-13.88	5.38	14.72
September	-17.22	8.68	18.95	September	-17.35	9.31	19.32
October	-22.50	8.47	23.74	October	-18.32	9.89	20.35
November	-19.74	6.82	20.70	November	-18.04	12.01	21.11
December	-20.30	15.11	24.54	December	-12.85	9.11	15.31
MODEL INFO				MODEL INFO			
Water Index	NDWI.MCF			Water Index	WI2015		
Correlation Coefficient	0.33			Correlation Coefficient	0.23		

Altinkaya Trained Mode Approach Over Altinkaya Dam with ASTER DEM:

	μ	σ	RMSE		μ	σ	RMSE
All Months Combined	-8.20	10.85	13.54	All Months Combined	-7.64	8.44	11.34
Month Based				Month Based			
January	-6.74	9.65	11.09	January	-9.88	6.98	11.76
February	-10.22	12.39	15.25	February	-12.57	17.57	20.38
March	-6.76	3.50	7.48	March	-5.57	8.10	9.26
April	-6.37	9.73	10.93	April	-3.11	6.46	6.66
May	-4.95	5.24	6.93	May	-4.89	7.94	8.83
June	-11.54	25.90	26.62	June	-3.60	5.98	6.60
July	-3.77	5.98	6.64	July	-9.70	10.23	13.47
August	-7.08	5.13	8.49	August	-4.44	5.49	6.69
September	-10.31	15.39	17.43	September	-6.61	4.89	7.98
October	-5.52	5.15	7.19	October	-12.63	5.78	13.65
November	-12.36	5.25	13.26	November	-9.71	5.91	11.11
December	-12.34	5.65	13.38	December	-10.94	7.84	13.07
MODEL INFO				MODEL INFO			
Water Index	AWEIS			Water Index	NDPI		
Correlation Coefficient	0.24			Correlation Coefficient	0.54		
	μ	σ	RMSE		μ	σ	RMSE
All Months Combined	-10.79	15.78	19.03	All Months Combined	-5.87	10.31	11.80
Month Based				Month Based			
January	-2.15	4.31	4.48	January	-0.60	5.06	4.66
February	-17.60	21.38	26.28	February	-4.38	6.44	7.33
March	-15.85	27.09	29.37	March	-5.24	3.97	6.37
April	-15.00	24.00	26.55	April	-6.72	9.72	11.14
May	-3.75	4.46	5.58	May	-3.84	4.45	5.63
June	-14.10	25.28	27.33	June	-13.00	25.38	26.85
July	-8.53	7.69	11.04	July	-4.41	5.51	6.69
August	-7.08	5.13	8.49	August	-7.08	5.13	8.49
September	-8.84	12.11	14.15	September	-9.72	15.44	17.13
October	-12.29	16.89	19.47	October	-3.87	5.73	6.42
November	-11.77	5.96	12.97	November	-7.66	5.77	9.30
December	-13.42	13.89	18.46	December	-2.67	6.75	6.71
MODEL INFO				MODEL INFO			
Water Index	NDWLMCF			Water Index	WI2015		
Correlation Coefficient	0.38			Correlation Coefficient	0.15		

Altinkaya Trained Mode Approach Over Altinkaya Dam with SRTM DEM:

	μ	σ	RMSE		μ	σ	RMSE
All Months Combined	-12.79	11.01	16.83	All Months Combined	-11.55	8.50	14.31
Month Based				Month Based			
January	-9.53	7.75	11.87	January	-13.35	5.57	14.29
February	-10.51	12.97	15.84	February	-16.40	14.94	21.33
March	-11.52	4.66	12.28	March	-5.57	8.10	9.26
April	-12.65	7.42	14.35	April	-3.81	6.00	6.67
May	-10.22	5.53	11.43	May	-6.62	6.46	8.92
June	-15.48	25.26	28.04	June	-8.54	6.93	10.68
July	-9.93	5.62	11.17	July	-15.68	8.13	17.35
August	-12.58	7.11	14.16	August	-12.06	4.67	12.79
September	-16.15	18.18	23.16	September	-12.97	6.54	14.28
October	-10.78	4.97	11.66	October	-14.14	6.70	15.36
November	-14.86	3.24	15.15	November	-14.57	8.66	16.57
December	-18.86	8.88	20.53	December	-16.66	8.32	18.31
MODEL INFO				MODEL INFO			
Water Index	AWEI.S			Water Index	NDPI		
Correlation Coefficient	0.37			Correlation Coefficient	0.58		
	μ	σ	RMSE		μ	σ	RMSE
All Months Combined	-12.82	11.01	16.85	All Months Combined	-11.42	9.67	14.91
Month Based				Month Based			
January	-7.81	8.48	10.99	January	-7.89	8.34	10.97
February	-13.70	11.30	17.15	February	-11.26	6.95	12.93
March	-8.48	8.46	11.47	March	-7.98	7.53	10.53
April	-13.62	7.71	15.33	April	-12.60	8.62	14.86
May	-10.74	4.78	11.61	May	-5.29	4.11	6.52
June	-22.81	25.08	32.55	June	-14.76	16.90	21.51
July	-12.54	3.36	12.90	July	-13.46	9.66	16.09
August	-12.58	7.11	14.16	August	-10.44	6.11	11.84
September	-14.68	14.94	20.04	September	-14.04	10.04	16.77
October	-12.32	6.97	13.81	October	-15.48	11.67	18.67
November	-14.27	3.94	14.72	November	-15.28	11.92	18.76
December	-8.93	8.20	11.65	December	-9.62	9.97	13.24
MODEL INFO				MODEL INFO			
Water Index	NDWI.MCF			Water Index	WI2015		
Correlation Coefficient	0.38			Correlation Coefficient	0.31		

Altinkaya Trained Median Approach Over Altinkaya Dam with ASTER DEM:

	μ	σ	RMSE		μ	σ	RMSE
All Months Combined	-11.46	8.39	14.17	All Months Combined	-8.31	7.35	11.06
Month Based				Month Based			
January	-8.34	3.62	8.97	January	-11.00	3.36	11.42
February	-9.22	6.22	10.83	February	-8.44	8.84	11.68
March	-7.77	5.72	9.36	March	-2.01	5.64	5.53
April	-12.29	7.97	14.28	April	-2.33	6.30	6.20
May	-5.29	2.96	5.96	May	-4.81	6.87	7.98
June	-13.64	18.71	22.05	June	-4.24	7.22	7.91
July	-11.50	8.19	13.71	July	-12.43	9.44	15.12
August	-8.98	4.50	9.88	August	-7.37	3.48	8.02
September	-14.10	7.89	15.83	September	-11.04	6.99	12.75
October	-15.67	7.37	17.00	October	-10.64	4.84	11.49
November	-16.63	7.18	17.88	November	-10.64	2.93	10.97
December	-15.46	3.40	15.77	December	-16.44	7.74	17.90
MODEL INFO				MODEL INFO			
Water Index	AWEI.S			Water Index	NDPI		
Correlation Coefficient	0.38			Correlation Coefficient	0.52		
	μ	σ	RMSE		μ	σ	RMSE
All Months Combined	-14.08	10.32	17.41	All Months Combined	-11.98	8.74	14.79
Month Based				Month Based			
January	-8.34	5.17	9.58	January	-8.50	7.70	11.04
February	-13.71	10.32	16.63	February	-11.32	6.32	12.70
March	-18.39	20.93	26.52	March	-8.11	6.62	10.12
April	-15.83	10.18	18.35	April	-13.79	8.42	15.79
May	-8.91	4.89	10.00	May	-6.16	4.07	7.22
June	-14.33	13.03	18.73	June	-14.63	15.10	20.23
July	-13.72	10.13	16.55	July	-14.23	9.19	16.52
August	-10.18	6.57	11.82	August	-11.83	6.19	13.11
September	-14.32	8.34	16.22	September	-14.71	8.84	16.78
October	-18.38	7.82	19.67	October	-15.83	11.03	18.65
November	-17.67	5.12	18.28	November	-15.40	10.24	18.01
December	-16.71	13.06	20.53	December	-10.45	6.93	12.22
MODEL INFO				MODEL INFO			
Water Index	NDW1.MCF			Water Index	WI2015		
Correlation Coefficient	0.37			Correlation Coefficient	0.32		

Altinkaya Trained Median Approach Over Altinkaya Dam with SRTM DEM:

	μ	σ	RMSE		μ	σ	RMSE
All Months Combined	-12.82	9.23	15.76	All Months Combined	-9.67	7.31	12.09
Month Based				Month Based			
January	-9.83	3.60	10.36	January	-12.42	3.48	12.82
February	-10.45	6.28	11.92	February	-10.05	8.85	12.90
March	-9.32	5.79	10.72	March	-2.39	5.79	5.80
April	-14.25	8.15	16.08	April	-3.73	5.40	6.18
May	-5.85	3.85	6.85	May	-8.20	4.09	9.03
June	-14.88	20.71	24.27	June	-5.24	8.24	9.25
July	-13.04	8.74	15.29	July	-13.68	10.34	16.62
August	-9.69	4.25	10.44	August	-9.19	2.94	9.57
September	-16.13	8.66	17.97	September	-12.09	7.54	13.91
October	-17.07	8.82	18.81	October	-11.46	5.88	12.61
November	-18.13	9.24	19.99	November	-11.03	2.52	11.27
December	-16.76	4.49	17.25	December	-17.84	7.08	18.97
MODEL INFO				MODEL INFO			
Water Index	AWEI.S			Water Index	NDPI		
Correlation Coefficient	0.38			Correlation Coefficient	0.54		
	μ	σ	RMSE		μ	σ	RMSE
All Months Combined	-15.69	10.94	19.08	All Months Combined	-13.36	9.60	16.41
Month Based				Month Based			
January	-10.54	6.49	12.09	January	-9.89	8.27	12.44
February	-15.77	10.71	18.55	February	-13.22	6.83	14.62
March	-19.70	20.80	27.36	March	-9.97	7.49	12.09
April	-16.85	10.19	19.25	April	-14.56	8.53	16.51
May	-9.90	4.70	10.81	May	-7.35	4.09	8.27
June	-15.94	15.39	21.38	June	-16.41	17.02	22.75
July	-15.08	10.37	17.80	July	-15.43	9.57	17.73
August	-10.89	6.71	12.49	August	-12.45	6.01	13.60
September	-16.15	9.21	18.21	September	-16.00	9.90	18.38
October	-20.90	9.45	22.55	October	-17.42	11.54	20.25
November	-19.43	6.28	20.26	November	-17.21	11.79	20.30
December	-18.88	13.69	22.64	December	-11.61	9.87	14.70
MODEL INFO				MODEL INFO			
Water Index	NDWI.MCF			Water Index	WI2015		
Correlation Coefficient	0.36			Correlation Coefficient	0.31		

Altinkaya Trained Mean Approach Over Ermenek Dam with ASTER DEM:

	μ	σ	RMSE		μ	σ	RMSE
All Months Combined	-19.23	16.36	25.17	All Months Combined	-16.79	10.73	19.88
Month Based				Month Based			
January	-23.03	16.11	27.33	January	-19.52	14.53	23.60
February	-16.59	4.63	17.12	February	-13.79	8.30	15.74
March	-22.91	20.70	29.70	March	-12.90	3.00	13.19
April	-19.17	16.17	24.20	April	-25.77	12.89	28.32
May	-21.38	28.04	32.96	May	-12.76	2.55	12.97
June	-13.14	10.31	16.17	June	-18.42	9.99	20.56
July	-14.05	4.57	14.65	July	-14.05	4.59	14.66
August	-12.22	3.99	12.75	August	-12.22	4.03	12.76
September	-7.27	0.31	7.27	September	-8.56	0.42	8.56
October	-12.95	7.75	14.76	October	-19.32	8.78	20.92
November	-32.96	14.63	35.56	November	-22.50	12.20	25.11
December	-35.44	28.07	43.73	December	-20.95	21.22	28.54
MODEL INFO				MODEL INFO			
Water Index	AWEI.S			Water Index	NDPI		
Correlation Coefficient	0.32			Correlation Coefficient	0.33		
	μ	σ	RMSE		μ	σ	RMSE
All Months Combined	-14.90	20.66	25.35	All Months Combined	-14.48	16.84	22.12
Month Based				Month Based			
January	-14.56	17.49	21.61	January	-12.12	14.66	18.30
February	-11.60	24.11	24.88	February	-12.19	10.66	15.60
March	-21.86	29.81	34.91	March	-23.69	27.13	34.27
April	-23.69	17.06	28.35	April	-15.18	15.28	20.61
May	-28.34	47.66	51.19	May	-24.53	39.89	42.37
June	-14.33	11.79	17.92	June	-19.31	17.95	25.33
July	-2.43	2.08	3.08	July	-6.52	3.46	7.24
August	-3.16	2.11	3.70	August	-8.41	4.57	9.39
September	-2.83	1.67	3.21	September	-6.08	5.85	8.09
October	-17.58	15.41	22.52	October	-9.81	8.38	12.44
November	-19.83	17.54	25.49	November	-14.96	15.11	20.35
December	-20.84	21.02	28.33	December	-21.43	22.57	29.44
MODEL INFO				MODEL INFO			
Water Index	NDWLMCF			Water Index	WI2015		
Correlation Coefficient	0.06			Correlation Coefficient	0.10		

Altinkaya Trained Mean Approach Over Ermenek Dam with SRTM DEM:

	μ	σ	RMSE		μ	σ	RMSE
All Months Combined	-14.57	17.01	22.31	All Months Combined	-12.56	11.22	16.79
Month Based				Month Based			
January	-19.67	18.55	25.95	January	-16.13	16.36	21.98
February	-11.83	6.06	13.06	February	-9.32	9.64	12.81
March	-18.84	22.32	27.75	March	-9.54	4.09	10.24
April	-15.41	17.22	22.01	April	-22.18	13.12	25.21
May	-16.38	28.00	29.92	May	-12.25	3.87	12.73
June	-8.43	10.71	12.91	June	-15.12	10.18	17.75
July	-9.21	4.51	10.09	July	-9.22	4.54	10.10
August	-7.13	4.03	8.03	August	-7.13	4.06	8.04
September	-2.17	0.31	2.19	September	-3.42	0.56	3.46
October	-7.86	7.98	10.72	October	-13.88	8.61	15.95
November	-27.91	14.79	31.01	November	-16.88	12.33	20.29
December	-30.36	29.19	40.39	December	-15.59	22.18	25.56
MODEL INFO				MODEL INFO			
Water Index	AWEI.S			Water Index	NDPI		
Correlation Coefficient	0.29			Correlation Coefficient	0.27		
	μ	σ	RMSE		μ	σ	RMSE
All Months Combined	-10.81	21.32	23.77	All Months Combined	-10.18	17.31	19.97
Month Based				Month Based			
January	-11.56	19.29	21.06	January	-9.68	15.35	17.32
February	-7.57	24.94	23.99	February	-7.95	12.48	13.90
March	-17.76	30.60	33.10	March	-19.15	27.82	31.81
April	-19.96	17.47	25.55	April	-12.20	15.55	18.72
May	-24.78	47.92	49.51	May	-20.14	40.04	40.10
June	-9.74	12.20	14.79	June	-14.70	18.41	22.33
July	1.76	1.75	2.38	July	-2.10	2.75	3.27
August	1.34	1.62	1.99	August	-3.69	3.85	5.10
September	1.52	1.37	1.97	September	-1.71	5.36	5.18
October	-13.17	16.01	19.67	October	-5.20	8.75	9.53
November	-15.44	18.70	23.02	November	-9.89	15.06	16.94
December	-16.67	23.14	26.91	December	-17.03	23.87	27.31
MODEL INFO				MODEL INFO			
Water Index	NDWI.MCF			Water Index	WI2015		
Correlation Coefficient	0.04			Correlation Coefficient	0.08		

Altinkaya Trained Mode Approach Over Ermenek Dam with ASTER DEM:

	μ	σ	RMSE		μ	σ	RMSE
All Months Combined	-22.64	22.25	31.64	All Months Combined	-21.45	14.78	25.99
Month Based				Month Based			
January	-34.03	33.06	45.49	January	-24.47	19.35	30.18
February	-19.96	8.45	21.40	February	-15.20	11.70	18.57
March	-20.00	16.72	25.16	March	-23.43	14.55	26.93
April	-28.63	23.63	35.85	April	-39.51	15.35	41.92
May	-25.74	38.12	42.72	May	-35.04	13.97	37.20
June	-9.83	4.46	10.64	June	-20.24	8.13	21.56
July	-14.67	9.68	17.13	July	-14.67	9.68	17.13
August	-13.76	6.36	14.93	August	-13.81	6.33	14.97
September	-9.40	1.62	9.51	September	-9.66	1.24	9.73
October	-12.50	6.26	13.74	October	-20.22	13.33	23.60
November	-41.51	23.28	46.63	November	-26.24	18.35	31.13
December	-42.23	34.84	52.86	December	-17.19	15.64	22.35
MODEL INFO				MODEL INFO			
Water Index	AWEL.S			Water Index	NDPI		
Correlation Coefficient	0.29			Correlation Coefficient	0.15		
	μ	σ	RMSE		μ	σ	RMSE
All Months Combined	-18.97	26.50	32.44	All Months Combined	-19.54	24.60	31.27
Month Based				Month Based			
January	-17.00	13.63	21.06	January	-20.24	30.17	34.73
February	-20.37	36.68	39.19	February	-18.56	24.78	29.26
March	-35.79	46.50	55.52	March	-36.54	41.40	52.57
April	-39.98	28.71	47.81	April	-27.00	23.92	34.72
May	-37.56	54.00	61.19	May	-32.23	51.08	54.73
June	-9.49	3.80	10.11	June	-19.03	12.31	22.10
July	-4.07	1.53	4.30	July	-8.50	4.66	9.50
August	-3.59	4.40	5.39	August	-8.12	6.44	10.03
September	-4.42	2.77	5.09	September	-7.56	5.82	9.24
October	-12.77	8.12	14.77	October	-10.97	7.69	13.03
November	-22.05	21.62	29.59	November	-17.01	19.45	24.59
December	-23.66	13.57	26.71	December	-27.46	31.16	39.12
MODEL INFO				MODEL INFO			
Water Index	NDWI.MCF			Water Index	WI2015		
Correlation Coefficient	0.02			Correlation Coefficient	0.03		

Altinkaya Trained Mode Approach Over Ermenek Dam with SRTM DEM:

	μ	σ	RMSE		μ	σ	RMSE
All Months Combined	-23.32	26.08	34.85	All Months Combined	-24.10	23.71	33.69
Month Based				Month Based			
January	-28.20	33.17	41.38	January	-29.55	31.62	41.31
February	-23.97	16.90	28.51	February	-16.26	19.76	24.29
March	-29.91	32.68	42.25	March	-23.88	11.51	26.09
April	-28.03	27.97	37.92	April	-54.05	29.95	60.57
May	-21.05	36.67	38.97	May	-29.63	15.89	32.86
June	-17.74	25.89	29.55	June	-31.41	23.94	38.26
July	-19.09	13.48	22.71	July	-19.07	13.49	22.70
August	-5.73	5.88	7.85	August	-9.04	7.76	11.49
September	-3.88	3.21	4.86	September	-4.16	2.83	4.90
October	-13.01	9.64	15.71	October	-19.64	15.45	24.18
November	-42.54	27.15	49.23	November	-24.61	18.73	29.97
December	-46.36	35.78	56.71	December	-28.78	41.49	47.57
MODEL INFO				MODEL INFO			
Water Index	AWEI.S			Water Index	NDPI		
Correlation Coefficient	0.20			Correlation Coefficient	0.04		
	μ	σ	RMSE		μ	σ	RMSE
All Months Combined	-20.86	31.74	37.79	All Months Combined	-18.85	26.51	32.37
Month Based				Month Based			
January	-27.62	32.45	40.50	January	-20.61	31.92	36.28
February	-17.64	37.34	38.38	February	-15.60	25.78	28.24
March	-32.86	51.58	57.42	March	-35.71	46.94	55.78
April	-36.80	27.97	44.79	April	-26.31	26.64	35.83
May	-34.46	55.13	60.16	May	-19.67	29.86	32.49
June	-18.67	27.06	30.96	June	-25.77	32.53	39.32
July	-1.88	2.92	3.26	July	-7.46	2.82	7.89
August	-2.27	3.30	3.77	August	-9.07	5.68	10.45
September	-1.97	2.47	3.00	September	-8.27	10.80	12.86
October	-21.99	25.80	32.22	October	-10.80	14.56	17.12
November	-25.13	30.30	37.37	November	-14.78	20.82	24.08
December	-31.30	35.70	45.19	December	-26.95	39.45	44.40
MODEL INFO				MODEL INFO			
Water Index	NDWI.MCF			Water Index	WI2015		
Correlation Coefficient	-0.04			Correlation Coefficient	0.03		

Altinkaya Trained Median Approach Over Ermenek Dam with ASTER DEM:

	μ	σ	RMSE		μ	σ	RMSE
All Months Combined	-18.21	16.36	24.41	All Months Combined	-15.04	9.96	18.00
Month Based				Month Based			
January	-21.29	15.64	25.63	January	-17.87	13.44	21.67
February	-14.73	3.79	15.13	February	-12.98	8.17	14.97
March	-22.25	20.10	28.84	March	-10.74	2.79	11.03
April	-17.63	15.39	22.54	April	-21.14	9.87	22.99
May	-21.85	29.60	34.32	May	-9.39	2.87	9.74
June	-12.19	8.73	14.57	June	-15.79	9.05	17.82
July	-12.36	3.35	12.74	July	-12.36	3.38	12.74
August	-11.06	3.31	11.46	August	-11.05	3.35	11.47
September	-7.17	0.32	7.18	September	-8.46	0.42	8.47
October	-12.54	7.40	14.24	October	-18.24	8.56	19.84
November	-31.45	15.63	34.53	November	-21.68	12.70	24.58
December	-34.63	28.74	43.44	December	-19.87	20.08	27.03
MODEL INFO				MODEL INFO			
Water Index	AWEL.S			Water Index	NDPI		
Correlation Coefficient	0.32			Correlation Coefficient	0.40		
	μ	σ	RMSE		μ	σ	RMSE
All Months Combined	-14.33	20.30	24.73	All Months Combined	-13.92	16.76	21.70
Month Based				Month Based			
January	-13.22	15.33	19.25	January	-10.76	13.74	16.76
February	-11.62	24.09	24.88	February	-12.13	11.71	16.16
March	-21.32	29.05	34.03	March	-23.53	27.00	34.07
April	-22.33	17.18	27.28	April	-13.47	15.06	19.25
May	-28.33	48.24	51.61	May	-24.41	39.74	42.20
June	-12.91	9.87	15.75	June	-18.62	17.72	24.67
July	-2.40	2.06	3.05	July	-6.31	3.40	7.03
August	-3.14	2.10	3.68	August	-7.86	4.02	8.68
September	-2.78	1.66	3.17	September	-5.64	4.99	7.25
October	-16.70	14.37	21.23	October	-9.54	8.04	12.03
November	-19.22	16.86	24.62	November	-14.86	15.35	20.43
December	-20.33	21.25	28.10	December	-21.06	22.68	29.24
MODEL INFO				MODEL INFO			
Water Index	NDWI.MCF			Water Index	WI2015		
Correlation Coefficient	0.07			Correlation Coefficient	0.09		

Altinkaya Trained Median Approach Over Ermenek Dam with SRTM DEM:

	μ	σ	RMSE		μ	σ	RMSE
All Months Combined	-13.56	17.08	21.72	All Months Combined	-10.90	10.43	15.04
Month Based				Month Based			
January	-18.26	18.60	24.94	January	-14.84	15.88	20.75
February	-9.74	5.03	10.77	February	-8.30	9.29	11.87
March	-18.30	22.00	27.17	March	-7.46	2.41	7.77
April	-14.29	16.48	20.75	April	-17.71	9.97	19.91
May	-16.84	29.64	31.41	May	-9.46	2.59	9.74
June	-7.42	9.18	11.20	June	-13.00	9.05	15.40
July	-7.45	3.29	8.04	July	-7.47	3.32	8.06
August	-5.86	3.28	6.58	August	-5.87	3.32	6.60
September	-2.01	0.31	2.03	September	-3.24	0.52	3.27
October	-7.36	7.55	10.08	October	-12.53	8.07	14.54
November	-26.31	16.02	30.10	November	-16.05	13.14	20.04
December	-29.43	29.83	40.09	December	-14.63	21.50	24.48
MODEL INFO				MODEL INFO			
Water Index	AWEL.S			Water Index	NDPI		
Correlation Coefficient	0.29			Correlation Coefficient	0.33		
	μ	σ	RMSE		μ	σ	RMSE
All Months Combined	-10.25	21.09	23.31	All Months Combined	-9.52	17.26	19.60
Month Based				Month Based			
January	-10.25	17.33	18.85	January	-8.32	14.34	15.79
February	-7.41	24.69	23.73	February	-7.42	12.73	13.79
March	-17.35	30.12	32.51	March	-19.02	27.91	31.79
April	-19.01	17.39	24.77	April	-9.91	14.63	16.63
May	-24.82	48.56	50.03	May	-20.24	40.44	40.45
June	-8.24	10.34	12.53	June	-14.00	18.35	21.83
July	1.84	1.68	2.40	July	-1.79	2.67	3.03
August	1.42	1.56	2.01	August	-3.11	3.39	4.39
September	1.64	1.32	2.04	September	-1.17	4.58	4.34
October	-12.25	15.02	18.38	October	-4.84	8.34	9.02
November	-14.66	18.06	22.06	November	-9.78	15.36	17.09
December	-16.33	24.35	27.58	December	-16.66	24.20	27.32
MODEL INFO				MODEL INFO			
Water Index	NDWI.MCF			Water Index	WI2015		
Correlation Coefficient	0.05			Correlation Coefficient	0.08		